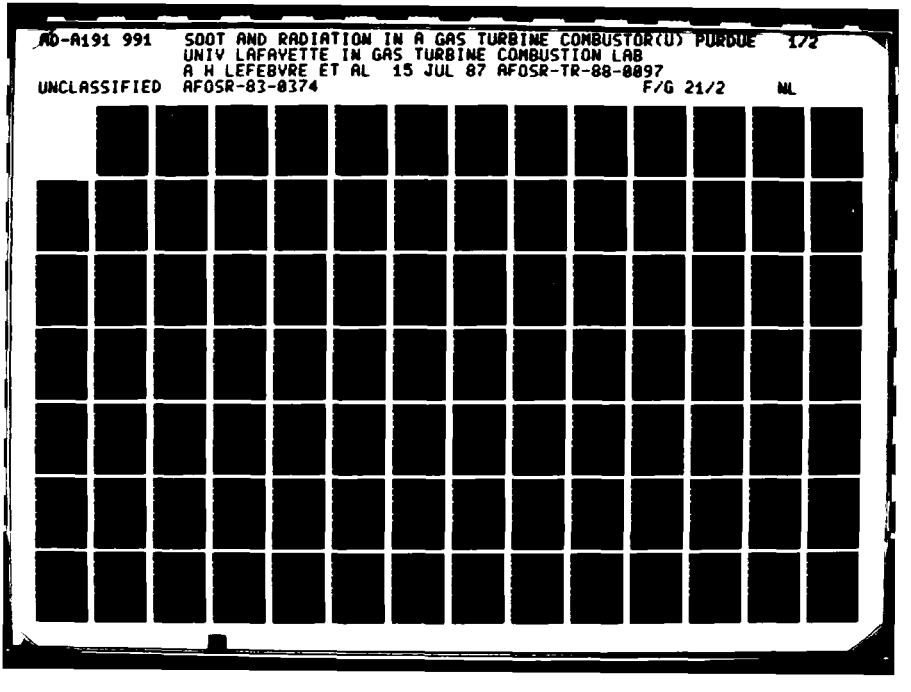
AD-A191 991 SOOT AND RADIATION IN A GAS TURBINE COMBUSTOR(U) PURDUE 1/2
UNIV LAFAYETTE IN GAS TURBINE COMBUSTION LAB
A H LEFEBVRE ET AL 15 JUL 87 AFOSR-TR-88-0897
UNCLASSIFIED AFOSR-83-0374 F/G 21/2 NL

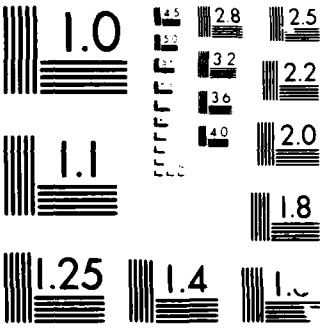

MICROCOPY RESOLUTION TEST CHART
NATIONAL BUREAU OF STANDARDS 1963-A

DTIC FILE COPY

Unclassified
SECURITY CLASSIFICATION OF THIS PAGE

REPORT DOCUMENTATION PAGE

Form Approved
OMB No. 0704-0188

DTIC ELECTE MAR 03 1988 H

AD-A191 991

1a. REPORT SECURITY CLASSIFICATION: Unclassified	1b. RESTRICTIVE MARKINGS
2a. SECURITY CLASSIFICATION AUTHORITY	3. DISTRIBUTION/AVAILABILITY OF REPORT: Approved for public release; distribution is unlimited.
2b. DECLASSIFICATION/DOWNGRADING SCHEDULE	
4. PERFORMING ORGANIZATION REPORT NUMBER(S)	5. MONITORING ORGANIZATION REPORT NUMBER(S): AFOSR-TR- 88-0097
6a. NAME OF PERFORMING ORGANIZATION: Purdue University	6b. OFFICE SYMBOL (If applicable):
6c. ADDRESS (City, State, and ZIP Code): School of Mechanical Engineering, West Lafayette, IN 47907	7a. NAME OF MONITORING ORGANIZATION: AFOSR/NA
8a. NAME OF FUNDING/SPONSORING ORGANIZATION: AFOSR/NA	8b. OFFICE SYMBOL (If applicable): NA
8c. ADDRESS (City, State, and ZIP Code): Building 410, Bolling AFB DC 20332-6448	7b. ADDRESS (City, State, and ZIP Code): Building 410, Bolling AFB DC 20332-6448
	9. PROCUREMENT INSTRUMENT IDENTIFICATION NUMBER: AFOSR 83-0374
	10. SOURCE OF FUNDING NUMBERS: PROGRAM ELEMENT NO. 61102F; PROJECT NO. 2308; TASK NO A2; WORK UNIT ACCESSION NO.

11. TITLE (Include Security Classification)
(U) Soot and Radiation in a Gas Turbine Combustor

12. PERSONAL AUTHOR(S)
A.H. Lefebvre, P.E. Sojka, W.G. Cummings III

13a. TYPE OF REPORT	13b. TIME COVERED	14. DATE OF REPORT (Year, Month, Day)	15. PAGE COUNT
Final Technical	FROM 9/30/83 TO 9/29/86	87/7/15	134

16. SUPPLEMENTARY NOTATION

17. COSATI CODES		
FIELD	GROUP	SUB-GROUP

18. SUBJECT TERMS (Continue on reverse if necessary and identify by block number)
Incipient soot formation, flame radiation and emissivity, premixed flames, pressure dependence

19. ABSTRACT (Continue on reverse if necessary and identify by block number)

The effects of pressure, inlet air temperature, and fuel type on the soot threshold, or critical equivalence ratio, are presented. Higher pressures yield lower soot thresholds, while no dependence on fuel type, as described by either the fuel hydrogen-to-carbon ratio, fuel molecular weight, number of carbon atoms, or number of carbon-carbon bonds, is observed. Variations in inlet air temperature have a complex effect; however, the results clearly show that the experimentally measured flame temperature is central to a description of the incipient soot formation process. The critical equivalence ratio dependence on pressure and temperature is shown to agree with a two-step semi-global model for soot precursor evolution for pressures form 0.1 to 0.8 MPa, and measured flame temperatures between 1600 and 2400K.

The effects of equivalence ratio, pressure, and fuel chemistry on total non-luminous flame radiation were also studied. Radiant intensity was highest for an equivalence ratio of unity and increased linearly with pressure from 0.4 to 0.8 MPa. The number of

20. DISTRIBUTION/AVAILABILITY OF ABSTRACT: ☒ UNCLASSIFIED/UNLIMITED ☒ SAME AS RPT ☐ DTIC USERS	21. ABSTRACT SECURITY CLASSIFICATION: Unclassified
22a. NAME OF RESPONSIBLE INDIVIDUAL: Julian M Tishkoff	22b. TELEPHONE (Include Area Code): (202) 767-4935 / 22c. OFFICE SYMBOL: AFOSR/NA

DD Form 1473, JUN 86 — Previous editions are obsolete. — SECURITY CLASSIFICATION OF THIS PAGE

Unclassified

carbon-carbon bonds and the H/C mass ratio are shown to influence flame radiation. Empirical non-luminous emissivities increase with pressure and decrease with axial location and equivalence ratio; calculated emissivities show no trends.

SOOT AND FLAME RADIATION IN A GAS TURBINE COMBUSTOR

Final Report

for

AFOSR Contract
Number 83-0374A

prepared by

A. H. Lefebvre,
P. E. Sojka, and
W. G. Cummings III

Gas Turbine Combustion Laboratory
Thermal Sciences and Propulsion Center
School of Mechanical Engineering
Purdue University
West Lafayette, IN 47907

July, 1987

TABLE OF CONTENTS

Page

LIST OF TABLES

LIST OF FIGURES

ABSTRACT

The effects of pressure, inlet air temperature, and fuel type on the soot threshold, or critical, equivalence ratio are presented. Higher pressures yield lower soot thresholds, while no dependence on fuel type, as described by either the fuel hydrogen-to-carbon ratio, fuel molecular weight, number of carbon atoms, or number of carbon-carbon bonds, is observed. Variations in inlet air temperature have a complex effect; however, the results clearly show that the experimentally measured flame temperature is central to a description of the incipient soot formation process. The critical equivalence ratio dependence on pressure and temperature is shown to agree with a two-step semi-global model for soot precursor evolution for pressures from 0.1 to 0.8 MPa, and measured flame temperatures between 1600 and 2400K.

The effects of equivalence ratio, pressure, and fuel chemistry on total non-luminous flame radiation were also studied. Radiant intensity was highest for an equivalence ratio of unity and increased linearly with pressure from 0.4 to 0.8 MPa. The number of carbon-carbon bonds and the H/C mass ratio are shown to influence flame radiation. Empirical non-luminous emissivities increase with pressure and decrease with axial location and equivalence ratio; calculated emissivities show no trends.

INTRODUCTION

Soot is an undesirable product of combustion. It is suspected of being harmful to human health, it leaves a visible exhaust plume, and it can overheat combustor walls via radiative heat transfer. It is therefore advantageous to minimize soot formation and to promote oxidation of any soot that is formed. An understanding of the basic relationship between operating conditions and soot formation is necessary to accomplish this. In particular, this study undertook as a first major objective the determination of the dependence of soot formation on equivalence ratio, pressure, temperature, and fuel being burnt.

Flame radiation is a second important phenomenon associated with the combustion process. In some applications, for example in a power plant furnace, high radiative wall heat fluxes are desirable [Wark, 1977]. In other systems radiative heat loads can overheat vital components. Excessive radiative heat flux is particularly critical in gas turbine combustion chambers because film cooling of the combustor liner provides an effective barrier against convective heating but not against radiative transfer.

The gas turbine combustor has been used as a test bed in previous flame radiation studies at high pressures; however, those studies have all used

multicomponent, heavy-hydrocarbon liquid fuels. Consequently, they were unable to isolate the effects of fuel structure on flame radiation at high pressures. This study therefore undertook as a second major objective an investigation into flame radiation from gas-fueled flames.

The overall goal of this investigation is to extend the fundamental knowledge of soot formation and flame radiation to combustion at elevated pressures. The principal application of this information lies in the design of high-pressure combustors for minimum soot emission and optimum radiative heat transfer characteristics.

Soot Formation

The detailed chemical mechanism for soot formation is not well understood but can be modeled in a semi-global manner as a two-stage process [Harris et al, 1986]. The first step occurs when fuel molecules enter the pyrolysis zone of a flame and are converted to a variety of compounds, including soot precursors. The soot precursors are subsequently converted to either soot or oxides of carbon, depending upon the nature of the flame. When the formation of soot precursors occurs at the same rate as their oxidation, the precursor concentration is at steady state, and the flame is at the soot threshold. The equivalence ratio at this point is termed the critical equivalence ratio, ϕ_c.

The soot threshold itself is an important experimental quantity for several

reasons. Since it is the fuel/air mixture at which the rates of soot precursor formation and destruction balance each other, its measurement can provide information to determine the extent of applicability of the two-stage model described above. The measurement is very simple and repeatable, depending only upon the visual acuity of the observer. Finally, the soot threshold provides a quantitative measure of the onset of flame luminosity, obviously important when analyzing radiation characteristics.

Several important questions about soot thresholds remain to be answered.

— Is the two-step global model valid for combustion pressures above one atmosphere?

— Which flame temperature best describes the sooting condition: adiabatic or measured? And which measured temperature?

— Will an effective equivalence ratio, based on products of carbon monoxide and water vapor, describe results more accurately than the standard equivalence ratio, based on products of carbon dioxide and water vapor?

— How important are fuel properties, such as molecular weight, hydrogen-to-carbon ratio, and number of carbon-carbon bonds?

This study answers these questions by investigating soot thresholds at high pressures.

Since the experiments in this work were run at various temperatures and pressures and since the semi-global model requires the determination of OH

concentrations, a knowledge of equilibrium OH behavior with respect to these variables is required. For instance, an increase in temperature brings about an exponential increase in the OH concentration. Higher pressures, on the other hand, lead to decreases in the OH concentration. Thus, from these considerations we should expect high flame temperatures and/or low pressures to preclude sooting. The pyrolysis of the fuel, however, is also temperature dependent, higher temperatures giving higher concentrations of soot precursors. This effect, then, counteracts the higher OH concentrations brought about by higher temperatures. A significant contribution to the understanding of soot formation could be made if the two-stage model described above could be shown to describe the critical equivalence ratio behavior found in this investigation.

Flame Radiation

The thermal radiation spectrum encompasses wavelengths between 0.4 and 1000 μm and includes band as well as continuous radiation. Band radiation is emitted by gaseous combustion products, principally carbon dioxide and water vapor. The strongest carbon dioxide bands are centered at 2.7 μm and 4.3 μm, while the water bands are located at 1.9 μm, 2.8 μm, and 6.7 μm. Continuous radiation emitted by hot soot particles extends over all thermal wavelengths. However, even for a cool flame of 1600 K, 95% of the energy is emitted at wavelengths shorter than 8.0 μm. For a flame at 2000 K the 95% cut-off is 6.3 μm. The significant conclusion, then, is that by

measuring radiative energy at wavelengths between 0.7 μm and 8.0 μm one observes essentially all flame radiation pertinent to this study.

Radiation is important in this study because it is a major contributor to the heat flux at the combustor wall. Radiation is a complex phenomenon and is only partially understood; nevertheless, the following parameters are known to affect the wall heat flux [Lefebvre, 1983]. Combustor pressure can alter soot levels and emission band widths, thereby altering radiation fluxes. Flame temperature strongly influences flame radiation and is controlled by equivalence ratio and inlet air temperature. Equivalence ratio and differences in fuel chemical structure can lead to changes in the concentrations of CO_2 and H_2O, upon which flame radiation also depends. For these reasons this study focuses on measurement of thermal radiation emitted by flames at various values of pressure, inlet air temperature, equivalence ratio, and fuel type.

The studies of flame radiation at high pressures are numerous [Moses and Naegeli, 1979; Naegeli et al., 1983; Claus, 1981; and Humenik et al., 1983], but the results have been influenced by the interdependences of the variables involved. The goal of the radiation portion of this study is to isolate the effects of the various parameters studied. A particularly important aspect, then, is that the fuels be burned in the gaseous state thereby eliminating any complicating effects of fuel spray distribution and drop size, a problem common in liquid-fueled combustors. Furthermore, only pure hydrocarbon

fuels should be burned. The effect of fuel chemical structure is thus more evident than in studies using multi-component fuels.

The flame radiation intensity, I_f, is the radiant power emitted per unit area projected normal to the direction of passage, per unit solid angle. It is the radiometric quantity reported in this study. Because the field of view of the radiometer is centered on a diameter of the flame, the emitting area and the projected areas are the same. This is equivalent to stating that the numerical values of the normal emitted flux and the intensity normal to the flame are interchangeable when using this radiometric alignment. The significant point, however, is that these quantities were measured at the boundary of the cylindrical flame. As such, no consideration was given to attenuation by absorption or scattering or to inward scattering. The reported intensities are simply the bulk quantities emitted normal to the flame (i.e. along a diametral path) as measured from outside the boundary of the hot flame gases.

The radiation intensity reported here is of value to the combustion engineer as a design guideline. Many practical combustors burn gaseous fuels, most of them among the fuels studied here. An estimate of flame temperature and a knowledge of combustor geometry are all the information required to apply the results given in this work to an actual system.

LITERATURE REVIEW

Critical Equivalence Ratio

Recent studies of soot thresholds in premixed flames have used the minimum equivalence ratio at which soot was detected as the principal indicator of a fuel's tendency to form soot. This so-called critical equivalence ratio, ϕ_c, is most often based on complete combustion to carbon dioxide and water vapor. Other end conditions have been considered, however. Takahashi and Glassman [1984] suggested an effective equivalence ratio that assumed combustion products of carbon monoxide and water vapor. Olson and Pickens [1984] and Millikan [1962] discussed the use of the carbon-to-oxygen ratio in the unburnt mixture, based on combustion products of carbon dioxide and hydrogen. However, Olson and Pickens state that none of these effective equivalence ratios is superior to the others, probably because the combustion products vary so greatly for different equivalence ratios. Because the definition of equivalence ratio based on carbon dioxide and water vapor is the most widely known, it will be used here. (Note that a high value of ϕ_c indicates a low tendency to form soot.)

Effect of Temperature

Flame temperature has been widely studied as a parameter having an effect on ϕ_c. Glassman and Yaccarino [1981] found a distinct relationship between ϕ_c and $\frac{1}{T}$. Millikan found a linear relationship between his effective critical equivalence ratio (based on the carbon-to-oxygen atom ratio in the unburnt mixture) and measured flame temperature for ethylene/air flames. He also showed a linear relationship between ϕ_c and inverse temperature. He suggested that ln[OH] was a linear function of equivalence ratio and that higher temperatures led to higher [OH], which in turn led to more rapid oxidation of soot precursors within the pyrolysis zone.

Harris et al. extended this theory, arriving at a slightly different expression. They found a linear relationship between $\ln\frac{\phi_c}{[OH]}$ and inverse temperature that held for five different aliphatic fuels and postulated that the formation of soot precursors was first order in fuel concentration while the oxidation of the precursors was first order in [OH]. They reasoned that a two-step model--precursor formation followed by oxidation--would satisfactorily predict soot thresholds. They also postulated that at the critical equivalence ratio the rate of formation of soot precursors exactly balanced the rate of destruction of precursors, or

$$[\dot{P}] = k_f[F] - k_d[OH][P] = 0 \tag{1}$$

where

$[\dot{P}]$ = time rate of change of the precursor concentration

$[F]$ = fuel concentration

$[OH]$ = hydroxyl radical concentration

$[P]$ = precursor concentration

k_f = rate coefficient for precursor formation

k_d = rate coefficient for precursor destruction

Over a given narrow range of pressures and flame temperatures the fuel concentration is a linear function of equivalence ratio, so

$$[F] = c \cdot \phi \tag{2}$$

With the reaction rate coefficients taking an Arrhenius form, Eqn (1) can be reduced to

$$\ln \frac{\phi_c}{[OH]} = \frac{E_{a,f} - E_{a,d}}{R_u T} + C_{fuel} \tag{3}$$

where

E_a = activation energy (f = formation; d = destruction)

C_{fuel} = a constant specific to a given fuel

An unexpected result came from the work of Olson and Madronich [1985], who measured temperatures and soot threshold equivalence ratios in

aromatic-fueled flames as functions of the ratio of oxygen to nitrogen in the unburnt mixture. While they concur with Takahashi and Glassman that ϕ_c increases with adiabatic flame temperature, they found that measured flame temperatures were unrelated to soot threshold equivalence ratios. In a similar study Wright [1969] adjusted the flame temperature within a well stirred reactor by preheating the fuel/air mixture. Burning olefins and aromatics with air preheated to as high as 650 K, he demonstrated that an increase in pre-flame temperature gave a higher soot threshold equivalence ratio. A similar rise in soot threshold followed the introduction of diluents of lower heat capacity, an effect which he also attributed to an increase in flame temperature. His experimental method had an important difference, however, from all others cited here; his criterion for critical soot limit required his mixtures to be rich enough to leave soot in the end products of the flame. All other soot threshold measurements have been made at the point of incipient soot formation where even though soot may be forming at one point within the flame it can be burnt off in downstream locations. Thus, Wright's critical equivalence ratio values are expected to be higher than those of the other studies discussed here. Wright's pressure and temperature dependencies may also differ from those observed at the critical soot point.

Most of these studies, then, have concluded that a higher flame temperature, either measured or adiabatic, leads to a higher ϕ_c; however, the

precise relationship between flame temperature and soot threshold needs refinement. In addition, the dependence of ϕ_c on pressure is not currently known.

Effect of Pressure

Pressure effects on ϕ_c have been investigated less extensively than temperature effects. Calcote and Miller [1978], burning acetylene, benzene, and cumene, found that soot threshold equivalence ratios were independent of pressure between 9 and 100 kPa. MacFarlane et al. [1975] also determined the soot threshold to be independent of pressure over the range 0.5 to 2.0 MPa for gaseous pentanes and hexanes. In contrast, Fenimore et al. [1957] observed a decrease in ϕ_c as the pressure rose.

The results of Calcote and Miller and MacFarlane et al. [1975] are surprising since the concentration of OH radicals is known to be a function of pressure. Since OH radicals are believed to play an important role in the oxidation of soot precursors, one would expect that as pressure changes, [OH] would change. Based on the model of Harris et al., the soot threshold would also change. No experimental data exist, however, to either verify that ϕ_c does depend on pressure, or to quantify that dependence. For this reason the effect of pressure was investigated in the present study.

Effect of Fuel Type

Fuel effects on ϕ_c have been the subject of many investigations. Several prior studies have been performed with liquid fuels, but in many cases the results are pertinent here. Naegeli et al. [1983], for example, showed that the hydrogen-to-carbon ratio of a liquid fuel was a good indicator of a fuel's tendency to soot. An important corollary was that the internal structure of the fuel molecule was unimportant. These authors also pointed out that improved aeration of a flame reduces the dependence of soot on flame temperature, implying that premixed flames will be less sensitive to temperature than diffusion flames. Calcote and Manos [1983], in an exhaustive review of atmospheric pressure flames using a variety of fuels from several hydrocarbon families, listed several important trends for premixed flames. First, the result of changing the carbon-to-hydrogen ratio from fuel to fuel appeared to be ambiguous. All alkenes, for example, have a C/H value of 1/2; however, the soot thresholds for these fuels varied widely. Furthermore, acetylene (with its high C/H value of 1) had the highest soot threshold of any fuel examined. Second, soot thresholds fell as the molecular weight rose within a hydrocarbon family (e.g. alkane family). This was especially apparent for hydrocarbons of fewer than six carbon atoms. Finally, the effect of molecular structure showed the following trend for soot:

highest thresholds (least likely to soot)

alkynes (acetylenes)

alkenes (olefins)

iso-alkanes

n-alkanes (paraffins)

lowest thresholds (most likely to soot).

Takahashi and Glassman defined a new parameter for describing critical equivalence ratios in premixed flames, namely the total number of carbon-carbon bonds within a molecule. They showed that for a wide variety of aliphatic, alicyclic, and aromatic fuels, all burned at the same calculated adiabatic flame temperature, the critical equivalence ratio decreased as the number of carbon-carbon bonds increased. In an interesting discussion on the effects of flame temperature and fuel type Calcote and Olson [1982] stated that "although increasing the flame temperature of an individual fuel may decrease its tendency to soot, a series of different fuels with increasing flame temperatures at their soot points generally increase in tendency to soot (ethylene and acetylene are exceptions)." The important point here is that fuel structure may be the dominant factor in determining the soot threshold.

To facilitate comparison of data from all soot threshold investigations Calcote and Manos have devised a Threshold Soot Index (TSI) for premixed flames:

$$TSI = a - b \cdot \phi_c$$

where ϕ_c is the soot threshold equivalence ratio and a and b are constants specific to a given experimental system. The goal of the TSI is to remove variations from rig construction, operational procedures, and systematic experimental variations, thereby bringing together the results of many different authors. The constants, a and b, are computed by taking ϕ_c data for two fuels of very different molecular weights and fitting them to the now widely published TSI values. A high value of TSI reflects a greater tendency to soot (i.e. low ϕ_c), while a low value of TSI indicates a lesser tendency to soot (i.e. high ϕ_c).

The present study has two experimental characteristics that could cause the results to deviate from those of other investigators. First, the soot threshold is determined visually, subjecting the results to the sensitivity of the human eye. Second, the flame is subjected to significant cooling, especially from the water jacket surrounding the combustor. Neither of these characteristics is expected to diminish the precision of the study, but the results were different from those of flat flame burners, which in some cases approach adiabatic performance.

Flame Radiation

Little radiant heat transfer data exist for high-pressure, gaseous-fuel flames; however, many studies have been conducted on flame radiation from high-pressure combustors burning liquid fuels. The expressions derived from liquid-fuel data are included here in hopes of providing an insight into the

results of the present work. The complex interactions of fuel atomization and combustor geometry with flame radiation should be borne in mind, however, in any comparison between these dissimilar experiments.

Effect of Temperature

An analytical method developed by Kunitomo and Kodama [1974] predicts that the contributions to flame emissivity from soot and non-luminous gasses are completely independent of flame temperature for any rich fuel/air mixture at pressures of 0.3 and 0.5 MPa. No experimental evidence has been found to support this result.

Effect of Pressure

Several investigators have examined the effect of pressure on flame radiation in practical gas turbine combustors [MacFarlane et al., 1975; Marsland et al., 1975; Humenik et al., 1983]. All concur that higher pressures yield considerably higher radiative fluxes at the combustor walls with a diminishing effect at very high pressures (1.2 to 1.5 MPa). The work of MacFarlane et al. [1975] is especially relevant since he measured flame radiation and emissivity for premixed methane/air flames. Using the Schmidt technique he found that the radiative flux also rose with pressure for rich fuel/air mixtures. In addition, he found that an increase in pressure brought about a substantial increase in emissivity, especially for equivalence ratios above 2.0. While this information may be useful, discretion is

EXPERIMENTAL SYSTEM

This chapter describes the hardware and instrumentation included in the gaseous-fueled combustion rig. It begins with the air supply system, follows with the fuel delivery system, and then discusses the combustor as a whole. Finally, the three combustor subsystems (igniter, flameholder/fuel injector, and flame positioning mechanism) are discussed.

Air Supply System

The laboratory air supply system consists of two compressors connected to four reservoir tanks (see Figure 1). Tank refilling can proceed during an experimental run, if desired. A mechanical description of the compressors, the air delivery system, and the air regulators is presented below. A discussion of the uses of the four air subsystems, classified by their maximum working pressure, follows. Finally, a description of the air flow profile through the combustor, and its measurement, is presented.

Mechanical Components

The air is raised to its dry, high-pressure state using a set of two piston-type compressors and two drying systems. The first set of compressors boosts ambient air to 0.345 MPa and 533 K. The air then passes through a separator to remove liquid water and oil. Next, the air's dew point is reduced to 236 K in a chamber charged with activated aluminum. Dust is then removed from the air with a paper filter and the air is pumped to 15.2

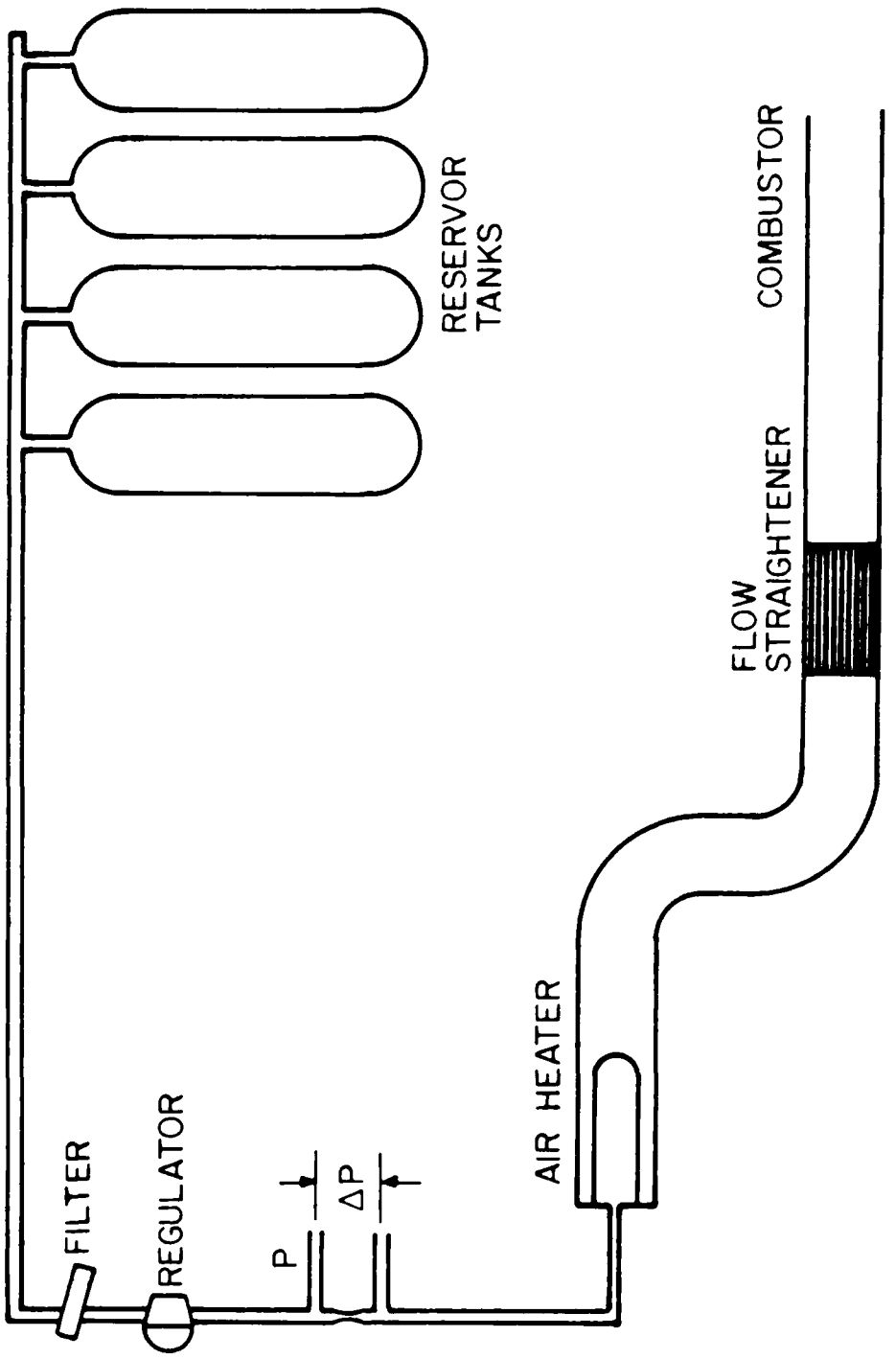

Figure 1. Air Supply System.

MPa. Finally, an activated carbon filter removes hydrocarbons from the air before it is sent to the reservoir tanks.

Combustion Air Pre-Treatment

Air entering the combustor was heated by means of a Wellman model W15000 immersion heater, comprised of three resistively heated cal rods powered by a 240 V, three-phase SCR controller. At the maximum current of 60 A, 14.4 kW of power was available. A 4-20 mA controller, located in the control room, regulated the current delivered to the heater. Its reference signal came from a thermocouple located at the combustor inlet.

Incoming air supply flow conditions were carefully maintained during these experiments. The combustor entrance incorporated two bends, installed to fit the rig within the test cell confines. These turns distorted the air flow field causing asymmetry of the velocity profile and imparting swirl; however, a set of flow straighteners and screens, located directly upstream of the combustor, re-established uniform flow. The length-to-diameter ratio of the flow straightener was 44 to 1, enough to provide an even velocity profile and to minimize swirl [Daily and Harleman, 1966]. A set of 60 x 60 mesh, 0.19 mm diameter wire screens were silver soldered upstream of the flow straightener in accordance with the work of Schubauer et al [1948]. For an inlet temperature of 600 K, a nominal velocity of 6 m/s through the combustor gave $Re_D = 4300$, far above the critical Re_D of 2300 for fully turbulent flow. Because the screens were placed in the flow and because the Reynolds number was well above the critical value for turbulence, all flames were considered to be fully turbulent.

Axial air velocity at several mass flow rates was measured with a traversing pitot-static probe connected to an inclined manometer. The velocity at any radial position, within a given plane normal to the flow, was found to lie within four percent of the average value across this plane. See Figure 2. All velocity measurements were made with the fuel injector/flameholder apparatus removed from the combustor.

Fuel Delivery System

The fuel system was designed to deliver gaseous fuels to the combustor and to control and measure their flow rates (see Figure 3). Most fuels had to be heated or pressurized, as described below, to propel them into the combustion chamber. This was accomplished by either warming the storage bottles to boost vapor pressures or driving the fuels in liquid form using nitrogen until they could be vaporized by an immersion heater. Three different modes of fuel storage were used: (1) Propane was stored as a two-phase mixture in a large bottle outside the laboratory building. (2) Butane, butylene, cyclopropane, and propylene were stored in the fuel room as two-phase mixtures within small bottles. (3) Methane, ethane, and ethylene were stored as gases in standard cylinders.

Pressurization

All fuels except methane, ethane, and ethylene had to be pressurized to force them into the high-pressure combustor.

The volume above the liquid in the propane storage tank was pressurized with facility nitrogen. A bottom-fed line tapped the pressurized liquid propane for delivery to the lab. The propane bottle was fitted with a 1.72

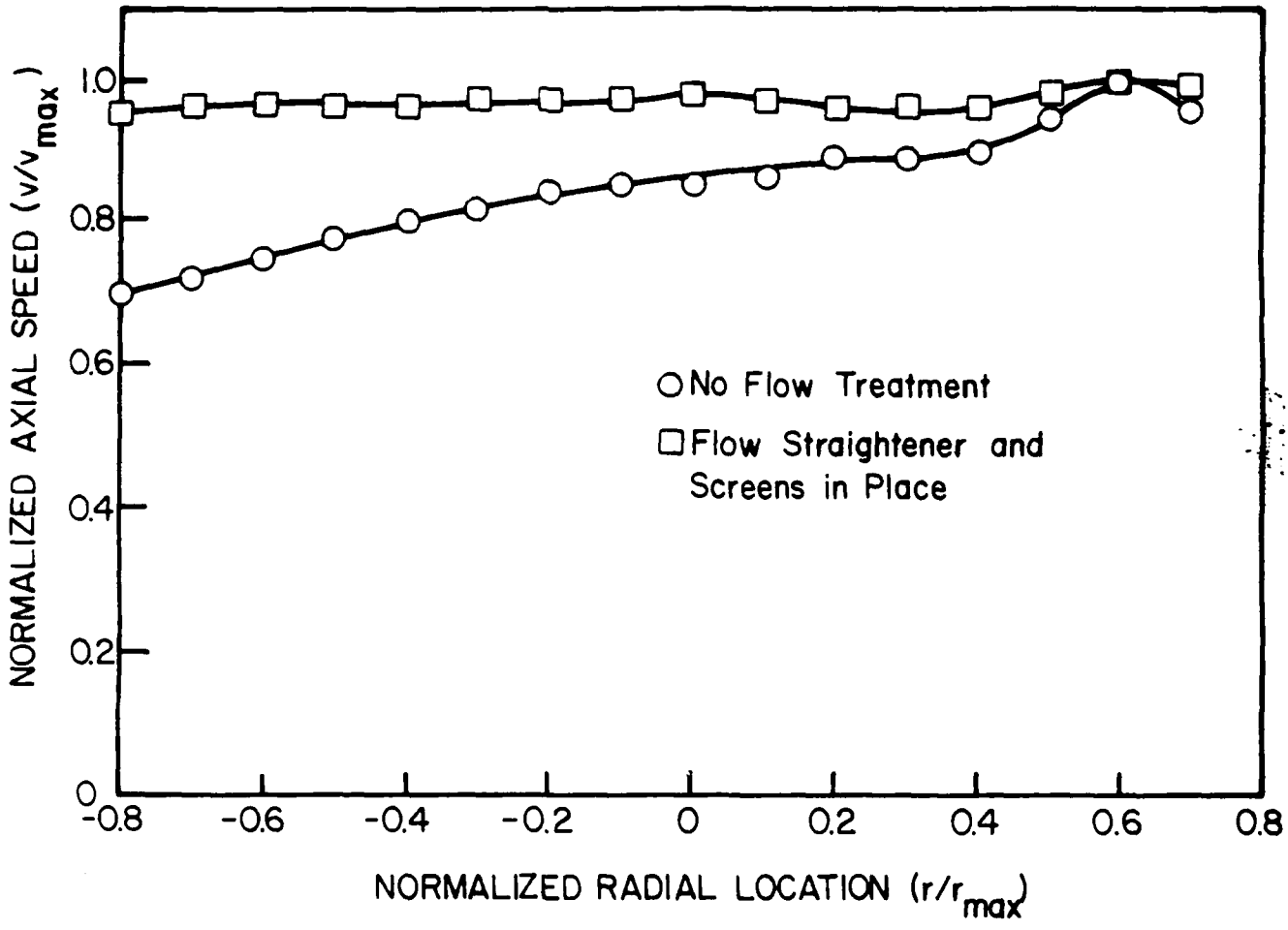

Figure 2. Air Velocity Profiles.

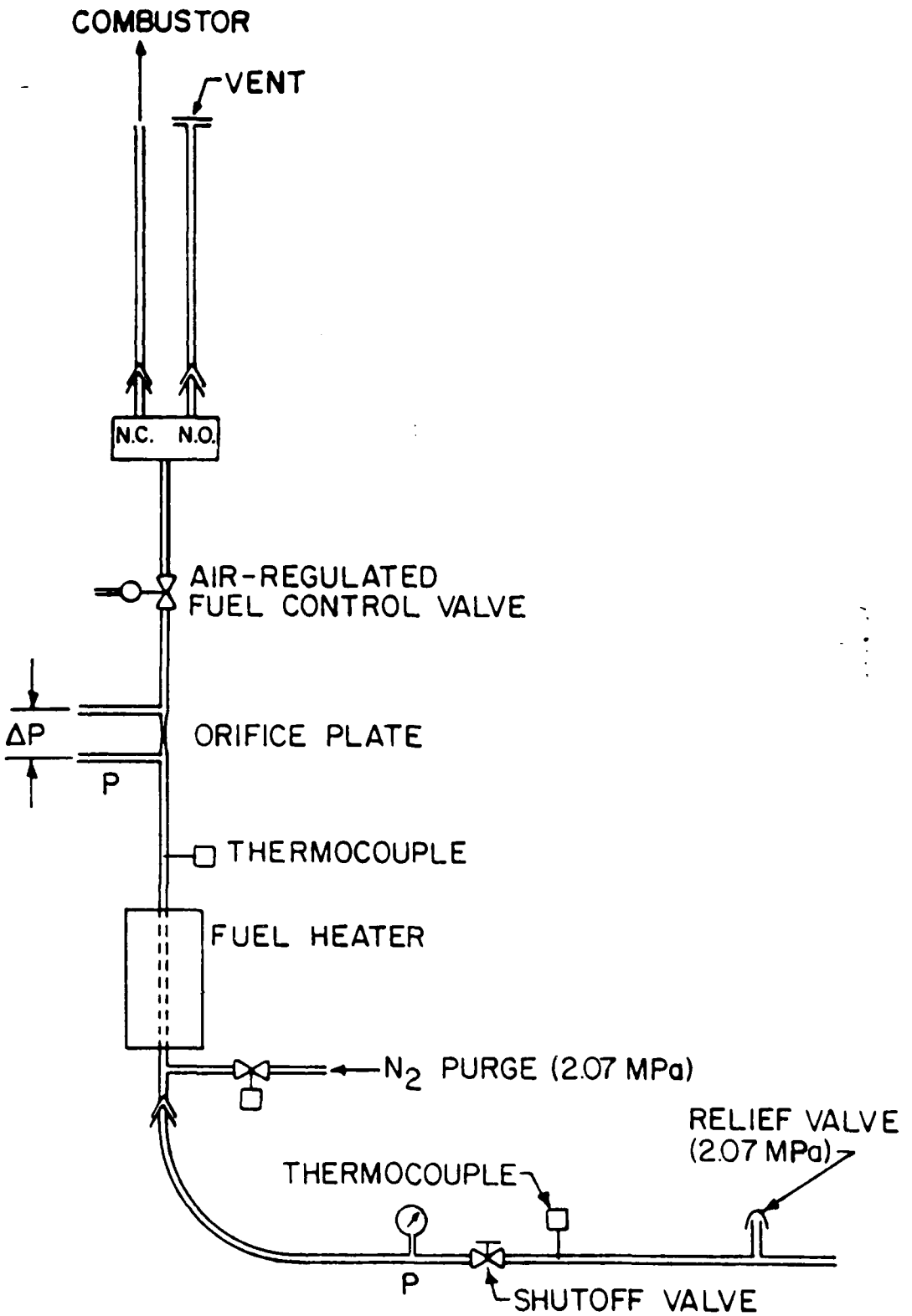

Figure 3. Fuel Delivery System.

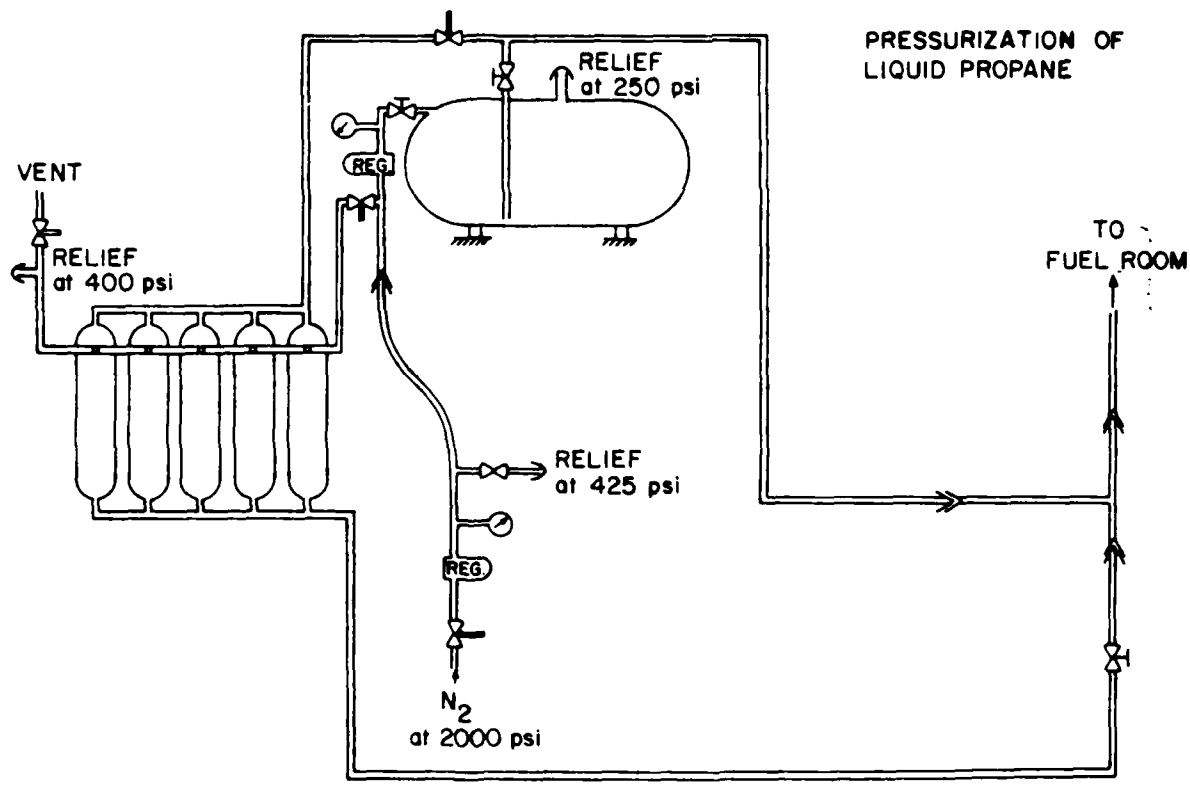

Figure 4. Pressurization of Liquid Propane.

MPa relief valve to prevent overpressurization. See Figure 4.

Bottles containing butane, butylene, cyclopropane and propylene were placed in a water bath (T = 70 C) to boost their vapor pressures. This technique allowed cyclopropane to be injected at pressures up to 0.4 MPa and propylene up to 0.6 MPa. Butane and butylene could be injected at pressures up to 0.3 MPa.

Fuel Pre-Heating

The fuel being tested was heated to the vapor state before being routed to the fuel injector. The fuel heater design was similar to that of the air heater, but was powered by a single-phase SCR controller and oriented vertically. Maximum heater power was 1.2 kW and, as with the air system, the heating rate was controlled using a 4-20 mA temperature monitor that received data from a thermocouple mounted in the fuel delivery tube. All fuels were heated to 375 K, a temperature sufficient to vaporize any of the fuels used here without pyrolysis occurring but safely below the melting temperature of the buna O-rings present in the fuel supply lines.

Since the fuel did not pass immediately from the immersion heater to the injector, care had to taken to keep it in the vapor state. This was accomplished by means of an electrical pipe heater (3 W/m) wrapped around the delivery line from the heater to the injector. Fiberglass insulation was then wrapped around the heating strip/fuel delivery line to optimize heat transfer.

Control

The fuel regulating valve was located less than two meters from the fuel injection tube to minimize the lag between valve actuation and a change in combustor performance. Precise control of fuel flow rates was facilitated by two component modifications. First, the regulating valve, originally oversized for the fuel flow rates intended for this work (1.0-20.0 g/s), was recut in the pintle/seat chamber to give it a very gentle taper. Second, remote control, made possible by using a Grove hand loader delivering 69 to 86 kPa pressure to the valve diaphragm, was made more precise by replacing the hand loader spring that came from the factory with another of lower spring constant. Finally, fuel was routed through flexible hose between the on/off valve and the injector tube, thus permitting motion of the injector tube (described in the section on Flame Positioning).

Fuel Purge

Nitrogen was forced through the fuel heater and into the combustor to purge those lines of any residual combustibles. Actuation came from a 28 V DC on/off valve placed just upstream of the fuel heater, protected from fuel back flow by a check valve.

Nitrogen was also used during the warm-up of the fuel heater. Because the controlling thermocouple for the heater lay just downstream of its outlet, gas had to be flowing through the line so that the temperature could be read properly. Using fuel would have been wasteful and dangerous, so a small flow of nitrogen was used instead.

Combustion Chamber

The combustor consisted of a 5 cm OD, 3.8 cm ID, XX-347 stainless steel pipe, cooled by two water systems: (1) a spiraling, low-pressure, high-flow-rate, external jacket where the water was confined to an annulus between the external wall of the combustor pipe and the inner wall of the jacket and (2) direct injection of water downstream of the windows to quench the flame, cool most of the length of the suction thermometer and keep the back-pressure valve cool (see Figure 5). The high pressure water for the direct injection cooling system was provided by a centrifugal pump driven by an electric motor. The pump was plumbed in parallel with the low-pressure water supply so that a hand loaded valve, when closed, forced water from the low-pressure branch to the pump.

Two diametrically opposed windows were installed in the combustor to permit measurement of radiative flux and observation of soot thresholds. Three items were considered when designing these windows. (1) The windows had to provide a clear view of the interior of the combustor over all wavelengths pertinent to thermal radiation measurements; (2) they had to withstand the thermomechanical stresses imposed upon them by the high-pressure, hot, reactive flame; (3) they had to be easily removable to allow for periodic cleaning.

Calcium fluoride was chosen as the window material, in part for its high, unvarying transmissivity between 0.4 and 8.0 μm. The transmissivity, for a 10mm thick window, is approximately 95% over the entire wavelength range [Lasers and App., 1985]. The actual windows, being 7.0 mm thick, have slightly higher transmissivities than the 10 mm value. However, the value of

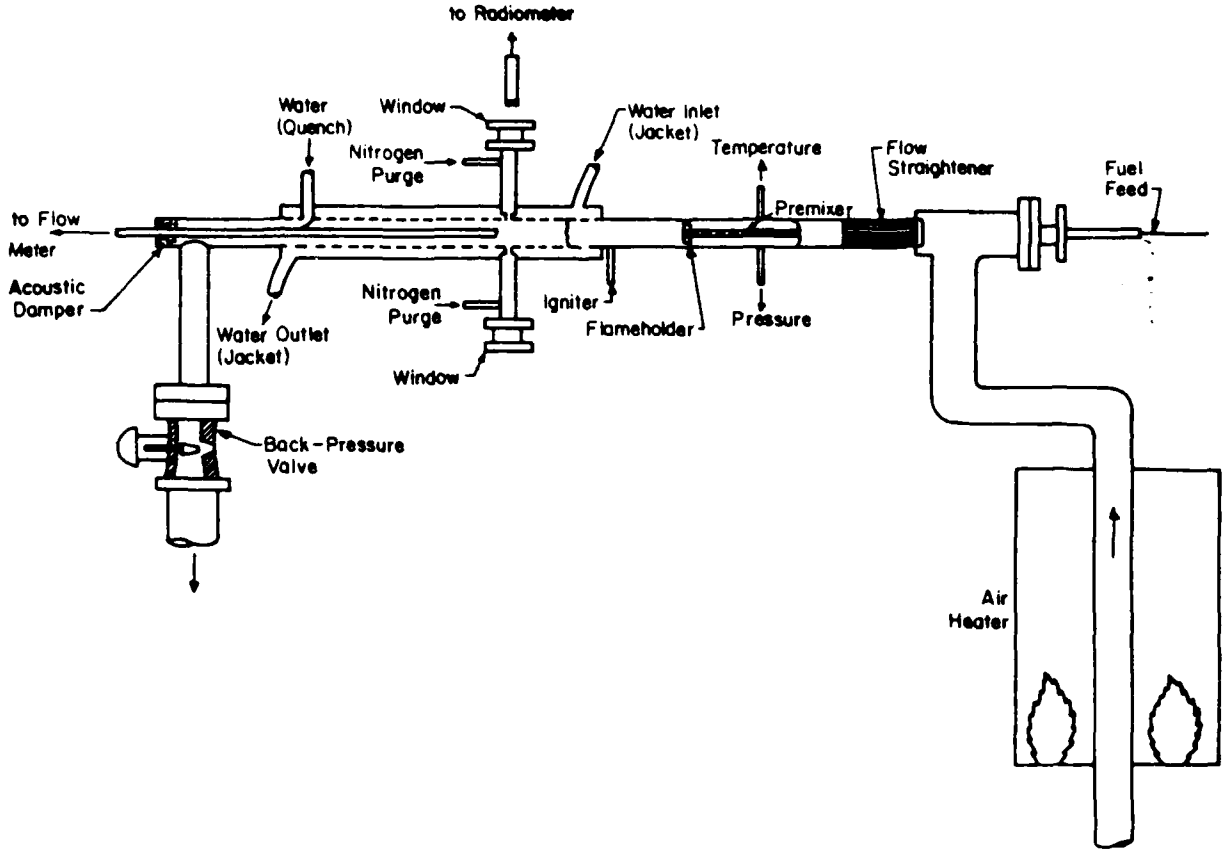

Figure 5. High-Pressure Gaseous Fuels Combustor.

transmissivity taken for corrections to radiative readings was that of the 10 mm windows.

The second optical design consideration was an appropriate window aperture--one that would provide observation of the flame through a known area while masking the hot combustor walls from the detector field of view. Obviously, since the combustor walls would be hot in a burning environment, they would emit radiation in the same spectral region as the flame itself, interfering with attempts to determine flame radiation. Figure 6 depicts the geometry discussed and gives appropriate dimensions.

Window overheating was avoided through the use of water cooling and a continuous nitrogen purge. The water cooling system was the same system used to cool the combustor. As Figure 6 shows, each window was mounted on a stainless steel supporting arm. Combustor cooling water flowed through the surrounding water jacket cooling the window support arms and hence the windows. A chromel/alumel thermocouple in each window arm provided a continuous readout of the temperature within each arm to ensure that it never rose above 35 C. A flow of dry nitrogen, injected into each window arm and exhausted to the combustor, kept soot, water vapor, carbon dioxide and other flame gases away from the window surfaces. The appropriate nitrogen flow rate (0.05-0.10 g/s) was determined by adjusting the flow control valve until the radiation reading was at its peak. Observation of the flame revealed that the nitrogen injection only slightly altered the flow field within the combustor.

The final combustor feature is the system controlling combustion pressure. It consisted of a back-pressure valve and an exhaust bleed. The extent to

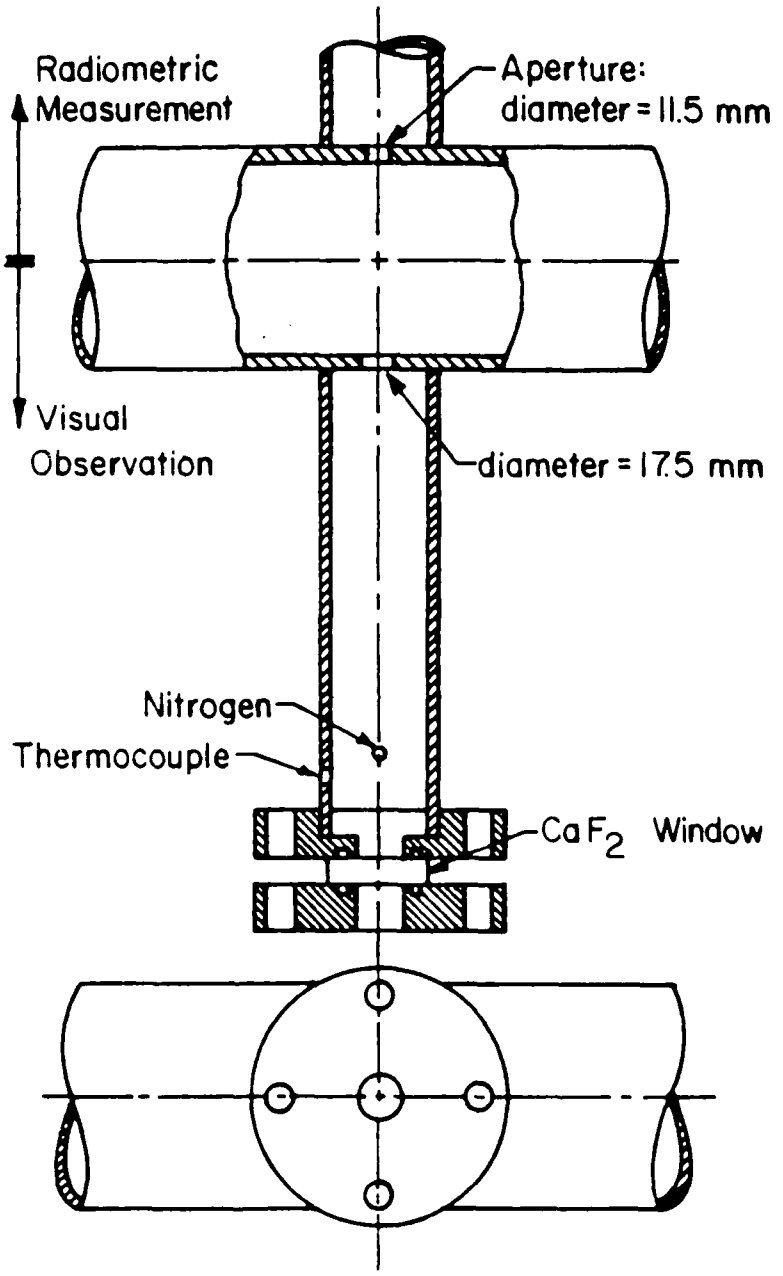

Figure 6. Combustor Window Detail.

which the valve was closed and the mass flow rate of air delivered determined the pressure within the combustor. Initial high pressure runs revealed difficulty in sustaining a flame when the back-pressure valve came close to shutting off the flow entirely. The solution was to include an exhaust bleed, vented directly to the atmosphere. Consequently, a 1.27 cm tube continuously exhausted a portion of the quenched combustion products thereby reducing the sensitivity of combustor performance to back-pressure valve actuation.

Igniter

Ignition was accomplished with an igniter spark arcing across a 3 mm gap at the wall of the combustor. The igniter itself consisted of a tungsten cathode centered in a stainless steel anode with the two electrodes being insulated from each other by ceramic and teflon spacers. A 110 V transformer provided a 5000 V spark, enough to jump the 3 mm gap at pressures as high as 0.5 MPa.

Flame ignition was assisted by heating the incoming air to a temperature of 500 K or higher. The ignition procedure consisted of warming the inlet air to at least 500 K, adding fuel at stoichiometric proportions, positioning the flameholder immediately upstream of the spark gap, and supplying a spark to the igniter. A stabilized flame was detected by observing a rapid increase in the output of a radiometer used to monitor flame zone emission.

Flameholder and Fuel Injector

If the flame speed is less than the flow speed of fuel and air in a subsonic flame zone, special attention must be given to keeping the flame burning

stably. In these experiments, the flow velocity was set at 6.0 m/s, far above the laminar flame speed of 0.4-0.5 m/s. This combustor, therefore, employed a flameholder of substantial blow-off speed--greater than 25 m/s at standard temperature and pressure.

The flameholder consisted of a Hastalloy disc with a diameter just smaller than the inside diameter of the combustor (3.8 cm). The disc had a hole of 1.1 cm diameter at its center through which the fuel/air mixture entered the combustion zone. See Figure 7. The flameholder could be translated relative to the fuel injector to provide varying degrees of premixing between the fuel and air.

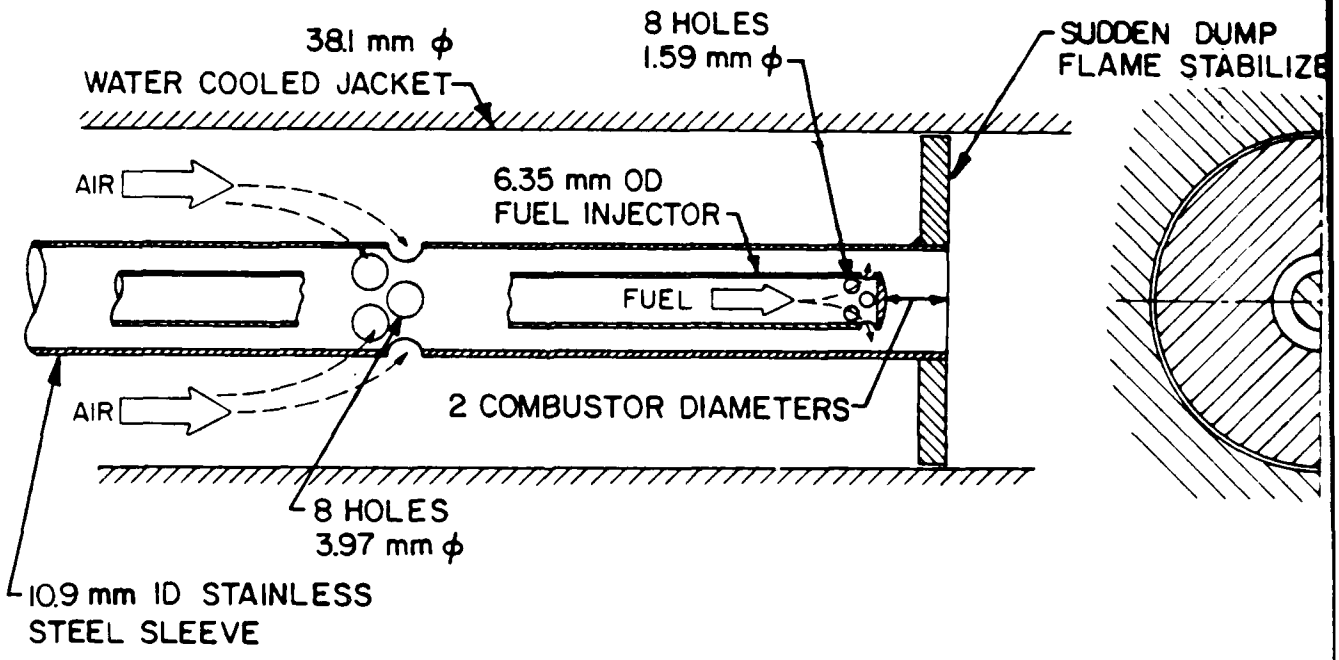

Figure 7. Fuel Injector/Flameholder.

The fuel injector forced the fuel and air to mix in a region of relatively high velocity immediately upstream of the flame zone. Since the speed in the mixing region was approximately fifteen times the nominal air speed in the combustor, the danger of flashback was minimal.

Because the flow within the combustor was turbulent, the length required for fuel-air mixing was expected to be negligible. Nevertheless, experiments were performed to verify that premixed fuel and air did enter the flame zone. To accomplish this, a stream of warm nitrogen was fed through the fuel injector to simulate fuel flow while ambient air flowed through the combustor. The difference in temperature between the two gases was 20 K, easily detectable by a chromel/alumel thermocouple. Such a thermocouple was translated across the injector outlet, reading temperatures at 15 different radial locations. For all equivalence ratios from 0.5 to 2.0 and for nominal air speeds of 5, 10, and 15 m/s the temperature profiles were uniform to within 1.5%, indicating that the two gases were fully premixed.

Originally, both diffusion and premixed flames were to be investigated with the fuel injector designed to make this possible. Early runs showed, however, that soot was present at nearly all conditions investigated in diffusion flames, so this portion of the program was not pursued.

Flame Positioning

One goal of this research was to study soot formation and flame radiation as a function of distance downstream of the flameholder. One way to provide radiometer access to several flame locations would be to build several pairs of observation ports. Many ports in the combustor wall would disturb the flow, however, and some arrangement for moving the radiometer's field of view (e.g. mirrors) would have to be developed. Moreover, the device used to monitor flame temperature would have to be relocated in order to measure the temperature at the axial location where radiometric data were being taken. The solution was to use a single pair of windows, a fixed

thermometric probe location and a sliding flameholder/fuel injector. In this way the flame could be scanned continuously for soot, radiation, and temperature, all from a single vantage point. Flow disturbances resulting from multiple windows were also minimized. A further advantage of the sliding flame was that the peak of radiation would never be lost due to its occurrence at a location between windows.

Flame positioning hardware consisted of a gas-over-hydraulic system, piping and solenoid values. Power for the slide arrangement was furnished by a hydraulic cylinder, with the hydraulic fluid pressurized by dry nitrogen. The liquid-gas interfaces lay inside two pipes, mounted vertically. Pressurization of one pipe forced hydraulic fluid into one end of the cylinder, driving the slide in one direction. Likewise, pressurization of the other pipe drove the slide in the opposite direction.

Flame position was monitored remotely on a 4-20 mA meter located in the control room. The meter was connected to a potentiometer, mounted next to the slide and attached to a pulley as shown in Figure 8.

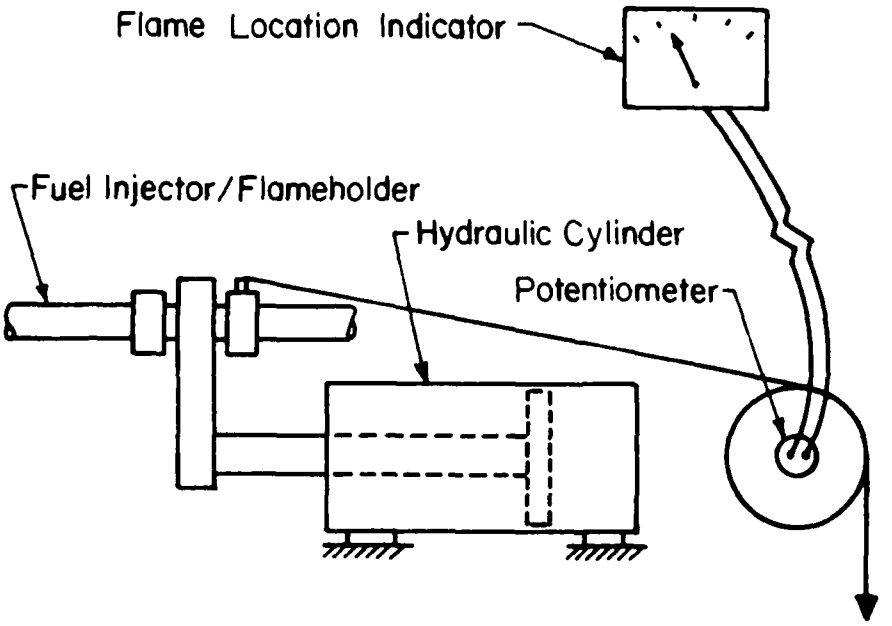

Figure 8. Hydraulic Slide Mechanism.

MEASUREMENTS AND DIAGNOSTICS

Descriptions of all devices used to take data during an experimental run are presented in this section. Calibration procedures are also described for each device.

Flame Temperature

Flame temperature is important when analyzing both soot thresholds and flame radiation. Soot thresholds depend exponentially on flame temperature through the rates of soot precursor formation and destruction. Flame radiation, in contrast, is proportional to T^4 for a gray medium and may also exhibit a weaker dependence since gas emissivities depend on temperature.

Two methods were originally considered for measuring flame temperatures. Both were line-of-sight optical techniques. One, the Schmidt technique, is useful for isothermal gray gases. The second, the monochromatic emissivity technique, is applicable to a sufficiently thick chamber of gases containing carbon dioxide. Brief explanations of each method and reasons for rejecting them are presented below.

If a gas/particle mixture is gray, i.e. has equal emissivities and absorptivities at all wavelengths, then the value of its overall emissivity can be determined by an absorption measurement. Three radiation readings are required:

(1) emission from the flame

(2) emission from a combination of the flame and a blackbody source placed behind the flame

(3) emission from the blackbody source

A simple calculation then yields flame emissivity. Once the emissivity is known, it can be used to calculate the flame temperature [Daws and Thring, 1955]. This procedure, known as the Schmidt technique, was rejected because it requires a gray medium. This may be an acceptable approximation for very sooty flames, but in this work most of the flames were either completely soot-free or at the verge of soot formation; therefore, the gray assumption does not apply for most flames and the resulting temperature calculations would have been erroneous.

The monochromatic emissivity technique uses an optical filter or monochromator to isolate radiant energy at a discrete wavelength. If the flame gas is known to have an emissivity of unity at that wavelength measurement of the monochromatic emissive power allows calculation of the flame temperature [Claus, 1981]. Carbon dioxide is known to have a very strong absorption band at 4.3 μm, so only a short path length is required to ensure an emissivity of unity. Such conditions occur for heavy hydrocarbon fuels, but are not always observed when burning lighter, gaseous fuels. The monochromatic emissivity technique was rejected for that reason.

Obviously, neither of the techniques originally proposed was applicable to this study. This was due, in part, to a shift in program goals from use of liquid fuels to use of gaseous fuels. Consequently, an alternative temperature measurement technique was employed: a pyrometric probe. The probe,

termed a suction thermometer, samples flame gases through a choked-flow orifice at the centerline of the combustor and passes them through a rotameter, yielding a temperature measurement via a mass-flow measurement. The orifice is located in the tip of a water-cooled, stainless steel probe, which is inserted through the back of the combustor with its inlet immediately downstream of the observation ports. Temperature is determined from a mass flow measurement by using the relationship between upstream stagnation pressure (combustor pressure in this case) and mass flow through the choked orifice. See Figure 9.

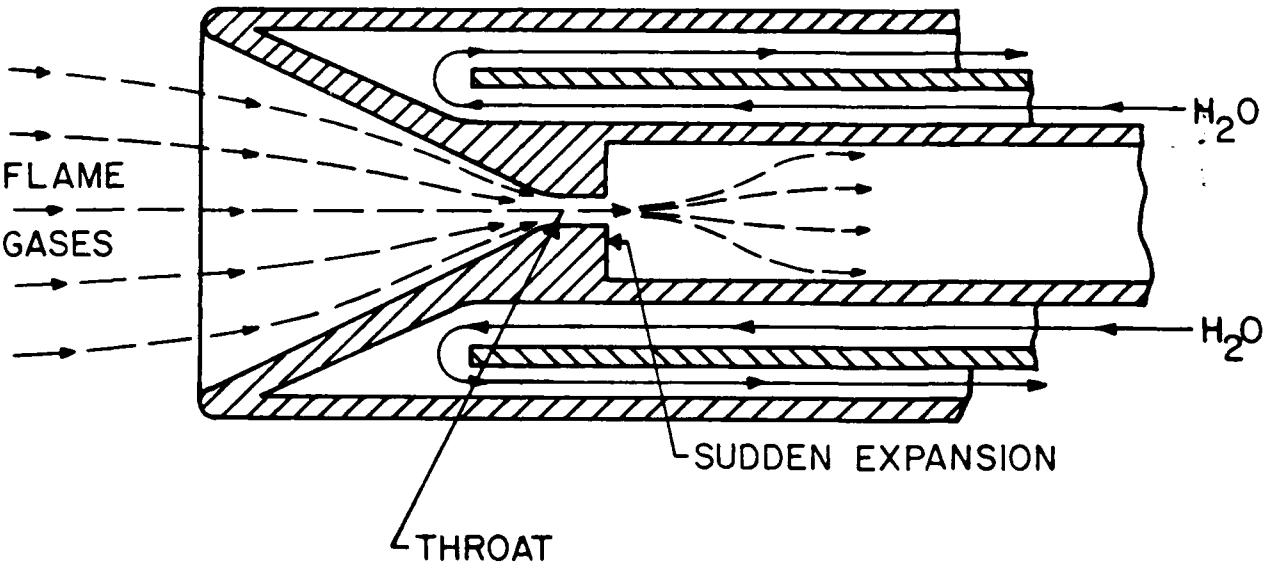

Figure 9. Suction Thermometer Inlet.

The probe's nozzle was carefully shaped in an effort to achieve frictionless flow in the converging section and sonic flow within the throat (diameter = 0.0838 cm). Standard construction codes [ASME, 1971] call for a circular profile for the nozzle inlet when sectioned along the flow axis and viewed from the side. This contour was approximated by a rounded inlet, a straight converging taper, and a rounded transition from taper to constant-area

throat. The probe also incorporated a sudden expansion downstream of the throat in order to maintain sonic flow in the constant-area throat.

Temperatures could be measured at any flame location visible through the window because the probe inlet was positioned immediately downstream of the observation plane. Axial flame-temperature profiles were collected by traversing the flame back and forth relative to the (fixed) probe. This accomplished two objectives. First, the temperature of the sooting region could be examined for its effects on soot thresholds. Second, overall emissivities could be mapped out from a knowledge of flame temperature and flame radiation.

A test was performed to determine how probe temperature measurements compared with theory. Air of known temperature and pressure was sampled by the probe with the volume flow rate measured using the rotameter. The mass flow rate was compared to $P_o \cdot T_o^{-1/2}$, as suggested by a one-dimensional gas dynamic analysis. Although the flow rate was lower than predicted, it was proportional to $P_o \cdot T_o^{-1/2}$ for pressures between 0.10 and 0.81 MPa and temperatures between 300 and 600 K.

A second test was performed to avoid extrapolating low temperature calibration results to high temperatures. This was accomplished by reconfiguring the rig in such a way that flame temperatures could also be monitored by a Pt/Pt-10%Rh thermocouple inserted into the combustion zone through an observation port. A lean flame was established, and the thermocouple reading was compared to simultaneous suction thermometer results. Thermocouple data were converted to temperatures and corrected for radiative losses. Because the calibration flames were lean, and therefore

non-sooting, the emissivities of the thermocouple junctions were not altered by soot deposition. As a further precaution, the thermocouple was coated with a thin layer of SiO_2 to prevent catalytic reactions. A calibration curve resulted from these tests, allowing determination of temperatures under sooting conditions from a knowledge of the probe mass flow rate.

Calculated Flame Properties

Some properties used in the analysis of the flame data were calculated rather than measured. For instance, the estimation of flame emissivity by Hottel's method required a knowledge of partial pressures of carbon dioxide and water vapor, while analysis of the critical equivalence ratio data required values for the hydroxyl radical mole fraction. These values were calculated for equilibrium conditions at the measured flame temperature and combustor pressure. In addition, the adiabatic flame temperature and equilibrium species mole fractions at that temperature were calculated for use in comparisons with the values at measured flame temperatures. All quantities were determined using a thermodynamic equilibrium computer code [Gordon and McBride, 1973].

Air Mass Flow

Combustion air flow was measured using an 8.86 mm, $\beta = 0.2$ orifice plate in conjunction with a Validyne model DP15-50 variable inductance pressure transducer. See Figure 10. The flow through the orifice plate was assumed to be incompressible and single-phase. The temperature at the orifice location was experimentally verified to be the same from day to day.

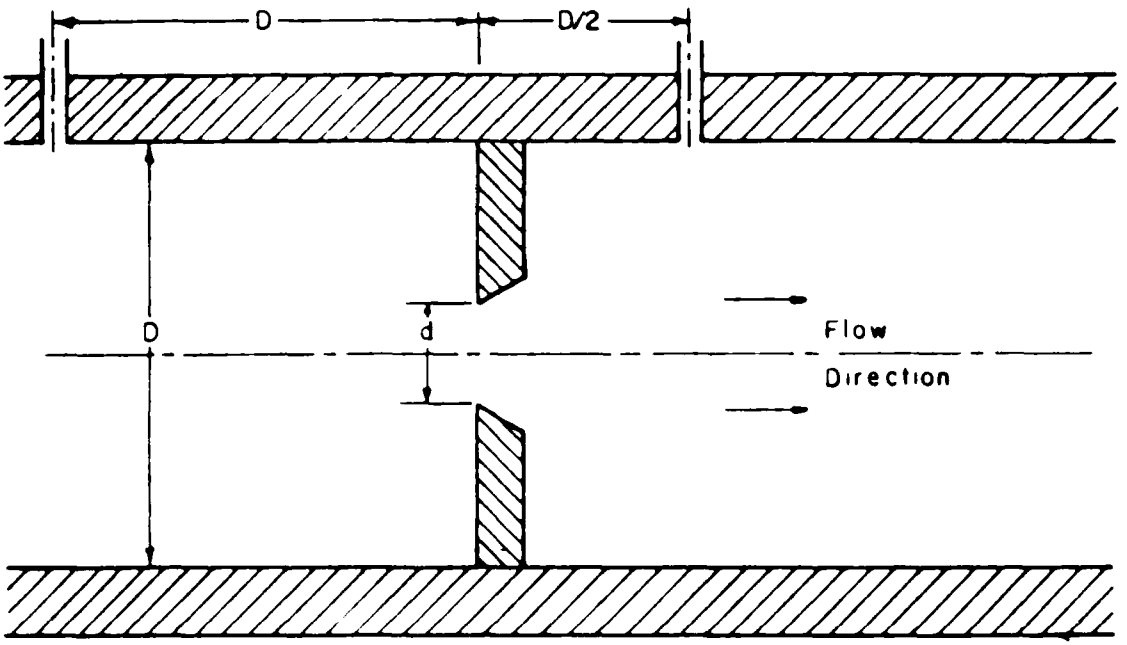

Figure 10. Fluid Measurement Orifice.

The associated signal analyzer, a Validyne model CD280, delivered a DC voltage in response to a given pressure drop across the orifice plate. The following equations, taken from Goldstein [1983], give the flow in g/s when p is in psi and Δp is in inches of water/15:

$$\dot{m} = \rho \dot{V} \tag{4}$$

$$\dot{V} = A \cdot C_D \left(\frac{2\,\Delta p}{\rho(1-\beta^4)} \right)^{1/2} \tag{5}$$

where

$\dot{m}$ = mass flow rate

$\dot{v}$ = volumetric flow rate

A = area at orifice ($= \frac{\pi}{4} d^2$)

C_D = discharge coefficient of the orifice

Δp = pressure drop across orifice

ρ = gas density

β = ratio of orifice diameter to internal pipe diameter

$$= \frac{d}{D}$$

Equations (4) and (5) give

$$\dot{m} = \hat{c}(p \cdot \Delta p)^{1/2} \tag{6}$$

where

$\hat{c}$ = encompasses all constants in (5)

p = pressure upstream of orifice

The peculiar units for Δp are a matter of experimental convenience. Calibration with a mass flow sensor (Micro Motion model D, accurate to 0.4% of reading) showed that Eqn (6) gave accurate values for the air flow rate.

Combustor Pressure

Provision was made to remotely monitor the combustor pressure by using an electromechanical transducer. A pressure tap was drilled normal to the combustor wall with the pressure sampled through a 6-mm stainless steel tube capped by a 0-172 MPa pressure transducer (Sensotec model A-10). An electrical signal ran from the transducer to a digital voltmeter in the control room. Calibration was accomplished by comparing readings of combustor pressure from a previously calibrated dial gauge with the voltage output of the transducer.

Combustor Temperature

Chromel/alumel thermocouples (Omega Type K) were used for all temperature measurements, except flame temperatures. The temperature was monitored at two locations within the combustor: in an insulated section of pipe ten diameters upstream of the water jacket and in an uninsulated section about one diameter upstream of the water jacket. The former recorded combustor inlet temperature. The latter was used during light-up to indicate when a flame stabilized on the flameholder and, because of its proximity to the burning zone, could also reveal flashback.

Fuel Mass Flow

Fuel flow rate measurements were also made using an orifice plate. The orifice, with a pressure tap one pipe diameter upstream and another tap one-half diameter downstream, was installed between the fuel heater and the fuel on/off valve (see Figure 3). The fuel orifice dimensions were smaller than those of the air orifice to allow for precise measurement of the small flow rates involved. (The inner diameter of the tube was 1.09 cm and the orifice diameter was 0.45 cm.) The pressure upstream of the orifice and the pressure drop across it were monitored by Validyne pressure transducers with the resulting signals read from voltmeters.

The fuel flow rate was calibrated as a function of upstream pressure and pressure drop across the orifice. To calibrate the pressure upstream of the orifice a known pressure of nitrogen was admitted to the fuel line and the flow control valve was shut so that a steady stagnation pressure could be read by the upstream transducer. Its output voltage was then read from a voltmeter.

The flow rate calibration employed both the upstream pressure and pressure drop transducers. A tank of known volume was filled with nitrogen from the fuel delivery system purge line. As the nitrogen flowed into the tank, the pressure and pressure drop across the orifice were noted. The gauge pressure after filling the tank and the time to fill were also noted. The mass of nitrogen in the tank was then calculated as follows:

$$m = \frac{p_g \cdot V}{R \cdot T} \tag{7}$$

where m = mass of nitrogen in the tank

p_g = gauge pressure after a trial

V = tank volume

R = gas constant for nitrogen

T = absolute temperature of the nitrogen

The resulting mass was divided by the tank fill time, yielding the mass flow rate. The mass flow rates of all trials were plotted against the square root of the product of upstream pressure and orifice pressure drop:

$$\dot{m}_{nitrogen} = 0.19\ (p \cdot \Delta p)^{1/2} \tag{8}$$

where

$\dot{m}_{nitrogen}$ = mass flow rate of nitrogen (g/s)

p = upstream pressure readout (V)

Δp = pressure drop readout (mV)

Solving for Δp gave

$$\Delta p = \frac{27.7\ \dot{m}^2_{nitrogen}}{p} \tag{9}$$

The desired value of $\dot{m}$ was determined from the nominal combustor air flow rate and desired equivalence ratio. The readout of upstream pressure was then used to give the necessary pressure drop, which was scaled to account for differences between the molecular weight of nitrogen and that of the fuel to be supplied. The procedure is illustrated by the following expressions.

$$\dot{m}_{fuel} = \dot{m}_{nitrogen} \cdot \left(\frac{\rho_{fuel}}{\rho_{nitrogen}} \right)^{1/2} \tag{10}$$

$$= \dot{m}_{nitrogen} \cdot \left(\frac{M_{fuel}}{M_{nitrogen}} \cdot \frac{T_{nitrogen}}{T_{fuel}} \right)^{1/2} \tag{11}$$

for the same upstream pressure where

$\dot{m}$ = mass flow rate

ρ = gas density

M = *molecular weight of the gas*

T = gas temperature

The nitrogen was at a temperature of 300 K while the fuel was held at 375 K by means of the fuel heater. Scaling of the temperatures then yielded:

$$\dot{m}_{fuel} = 0.17 \, (p \cdot \Delta p)^{1/2} \, M_{fuel}{}^{1/2}. \tag{12}$$

Radiometer

Proper measurement of flame radiation called for careful selection of radiometric components. The four principal components were the power meter, the rotating wheel chopper, the combustor window assemblies, and the calibration furnace. The power meter was a Laser Precision model RL-3610 of 1.0 cm^2 collection area used in conjunction with a Laser Precision model CTX-530 chopper operating at 30 Hz. It was able to detect radiant energy

from 0.4 μm to 12.0 μm. This wide response range is useful only if the window separating the power meter and the interior of the combustor is transparent to radiation throughout the same wavelength band. Consequently, calcium fluoride was chosen for the window material since it transmits approximately 95% of the incident energy from 0.7 μm to 8.0 μm. One important consideration concerns the space between the window surface and the flame itself (Figure 6). Had this space been allowed to fill with carbon dioxide or water vapor from either the atmosphere or the flame, radiative emission from the flame would have been attenuated. Because this path was continuously purged with nitrogen, however, no such attenuation occurred (nitrogen being transparent to infrared radiation). The final component of the radiometric system was an Infrared Industries model IR-464 blackbody furnace with a model IR-101C controller. With a maximum cavity temperature of 1473 K this blackbody provided a standard for calibration of the radiation power meter.

Calibration was accomplished by placing the radiometer and chopper directly in front of the blackbody furnace at a known distance of separation and measuring the output voltage of the radiometer at various blackbody temperatures. The following analysis describes the process in detail.

$$q_{e-r} = J_e \cdot A_e \cdot \omega_{e-r} \tag{13}$$

$$= I_e \cdot A_e \cdot A_r \,/\, d_{e-r}^2 \tag{14}$$

$$= S_e \tag{15}$$

where

A = area of emitting or receiving surface

d = distance from emitter to receiver

I = normal radiative intensity from the emitting surface

ω_{e-r} = solid angle between emitter and receiver

$\sigma = 5.67 \cdot 10^{-8}$ W/ $m^2 \cdot K^4$

q = radiant energy emission rate

S = signal from the radiometer

and the subscripts are

e = emitter

r = receiver

For a blackbody

$$I_e = \frac{E_b}{\pi} = \sigma \frac{T_b^4}{\pi} \tag{16}$$

where

E = emitted flux

with subscript

b = blackbody

Using Eqns (15) and (16)

$$S_b = \frac{\sigma T_b^4}{\pi} \cdot \frac{A_b \cdot A_r}{d_{b-r}^2} \tag{17}$$

For the flame as the emitter we can rearrange Eqn (14) to yield

$$I_f = \frac{q_{f-r} \cdot d_{f-r}^2}{A_f \cdot A_r} \tag{18}$$

and use Eqns (13) and (15) to give

$$q_{f-r} = \frac{S_f}{S_b} \cdot q_{b-r} \tag{19}$$

where the subscript f refers to the flame.

Finally, Eqns (18), (19), (14), and (16) give

$$I_f = \frac{S_f}{S_b} \cdot \frac{\sigma T_b^4}{\pi} \cdot \frac{A_b}{A_f} \left(\frac{d_{f-r}}{d_{b-r}} \right)^2 \qquad (20)$$

RESULTS AND ANALYSIS

This portion of the report consists of two sections. The first is devoted to soot threshold equivalence ratio data and analysis. The second discusses flame radiation results and analysis.

Soot Thresholds

Figures 11 through 17 show the results of variations in pressure on the critical equivalence ratio, ϕ_c, for all fuels studied. Critical equivalence ratio data are presented at multiple temperatures for three of the fuels, ethane, propane, and ethylene. Clearly, both combustor pressure and inlet temperature strongly affect ϕ_c.

Effect of Pressure

Examination of the data for any fuel shows that the critical equivalence ratio falls as combustor pressure rises. This agrees with the work of Fenimore et al. [1957], who studied the subatmospheric pressure dependence of ϕ_c. Further examination of the figures reveals that at higher pressures, 0.4 MPa and above for most fuels, the critical equivalence ratio becomes less sensitive to pressure, approaching a horizontal asymptote. For methane, ethane, ethylene, and propylene the high-pressure limiting value of ϕ_c is approximately 1.20, when the inlet air temperature is 700 K.

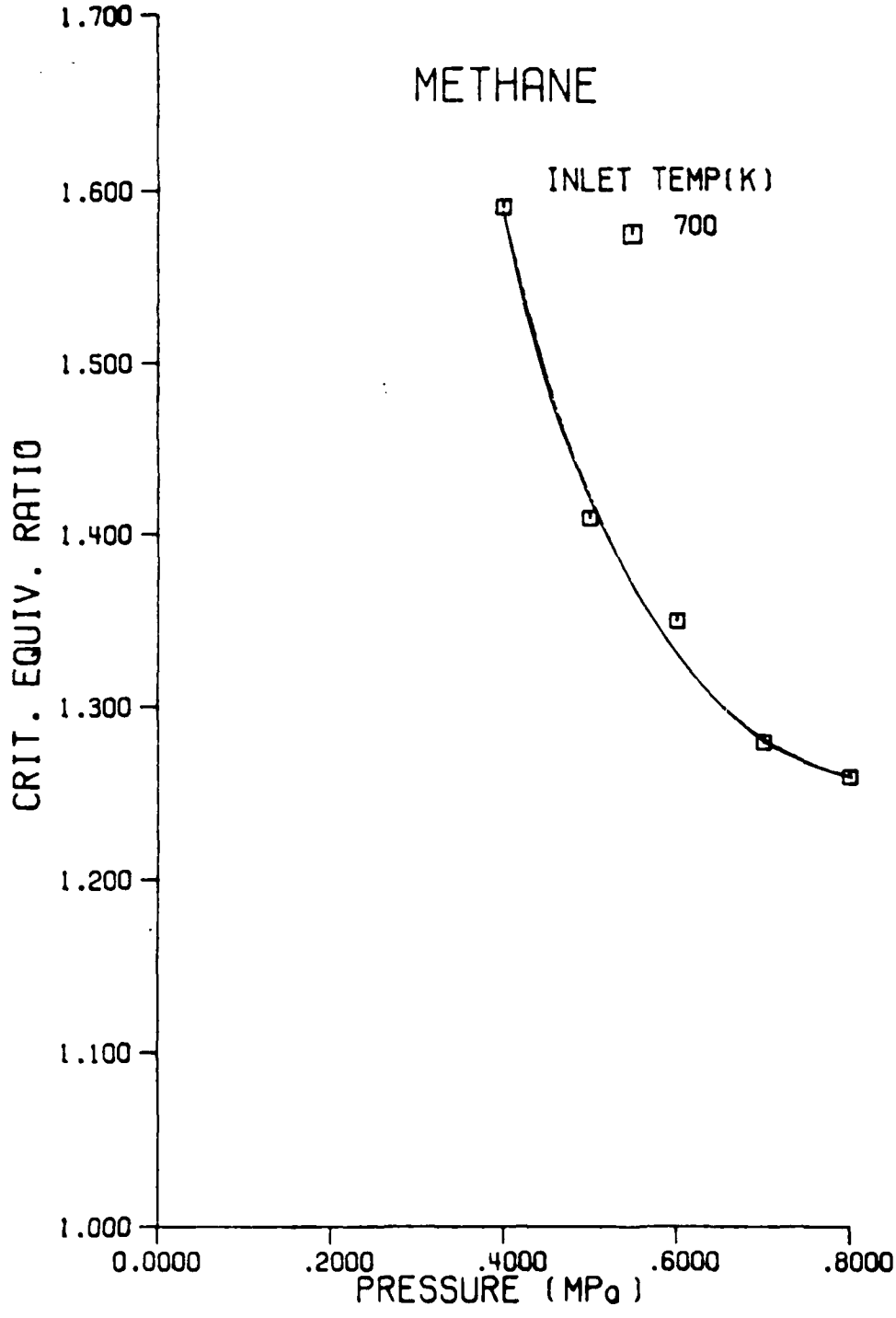

Figure 11. Methane: Critical Equivalence Ratio vs. Pressure.

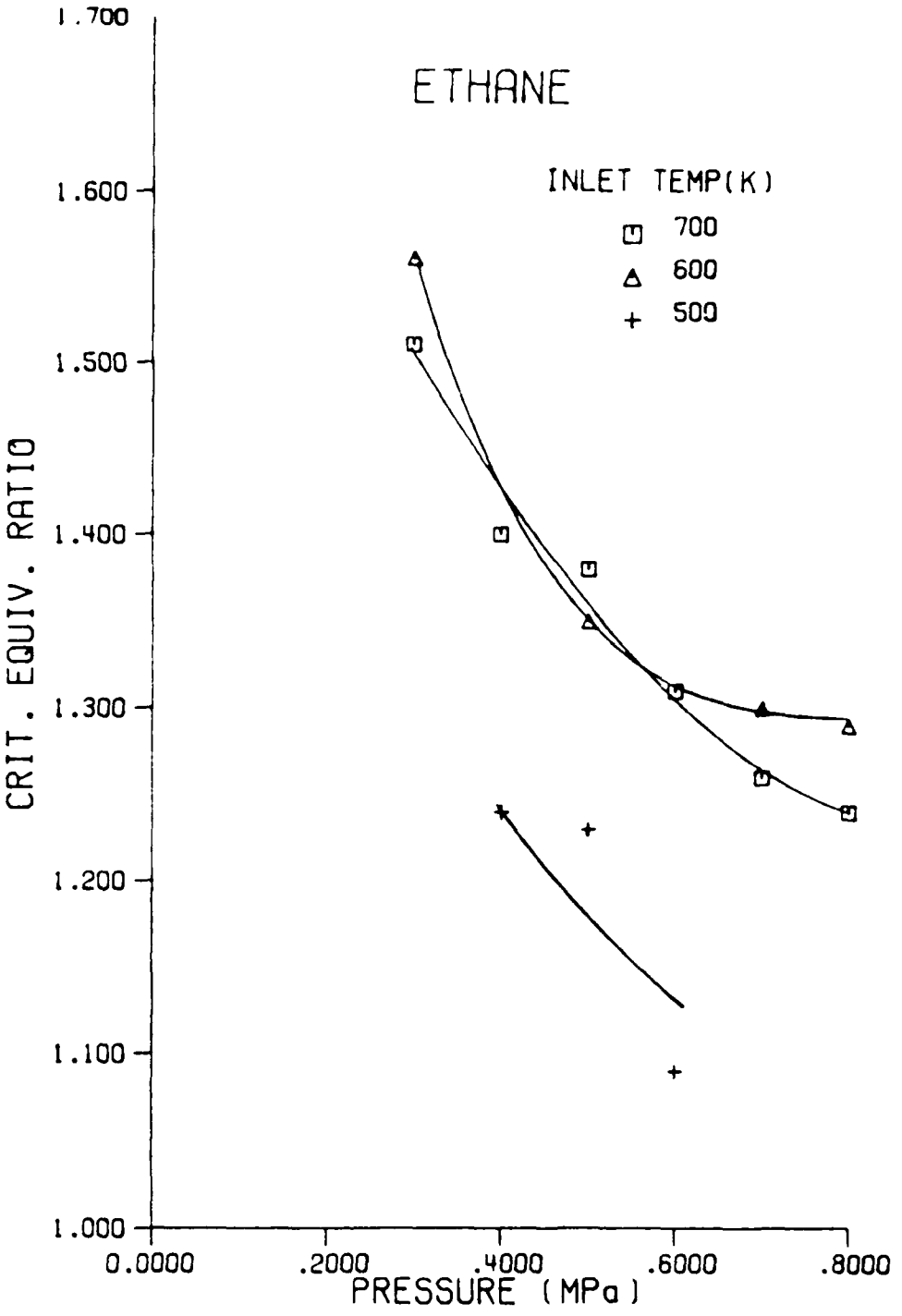

Figure 12. Ethane: Critical Equivalence Ratio vs. Pressure.

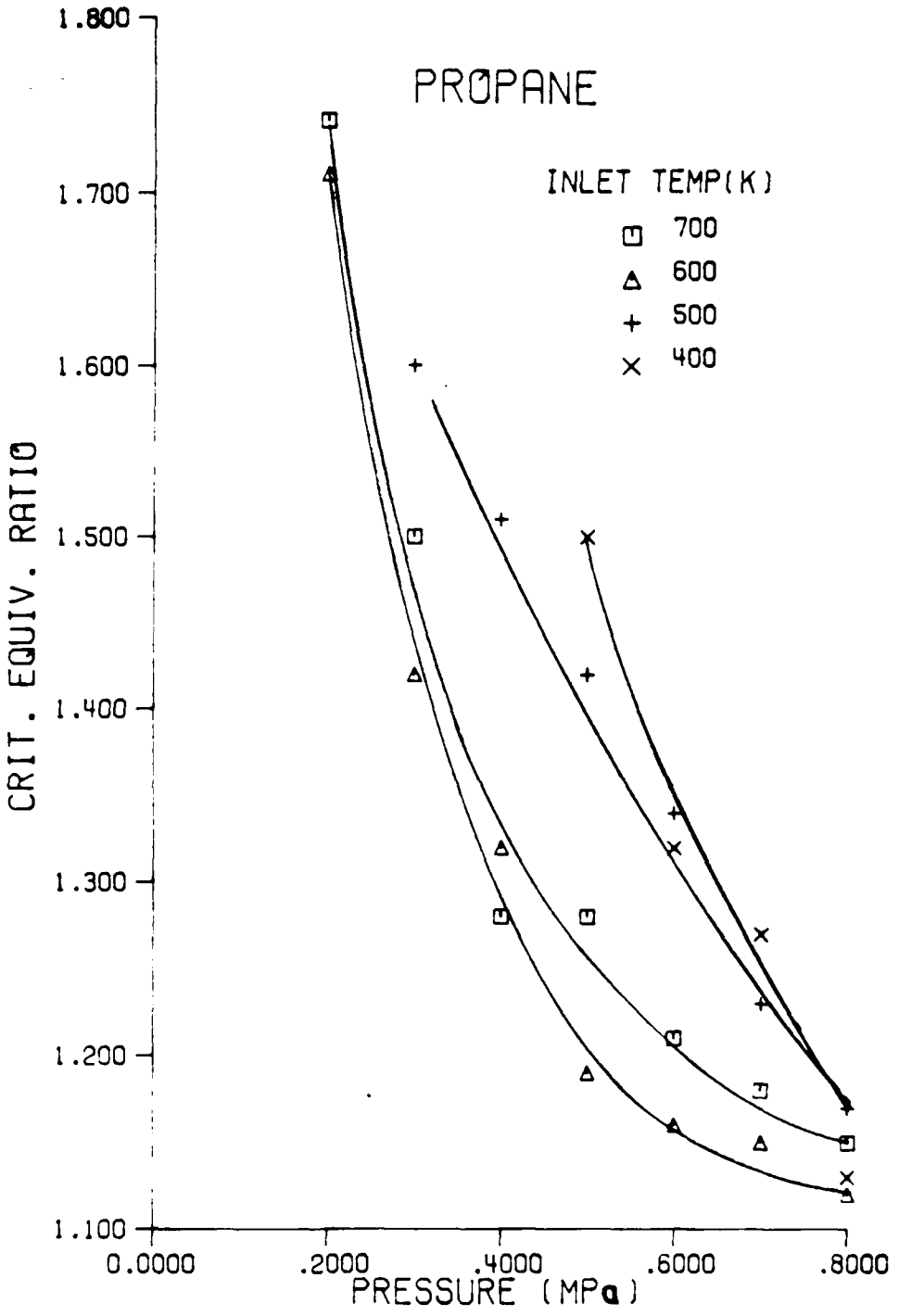

Figure 13. Propane: Critical Equivalence Ratio vs. Pressure.

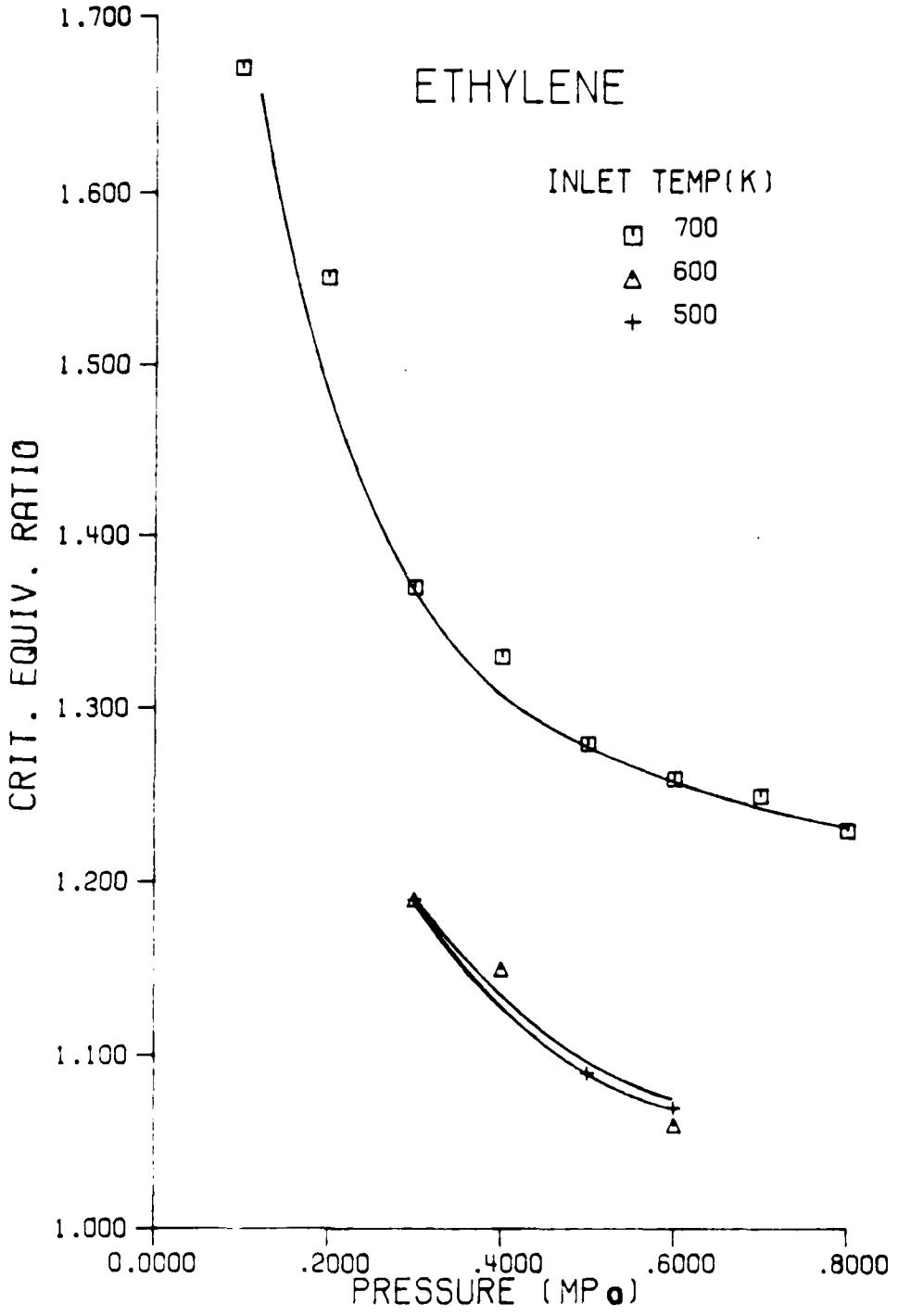

Figure 14. Ethylene: Critical Equivalence Ratio vs. Pressure.

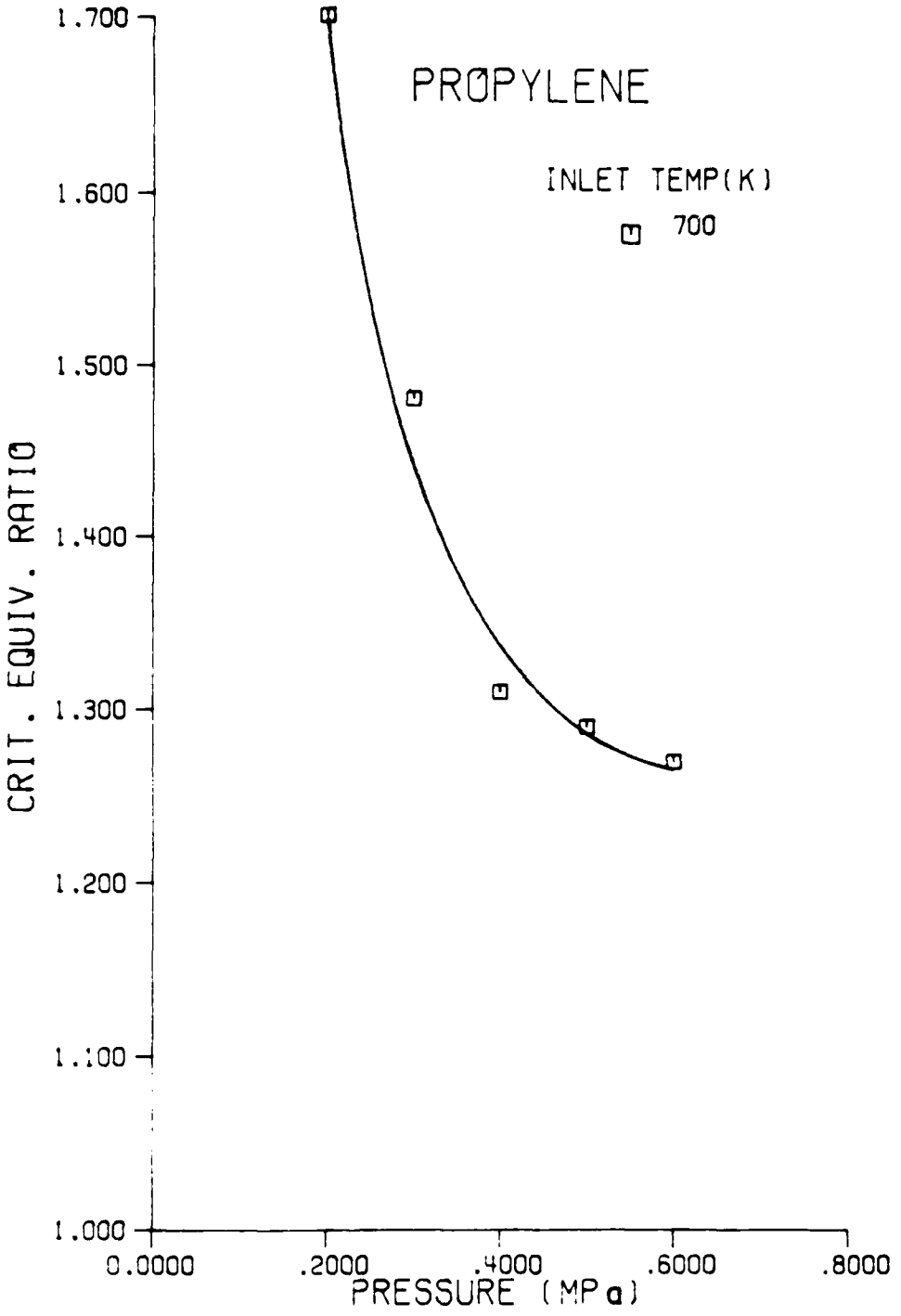

Figure 15. Propylene: Critical Equivalence Ratio vs. Pressure.

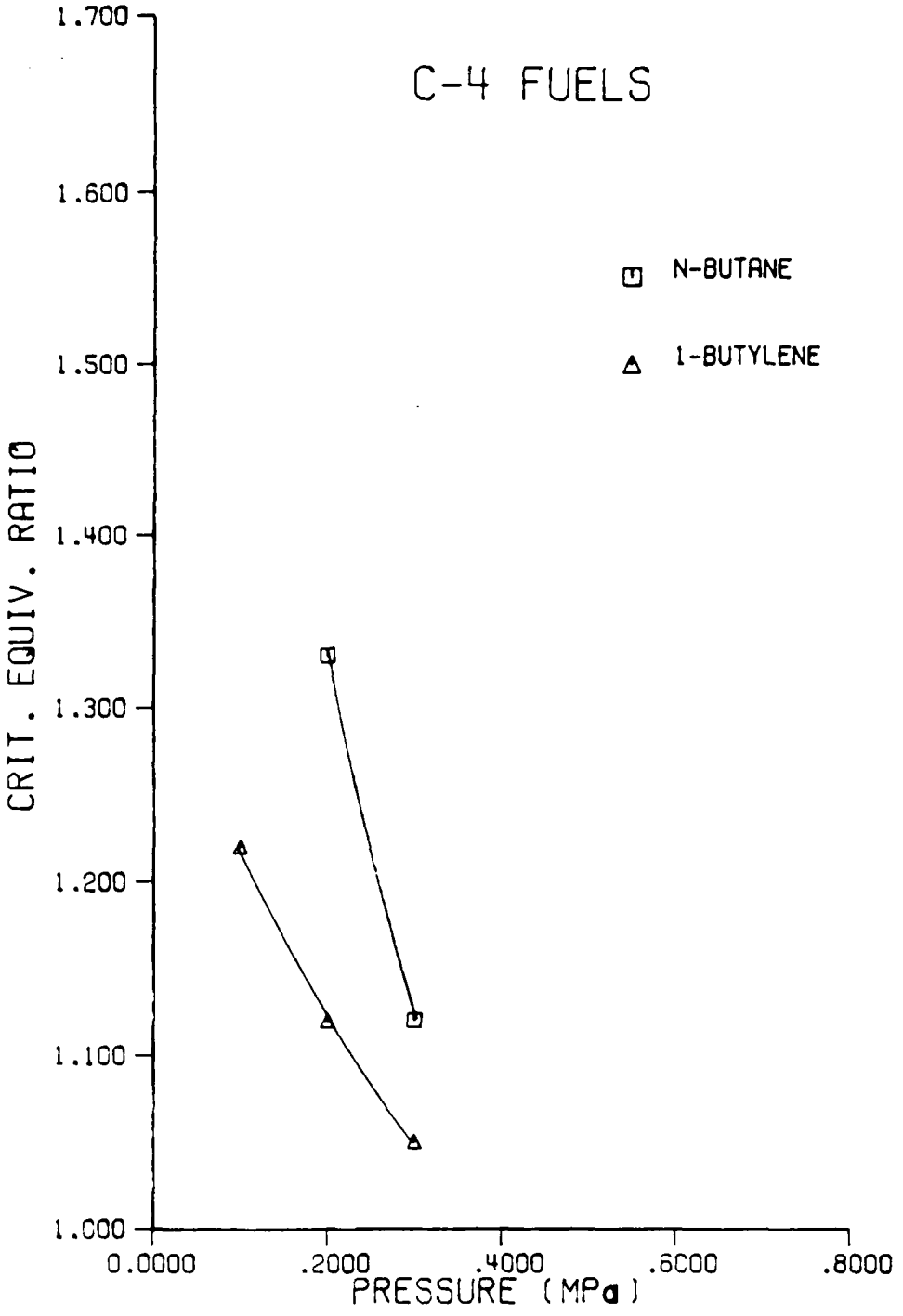

Figure 16. C-4 Fuels: Critical Equivalence Ratio vs. Pressure.

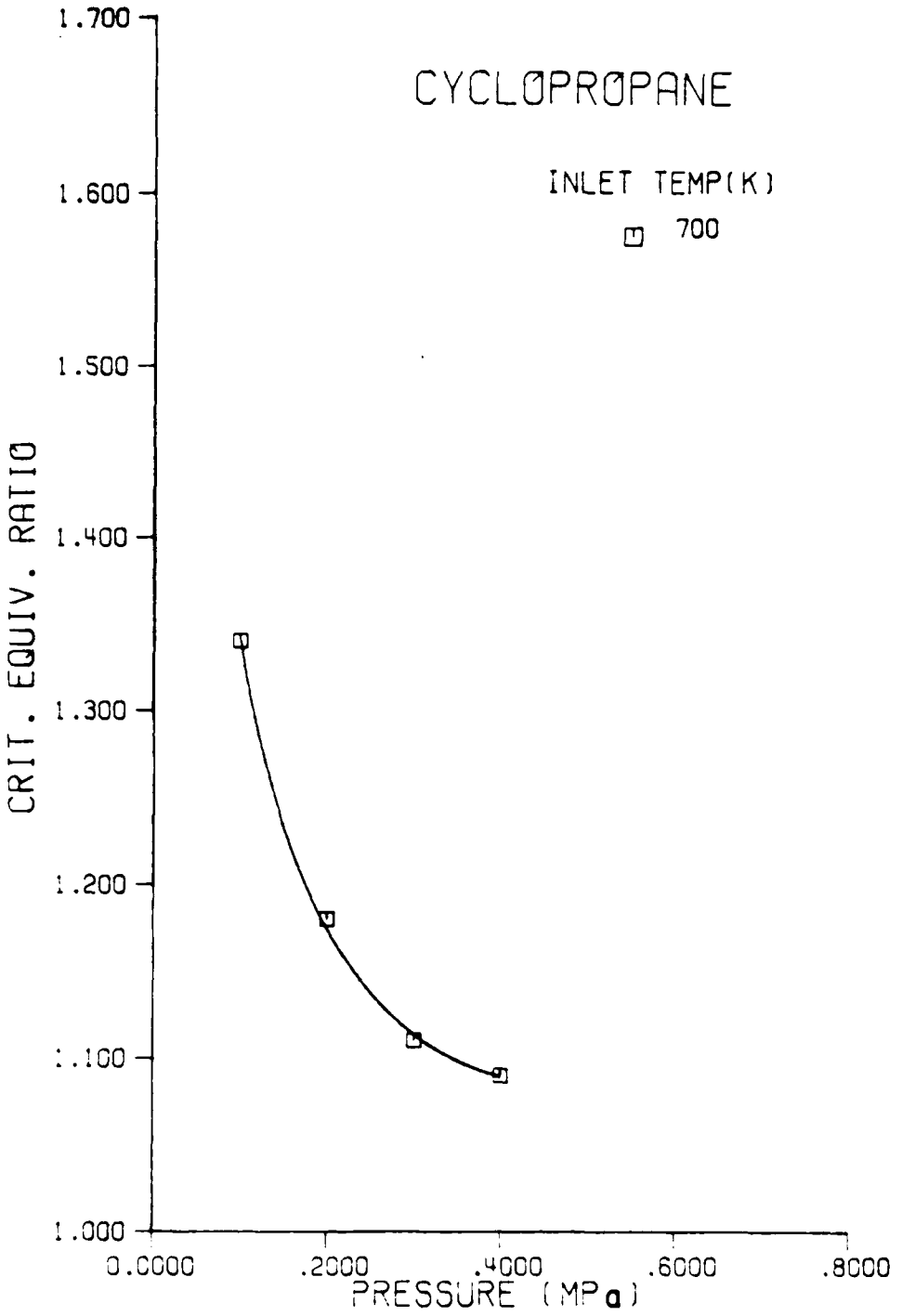

Figure 17. Cyclopropane: Critical Equivalence Ratio vs. Pressure.

For propane the value is about 1.15, for cyclopropane 1.05, and for the four-carbon fuels it appears to be lower, but no high-pressure data were taken to confirm this. The fact that methane, ethane, and propylene all approach the same value of ϕ_c at high pressures is interesting because these fuels differ markedly in their sooting tendencies at low pressures. Notice that methane did not produce soot at any equivalence ratio below a pressure of 0.4 MPa. Similarly ethane produced no soot below a pressure of 0.3 MPa. The two olefins, ethylene and propylene, both formed soot over the entire pressure range (0.1 to 0.8 MPa).

Effect of Temperature

Three fuels, ethane, propane, and ethylene, were burned at different inlet air temperatures, with all other fuels run at an inlet temperature of 700 K only. As Figures 12, 13, and 14 show, a change in inlet air temperature can change the value of ϕ_c at a given pressure. The ϕ_c versus pressure behavior is, however, qualitatively the same for all inlet temperatures. An interesting feature of the temperature curves is that for different fuels the inlet temperature at which ϕ_c is a minimum varies. Also, no simple relationship exists relating ϕ_c to inlet air temperature alone. Propane, for example, shows a decrease in soot threshold as the inlet air temperature rises to 600 K. The curve at 700 K, however, lies above the lower temperature curves. Ethane, on the other hand, has its lowest ϕ_c values at an inlet temperature of 500 K, while ethylene's lowest ϕ_c values are for inlet temperatures of 500 and 600 K. Our results for ethylene, the only fuel studied as such in another work, show the same behavior as reported by Wright [1969].

Effect of Fuel Type

As mentioned above, the various fuels had widely varying soot thresholds. For the purposes of comparison we will look at the different results for inlet temperatures of 700 K. More general comparisons will be made later in the analysis section of this chapter.

Several fuel parameters have been suggested as affecting critical equivalence ratio. For instance, a comparison of the ϕ_c versus pressure curves for the parafinic fuels (methane, ethane, propane, and n-butane) shows an increasing tendency to form soot as molecular weight increases (from 16 for methane to 58 for n-butane). Similar behavior is observed for the olefins (ethylene, propylene, and 1-butylene) from ethylene up to 1-butylene. A comparison of fuels with the same number of carbon atoms shows that paraffins generally soot less readily at low pressures than olefins, a result contrary to many atmospheric pressure studies (reviewed in Calcote and Manos [1983]). For the three-carbon fuels we can make the further comparison with cyclopropane, showing that cyclopropane forms soot more readily than either propylene or propane. No simple relationship is apparent, however, between ϕ_c and either the number of carbon-carbon bonds or the H/C ratio. In the following section we will see that explicit fuel effects are negligible and that it is the temperature and pressure that are needed to predict ϕ_c. It should be noted, however, that fuel type does have an implicit effect on ϕ_c through its determination of the equilibrium hydroxyl radical concentration.

Soot Threshold Analysis

Since soot threshold data depend on pressure and temperature, any model explaining the data must incorporate these variables. Also, in accordance with the work of Harris et al. [1986], possible fuel chemistry effects should be accounted for. The analysis presented below follows closely the work of Harris et al. and Takahashi and Glassman [1984]. It is based on three assumptions. First, that soot formation in premixed flames is directly related to the formation of precursors, and that only two chemical reactions are necessary to describe the evolution of the precursor concentration: (i) formation of precursors via fuel pyrolysis; (ii) oxidation of precursors via hydroxyl radicals. Second, that the hydroxyl radical concentration can be described by its equilibrium value, calculated using the temperature measured at that location in the flame where soot is first observed. Third, that the concentration of fuel is linearly proportional to the equivalence ratio.

Note that the second assumption differs from the works of Harris et al. and Takahashi and Glassman. Harris et al. assume ϕ_c depends on the maximum measured flame temperature while Takahashi and Glassman assume ψ_c depends on the adiabatic flame temperature. This point will be discussed again in a subsequent section.

The first assumption may be expressed as

$$[\dot{P}] = k_F\,[F] - k_D\,[OH]\,[P] \tag{21}$$

where $[\dot{P}]$ is the time rate of change of the precursor concentration, [F], [OH], and [P] are the fuel, hydroxyl radical and precursor concentrations, and k_F and k_D the rate coefficients for precursor formation and destruction. Back

reactions have been neglected in both cases. Note that Eqn (21) is based on the analysis proposed by Harris et al. and Takahashi and Glassman, which models precursor formation as a first order reaction and precursor destruction as a second order reaction.

By definition, the critical equivalence ratio occurs when the precursor concentration is at steady state. Consequently

$$[F]_{\phi_c} = [OH]_{\phi_c} [P]_{\phi_c} \frac{k_D}{k_F} \tag{22}$$

The second assumption allows determination of $[OH]_{\phi_c}$ using a standard chemical equilibrium code, if the "correct" temperature is known. Several candidate temperatures have been suggested, including the adiabatic flame temperature for products of either CO_2 and H_2O [Olson and Pickens, 1984] or CO and H_2O [Millikan, 1962]. Another, more physical, suggestion is an experimentally measured temperature [Harris et al.; MacFarlane et al., 1964; Flower and Bowman, 1986].

The final step in the analysis is to relate the fuel concentration at the critical equivalence ratio to the critical equivalence ratio. An expression, similar to those presented by Millikan, Takahashi and Glassman and Harris et al., is derived below.

The equivalence ratio is commonly defined as

$$\phi = \frac{m_F/m_A|_{actual}}{m_F/m_A|_{stoi}} \tag{23}$$

where m_F is the mass of fuel present and m_A is the mass of air present. Then,

$$\phi = \frac{\chi_F M_F M_T m_T / \chi_A M_A M_T m_T \mid act}{\chi_F M_A M_T m_T / \chi_A M_A M_T m_T \mid stoi} \tag{24}$$

with χ_F and χ_A the mole fractions of fuel and air, M_F, M_A and M_T the molecular weights of the fuel, air and fuel/air mix, and m_T being the total mass (fuel + air). Obviously, Eqn (24) reduces to

$$\phi = \frac{\chi_F / \chi_A \mid act}{\chi_F / \chi_A \mid stoi} \tag{25}$$

and can be rewritten as

$$\phi = \frac{\frac{\chi_F}{1-\chi_F} \mid act}{\frac{\chi_F}{\chi_A} \mid stoi} \tag{26}$$

The denominator is a constant, for a given class of fuels. For an alkane fuel, for instance, having CO_2 and H_2O as products

$$C_nH_{2n+2} + (\frac{3n+1}{2})(O_2 + 3.76\ N_2) = nCO_2 + (n+1)H_2O + 1.88(3n+1)N_2 \tag{27}$$

and

$$\chi_F / \chi_A \mid stoi = \frac{1/(\frac{4.76}{2}(3n+1) + 1)}{\frac{4.76}{2}\ (3n+1)/(\frac{4.76}{2}(3n+1) + 1)} \tag{28}$$

Equation (28) reduces to

$$\frac{\chi_F}{\chi_A} \mid stoi = \frac{1}{(3n+1)2.38} \tag{29}$$

If ψ (the equivalence ratio based on CO and H_2O) is used instead,

$$\frac{\chi_F}{\chi_A} \mid stoi = \frac{1}{(2n+1)2.38} \tag{30}$$

For any alkane, Eqn (26) shows $\chi_F < 0.2$ if $\phi < 2.0$ since $n \geq 1$. The same holds true for $\psi < 1.43$. For acetylene or an aromatic fuel

$$C_nH_n + (\frac{2n+\frac{n}{2}}{2})(O_2 + 3.76\ N_2) = nCO_2 + \frac{n}{2}\ H_2O + 4.7n\ N_2 \tag{31}$$

and

$$\frac{\chi_F}{\chi_A}\Big|_{stoi} = \frac{1}{\frac{5n}{4}(4.76)} \tag{32}$$

For acetylene, Eqn (26) shows $\chi_F < 0.17$ if $\phi < 2$. Aromatic fuels would have $\chi_F < 0.12$ for the same conditions. Equation (26) then, shows that in general

$$\phi = \frac{\frac{\chi_F}{1-\chi_F}}{c} \tag{33}$$

where c is a constant dependent on the fuel. Furthermore, since $\chi_F < 0.2$, the right hand side of Eqn (33) is approximately equal to χ_F/c. Thus,

$$\chi_F = c\ \phi \tag{34}$$

Notice that the expressions due to Takahashi and Glassman and Harris et al. implicitly assume constant pressure and temperature since they equate the fuel concentration, instead of the mole fraction, to ϕ. Their assumption of constant temperature and pressure is reasonable considering their temperatures varied by less than 20% and all their results were for a single pressure. In contrast, the expression given in Eqn (34) requires neither constant pressure nor temperature.

Transforming the concentrations in Eqn (22) into mole fractions, and recalling that

$$\chi_i = p_i/p = [i]R_uT/p \tag{35}$$

where p_i is the partial pressure of species i, R_u is the universal gas constant, T is the temperature, and p the mixture pressure shows

$$\frac{p\,\chi_F}{R_uT} = [F] = \frac{p\,\chi_{OH}}{R_uT}\,\frac{p\,\chi_P}{R_uT}\,\frac{k_D}{k_F} \tag{36}$$

Using Eqn (34) for χ_F, and dividing both sides by χ_{OH} and c yields

$$\frac{\phi_c}{\chi_{OH}} = \frac{k_D}{k_F}\,\frac{p}{R_uT}\,\frac{\chi_P}{c} \tag{37}$$

The rate coefficients are then written in Arrhenius form

$$k_i = A_i\, e^{-E_i/R_uT} \tag{38}$$

where A_i is the collision factor and E_i the activation energy. Taking the natural logarithm of both sides gives

$$\ln\frac{\phi_c}{\chi_{OH}} = \frac{E_F - E_D}{R_uT} + \ln\frac{\chi_P}{c}\,\frac{p}{R_uT}\,\frac{A_D}{A_F} \tag{39}$$

If we make the simplifying assumption that $\frac{\chi_P A_D}{cA_F}$ is independent of temperature and pressure, then for a single fuel

$$\ln\frac{\phi_c}{\chi_{OH}} - \ln\frac{p}{T} = \frac{E_F - E_D}{R_uT} + \ln\frac{\chi_P}{c}\,\frac{A_D}{A_F R_u} \tag{40}$$

Equation (40) forms the basis for analysis of our critical equivalence ratio data. In what follows we examine the outcome of the application of Eqn (40) to the critical equivalence ratio data presented in Figures 11 to 17, using both adiabatic and measured flame temperatures. We will also examine the applicability of using the effective equivalence ratio, ψ_c, as proposed by Takahashi and Glassman. Note that neither the H/C ratio of the fuel, nor

any other "fuel property" is included in the ϕ_c figures. This is in contrast to the results of several other studies. At the conclusion of this section we will see that such terms are insignificant and can therefore be ignored.

The goals in applying Eqn (40) are to show that the two-step model for soot precursor evolution correctly predicts soot threshold behavior over the pressure range 0.1-0.8 MPa, and to determine which temperature and equivalence ratio best describe the data.

Figure 18 shows results obtained using the adiabatic flame temperature and corresponding equilibrium OH concentration in Eqn (40). The curves for the various fuels are not linear and do not lie on top of one another. The use of the measured flame temperatures and associated equilibrium OH mole fractions, however, yields very good agreement between Eqn (40) and experimental data. This is illustrated in Figure 19. A linear least squares fit of these results gives

$$\frac{\Delta y}{\Delta x} = 0.040$$

where

$$y = \ln\left[\frac{\phi_c}{\chi_{OH}}\frac{T_f}{p}\right]$$

$$x = \frac{10^6}{T_f}$$

The correlation coefficient, r^2, is 0.967 for measured flame temperature data but only 0.850 for adiabatic flame temperature data. Thus, the measured flame temperature should be used when predicting critical equivalence ratio behavior. Significantly, Harris et al. arrived at a similar conclusion regarding measured versus adiabatic flame temperatures, although they compared the

adiabatic flame temperature with the maximum measured flame temperature, instead of the temperature *measured at* the point of incipient sooting.

It can easily be shown that the results presented here are sufficiently sensitive to discriminate between the use of measured and adiabatic flame temperatures. Starting with Eqn (40) and transforming it to

$$\frac{\phi_c}{\chi_{OH}} = C\, e^{-\Delta E/RT} \tag{41}$$

(where C is a temperature independent term containing the pre-exponential factors for the rates of precursor formation and destruction, the precursor mole fraction and the constant relating equivalence ratio to fuel concentration) we can show that if our results are insensitive to the choice of flame temperature either value used in the argument of the exponent (Eqn (41)) would yield the same functional form. To show that this is not so we substitute the measured and adiabatic temperatures into Eqn (41) and equate the two expressions. After canceling all temperature independent terms, we see that

$$e^{-\Delta E/RT_{meas}} = e^{-\Delta E/RT_{adia}} \tag{42}$$

Rewriting T_{adia}

$$T_{adia} = T_{meas} + \Delta T$$

and substituting into Eqn (42) gives

$$e^{-\Delta E/RT_{adia}(1-\Delta T/T_{adia})} \tag{43}$$

for the right hand side. If we expand the quantity $(1 - \Delta T/T_{adia})^{-1}$ and substitute it into Eqn (43), we get

$$e^{-\Delta E/RT_{adia}}\, e^{-\Delta E \Delta T/RT_{adia}^2} \tag{44}$$

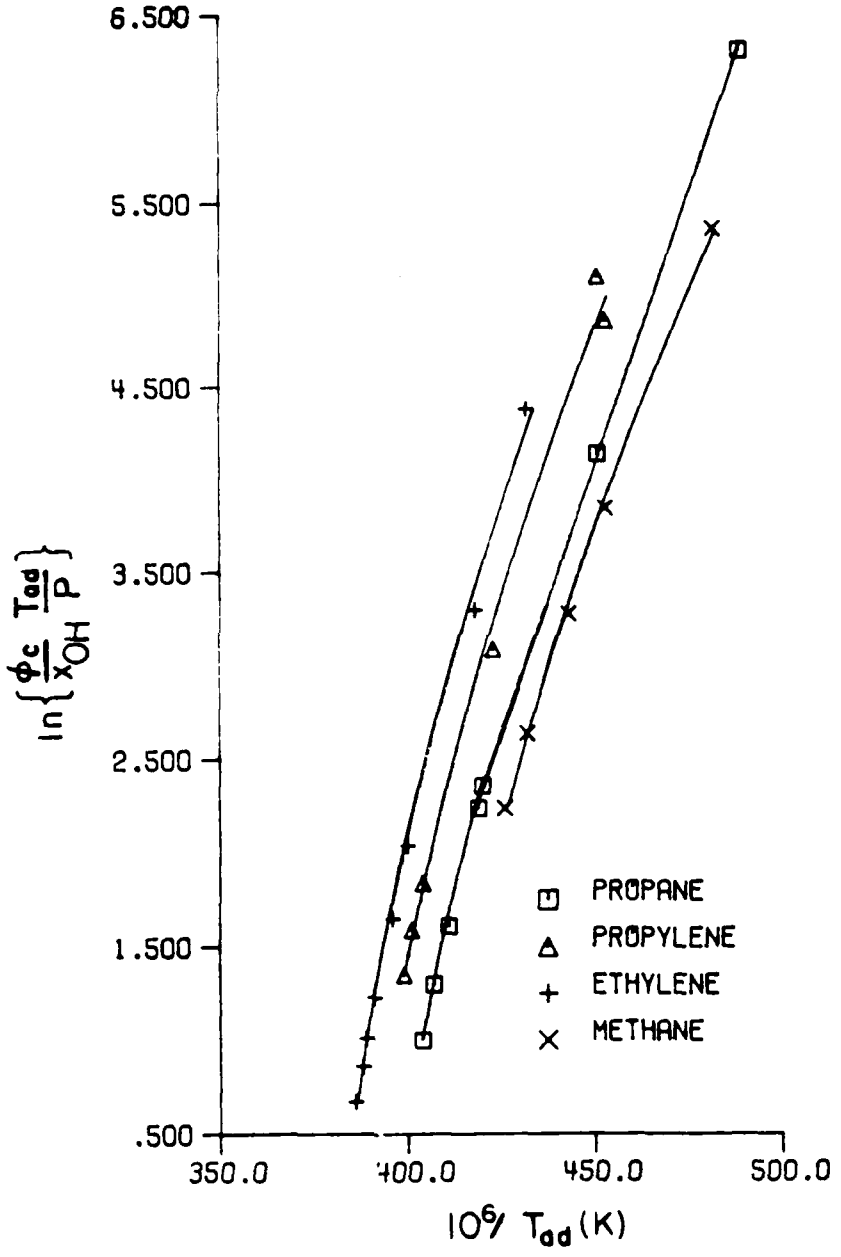

Figure 18. Critical Equivalence Ratio vs. $1/T_{ad}$.

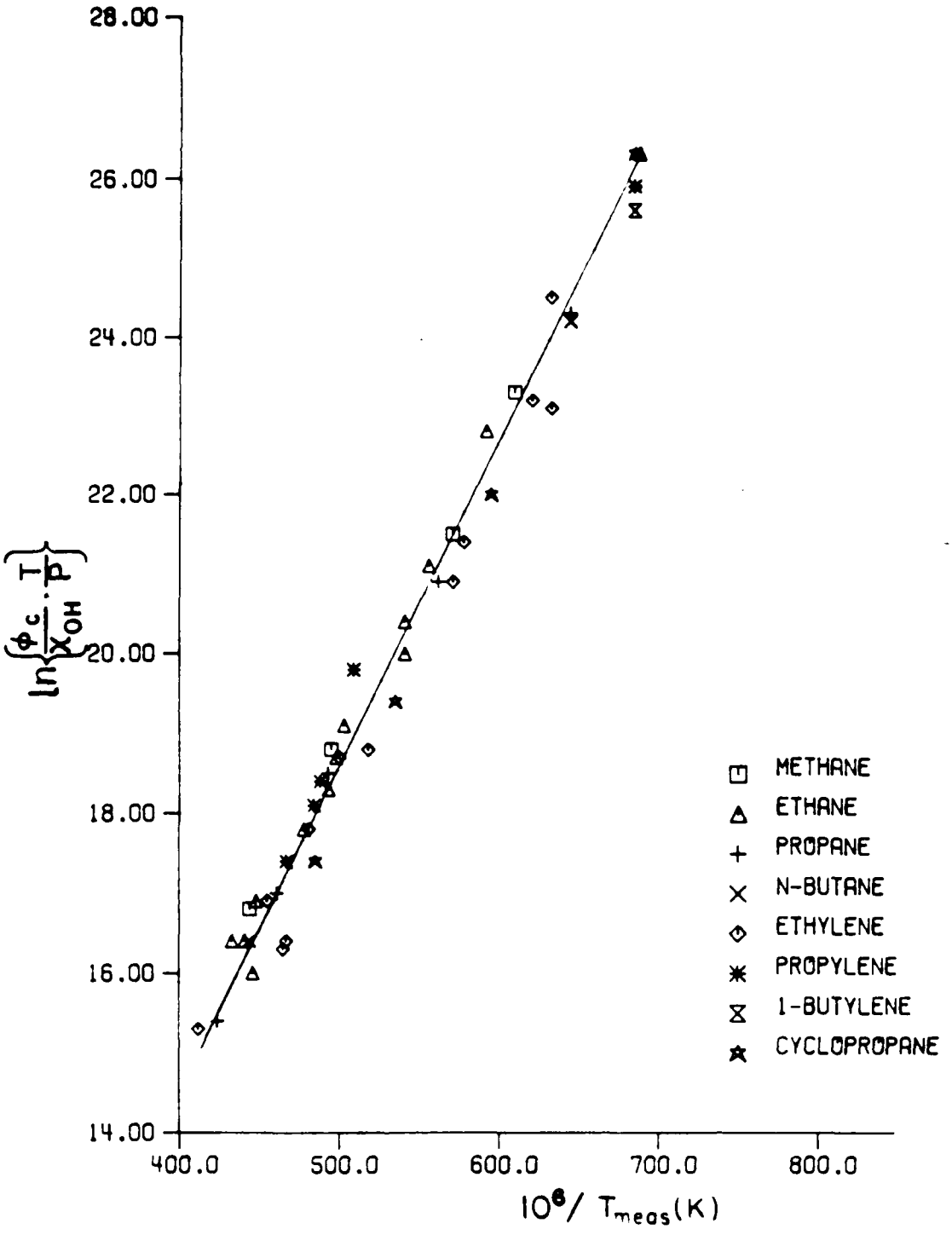

Figure 19. Critical Equivalence Ratio vs. $1/T_{meas}$.

If the measured and adiabatic temperatures give equivalent results, we can interchange them. The left hand side of Eqn (42) will cancel with the first term in Eqn (44), leaving

$$e^{-\Delta E \Delta T / R T_{adia}^2} = 1 \tag{45}$$

Consequently, if ΔT is quadratic in T_{adia}, we will be incapable of distinguishing between the two temperatures. Figure 20, which presents ΔT versus T_{adia}^2, immediately shows that ΔT is not quadratic in T_{adia} so we conclude that our results are sufficiently sensitive to distinguish between the T_{meas} and T_{adia}.

The effective equivalence ratio suggested by Takahashi and Glassman, ψ_c, was also employed to analyze the ϕ_c results. Results using this equivalence ratio, considered by those authors to be more pertinent to rich flames, are presented in Figures 21 and 22. Figure 21 presents results using measured flame temperatures while Figure 22 presents results using adiabatic flame temperature. The correlation coefficients from least squares linear fits are 0.967 and 0.863, respectively.

From this analysis we can see that the use of Eqn (40) with *measured* flame temperatures and either ϕ_c or ψ_c yields the best results. Significantly, the combination of either ϕ_c or ψ_c and *adiabatic* flame temperature is shown to give poor results.

Several groups have suggested ϕ_c (or ψ_c) should depend explicitly on some "fuel parameter," such as the H/C ratio [Harris et al.] or the number of carbon-carbon bonds [Takahashi and Glassman]. Consequently, Eqn (40) was modified to include an explicit dependence of ϕ_c on parameters such as H/C ratio, H/C mass ratio, number of carbon-carbon bonds, number of carbon

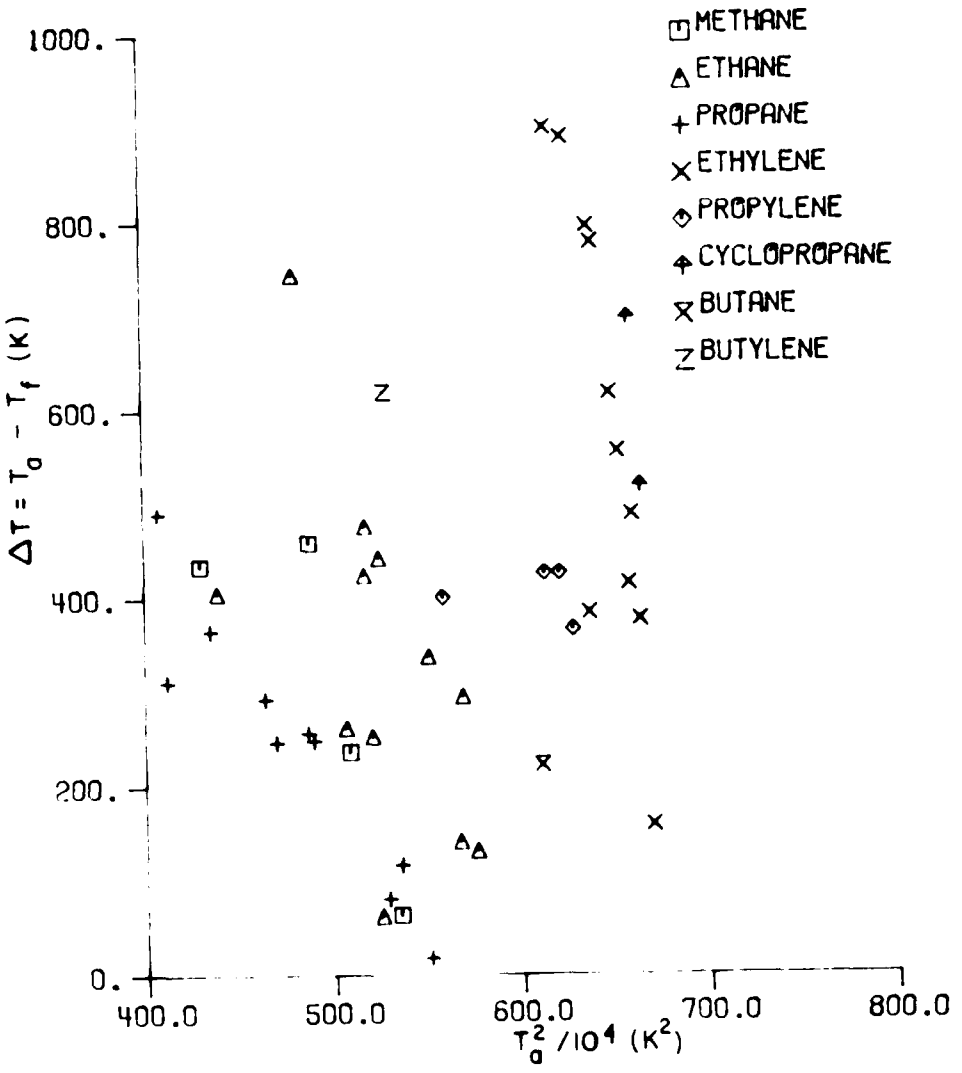

Figure 20. Temperature Difference vs. Flame Temperature, Squared.

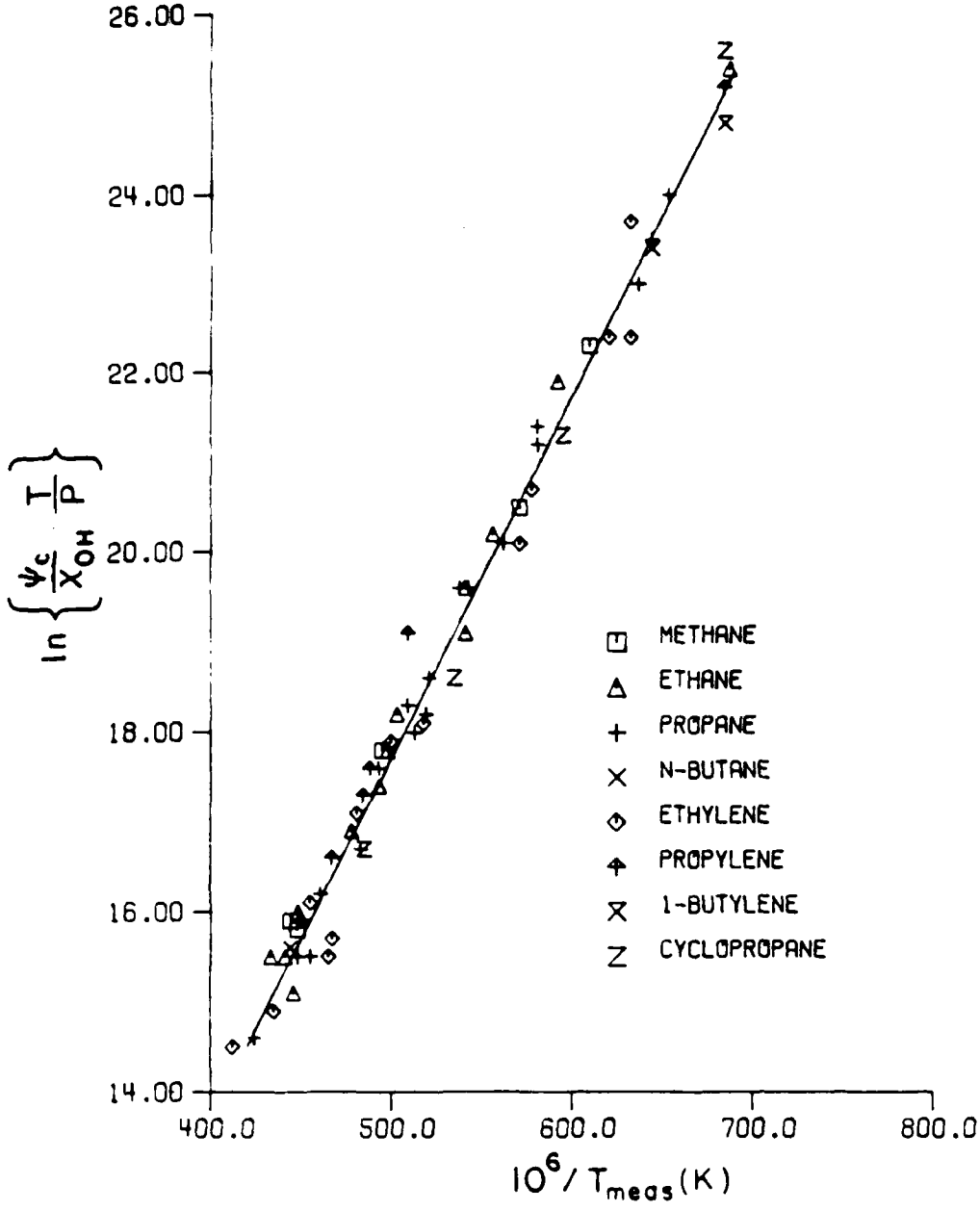

Figure 21. Effective Critical Equivalence Ratio vs. $1/T_{meas}$.

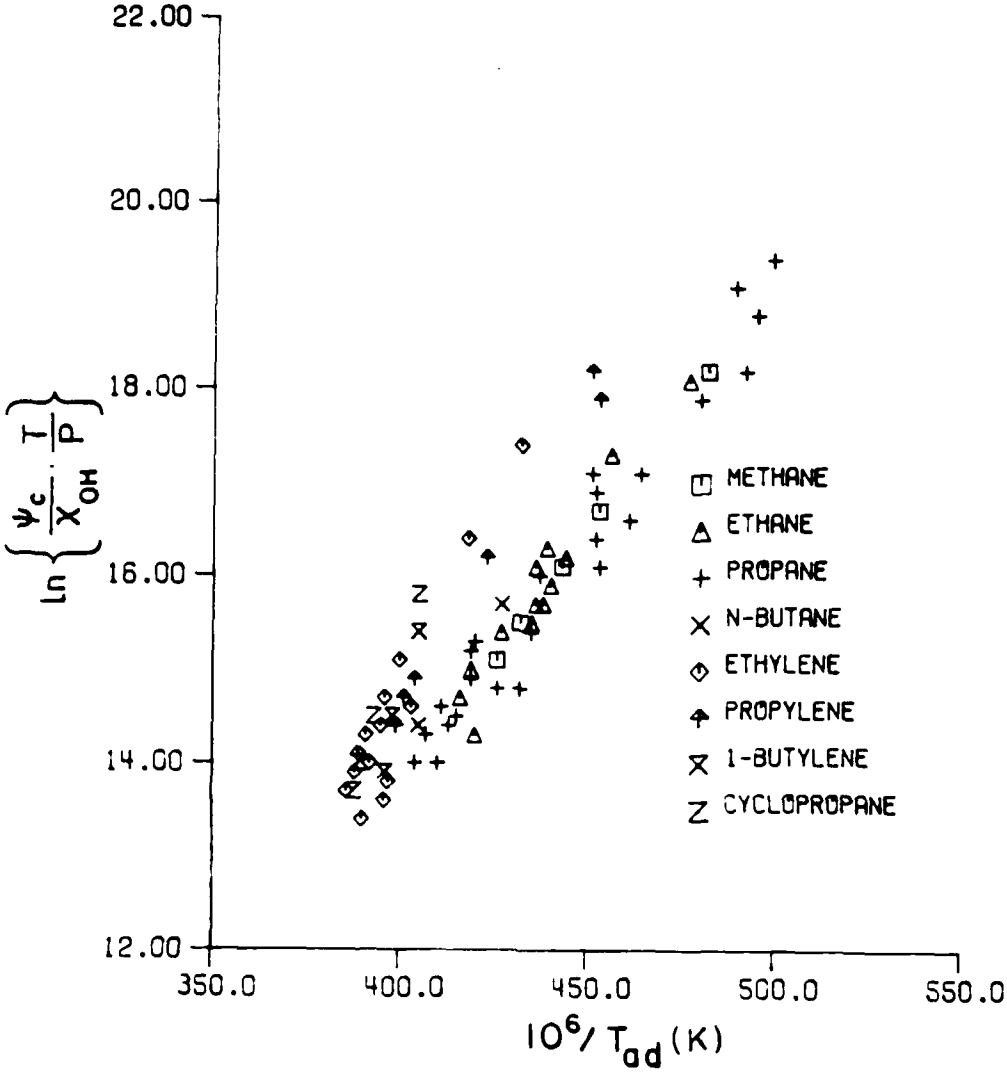

Figure 22. Effective Critical Equivalence Ratio vs. $1/T_{ad}$.

atoms and fuel molecular weight.

The data were reanalyzed with the results presented in Table 1 and Figure 23. It is readily apparent though, that none of the parameters exhibited improved agreement between the experimental results and Eqn (40) for the fuels and conditions studied here. We thus conclude that ϕ_c exhibits no explicit dependence on any "fuel parameter." However, fuel type does have an implicit effect on ϕ_c through its impact on the equilibrium hydroxyl radical concentration.

In summary several conclusions are apparent. First, the measured flame temperature predicts critical equivalence ratios better than the adiabatic flame temperature. In addition, the measured temperature should be that temperature occurring at the location where soot is first observed to form. This result is intuitively obvious since it should be the temperature occurring at the point where the precursor concentration is in steady state that controls the chemical kinetic processes leading to incipient sooting. Second, either the standard equivalence ratio, ϕ, or the equivalence ratio based on CO and H_2O as products, ψ_c, accurately predicts incipient sooting behavior. Finally, for the fuels and conditions investigated here no explicit dependence of ϕ_c (or ψ_c) on any "fuel parameter" is apparent, if the temperature occurring at the point of incipient soot formation is used in Eqn (40). No fuel parameter dependence inserted into a modified version of Eqn (40) gave any improvement.

The conclusions drawn here imply that the mechanism leading to soot formation is similar for all fuels. This hypotheses should be investigated further to confirm its validity.

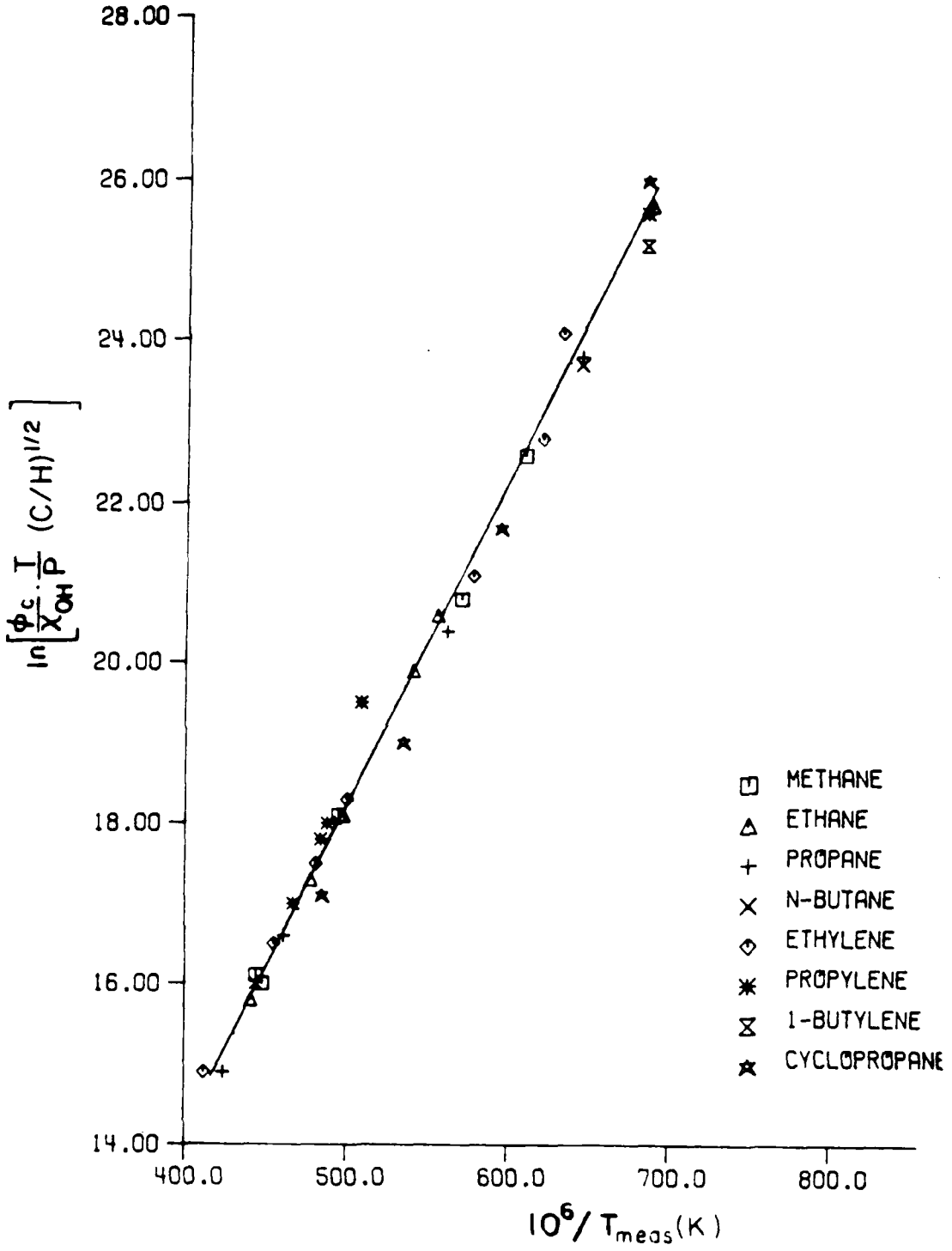

Figure 23. Effective Critical Equivalence Ratio vs. $1/T_{meas}$ With Fuel Type Depende

Table 1. Critical Equivalence Ratio Dependencies on Fuel Parameters

	ϕ_c			ψ_c		
Term	$\Delta E/R$	n	r^2	$\Delta E/R$	n	r^2
----	.039	---	.969	.039	---	.967
H/C mass	.041	-.016	.969	.041	-.012	.967
H/C no.	.041	-.19	.967	.041	-.14	.966
C no.	.041	.18	.967	.041	.16	.965
C-C bonds	.041	.13	.965	.041	.12	.964
MW	.041	2.6	.871	.041	2.5	.881

Flame Radiation

Figures 24 through 27 depict radiation intensity versus axial location for ethane, propane, ethylene, and propylene flames, respectively. The inlet temperature was 700 K for all tests, while the pressure was varied from 0.4 to 0.8 MPa (except for propylene, for which no 0.8 MPa data were taken). In addition, tests were run at three equivalence ratios, namely: 0.80, 1.00, and 1.25. These conditions produced flames of negligible or zero soot. Flame radiation intensity was then plotted vs x/D.

To obtain mappings of radiation intensity versus axial location, measurements were taken at integral values of x/D in most cases; however, at each pressure the radiometric output was monitored as a continuous function of axial location for 25% of the cases so that curves could be fitted accurately between integral x/D locations for all conditions.

Three quantities were varied to examine their effects on flame radiation levels. Two of these were combustor pressure and equivalence ratio, while the third, fuel type, covered two paraffins, ethane and propane, and two olefins, ethylene and propylene. Note that propane and ethylene have the same number of carbon-to-carbon bonds. The effects of the above parameters on flame radiation intensity are discussed below.

To simplify the discussion and to focus on the most important data, the analysis is restricted to the peak levels of radiation for each axial profile.

Effect of Pressure

An increase in combustion pressure yielded a linear increase in peak intensity for all fuels, as shown in Figures 24 through 27. However, Figure 28

shows that the slope of the line denoting peak intensity versus pressure differs between equivalence ratios. The slope is 1.0 for an equivalence ratio of unity, falling to 0.90 for $\phi = 1.25$ and 0.70 for $\phi = 0.80$. Evidently, the changes in flame gas density, flame temperature, species concentrations, and emission bandwidths brought about by changes in pressure are dependent on the equivalence ratio of the unburnt mixture. It is interesting to note that despite the complicated nature of the pressure effect, the intensity responds linearly to pressure changes in the range 0.4 to 0.8 MPa. This linear response agrees with results taken from liquid fuel studies for the pressure range covered here [Claus; Naegeli et al., 1983]. It is also corroborated by the results of MacFarlane, who burned gaseous methane in air.

Effect of Equivalence Ratio

The radiation intensity follows several clear trends as equivalence ratio varies. First, equivalence ratios of 0.80 and 1.25 have nearly equal peak intensities. This is shown in Figure 29, which depicts the maximum radiant intensity averaged over all fuels as functions of ϕ and p. In general, about 20% more CO_2 and 20% less H_2O is produced for $\phi = 0.80$ than for $\phi = 1.25$ at equilibrium flame conditions, as determined using the equilibrium code of Gordon and McBride. The temperatures in the experiment discussed here were, on the average, 10% higher for $\phi = 1.25$ than for $\phi = 0.80$, as demonstrated in Figures 30 and 31. An important conclusion is that the higher CO_2 concentration give the lean flame as great an emissive flux as the rich flame, despite its higher H_2O concentration and temperature. This is logical because the infrared emissivity of CO_2 is much higher than that of H_2O [Siegel and Howell]. Also, as shown in Figure 32, the stoichiometric

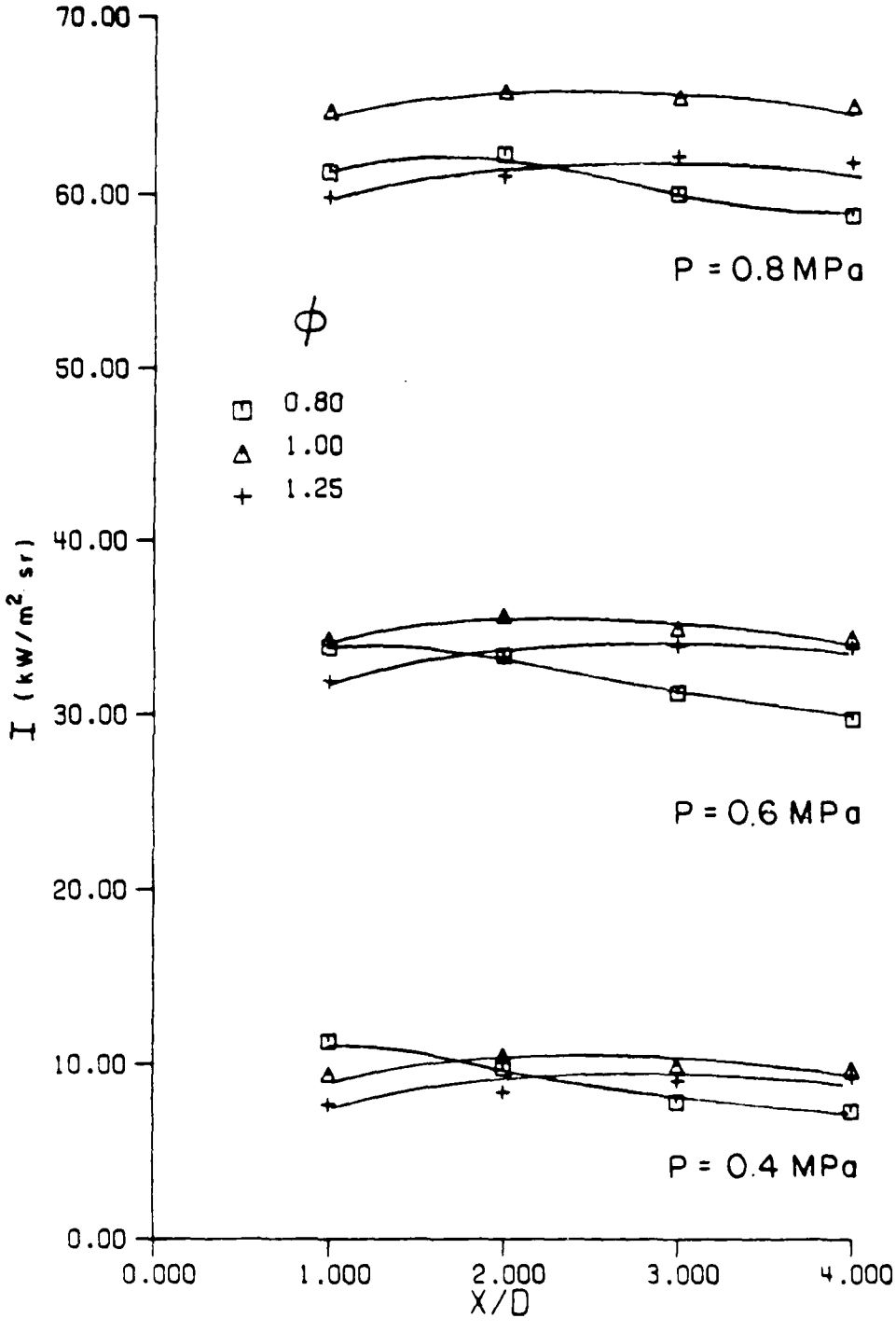

Figure 24. Ethane: Flame Radiation Profiles.

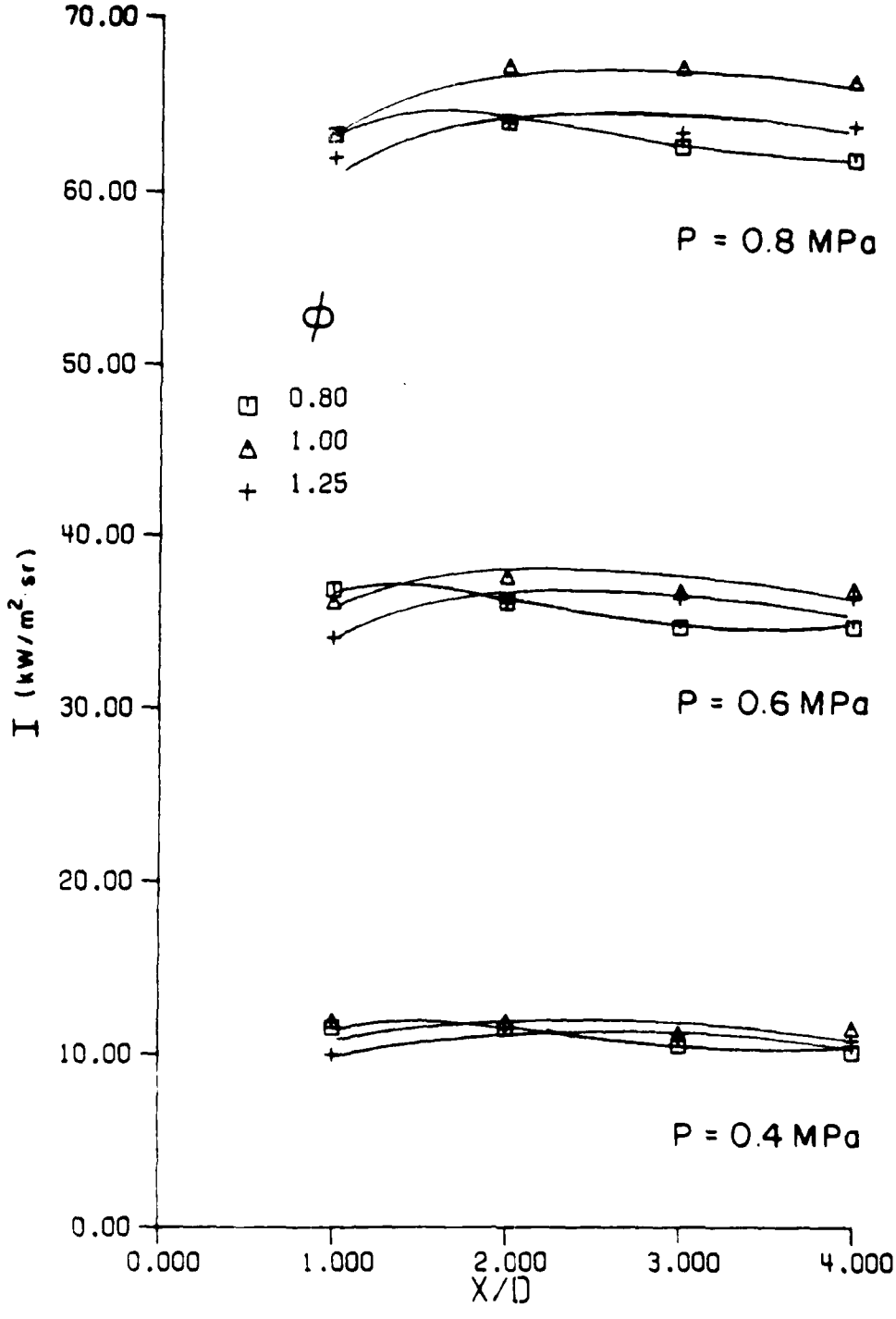

Figure 25. Propane: Flame Radiation Profiles.

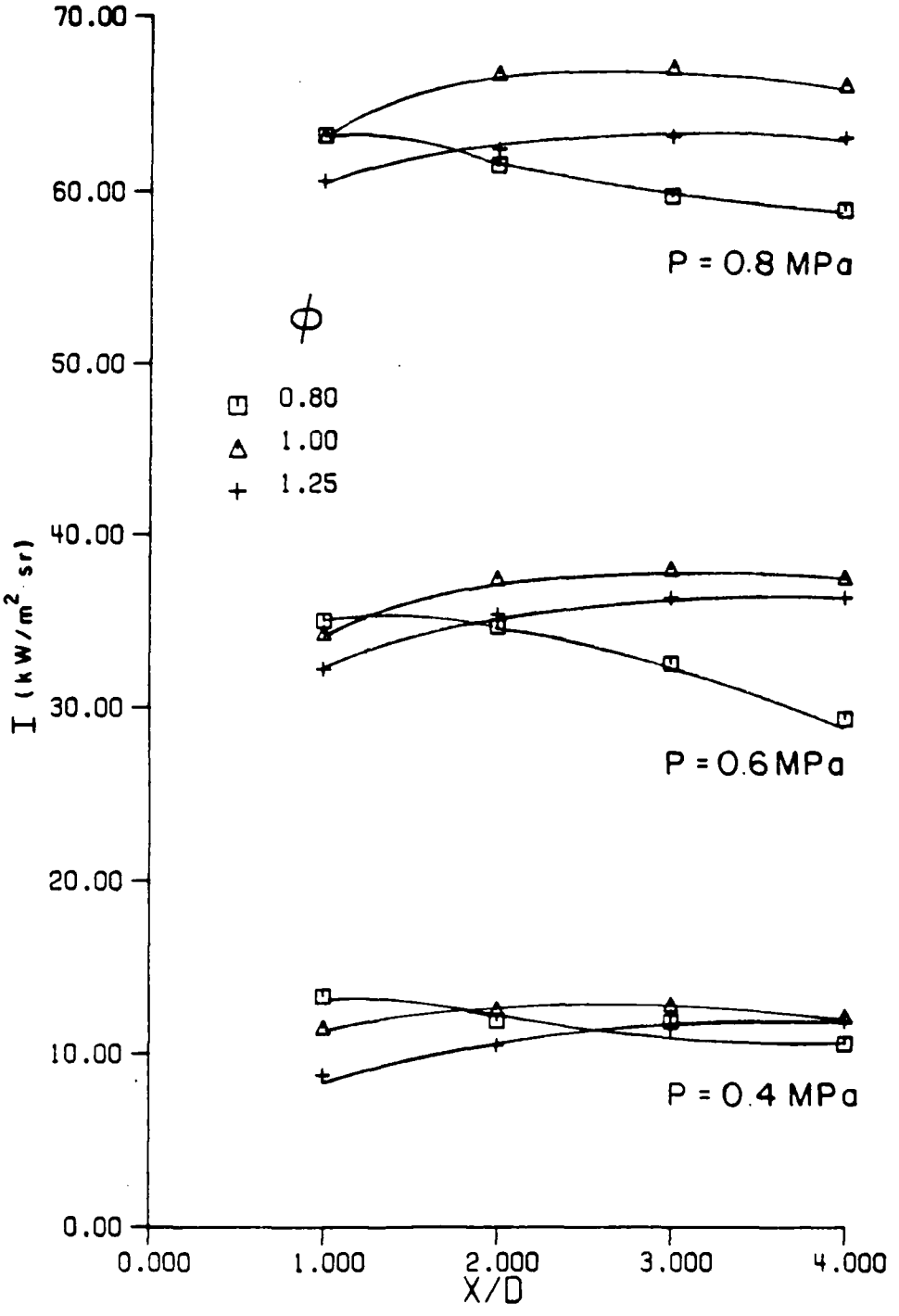

Figure 26. Ethylene: Flame Radiation Profiles.

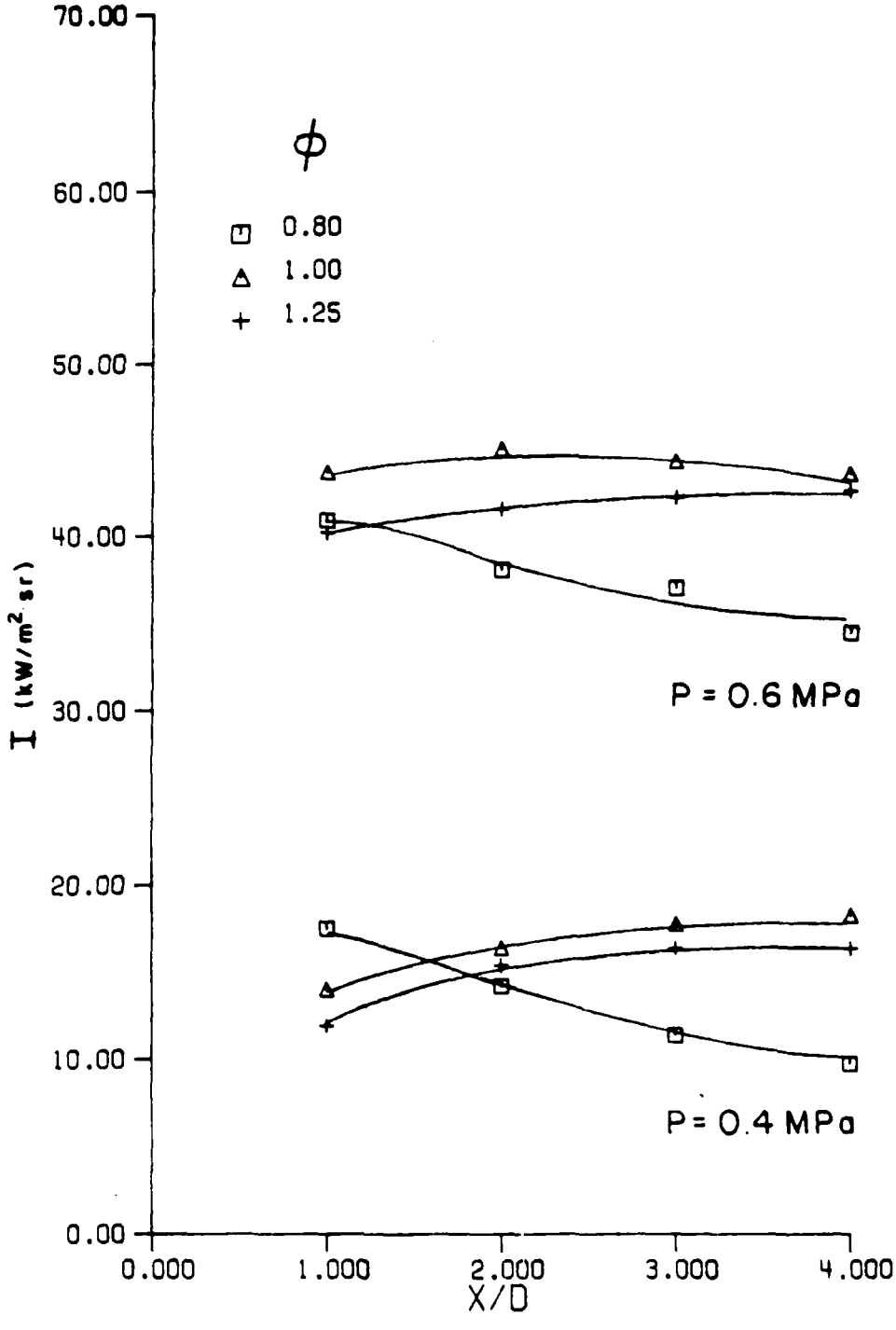

Figure 27. Propylene: Flame Radiation Profiles.

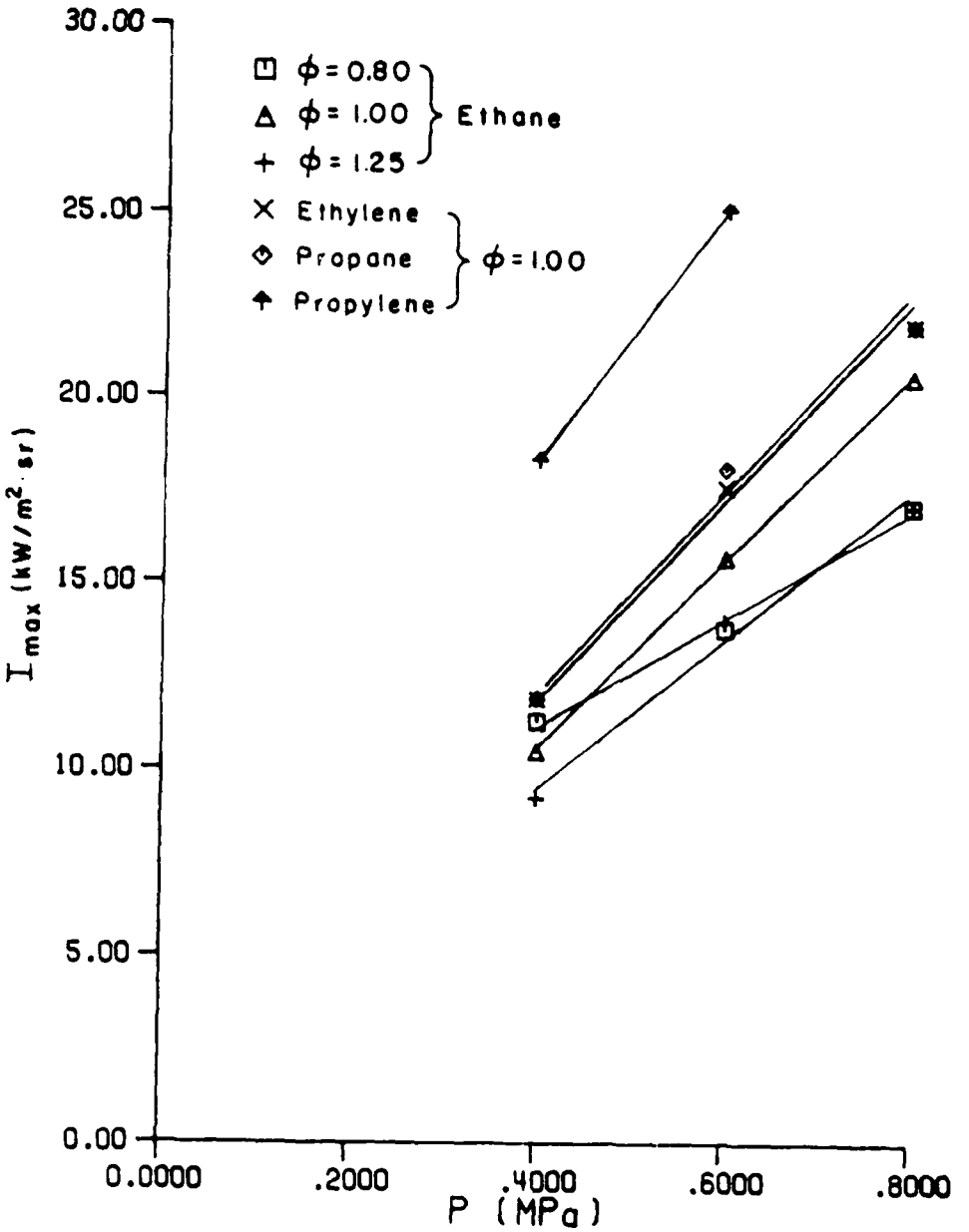

Figure 28. Peak Flame Radiation Intensity vs. Pressure.

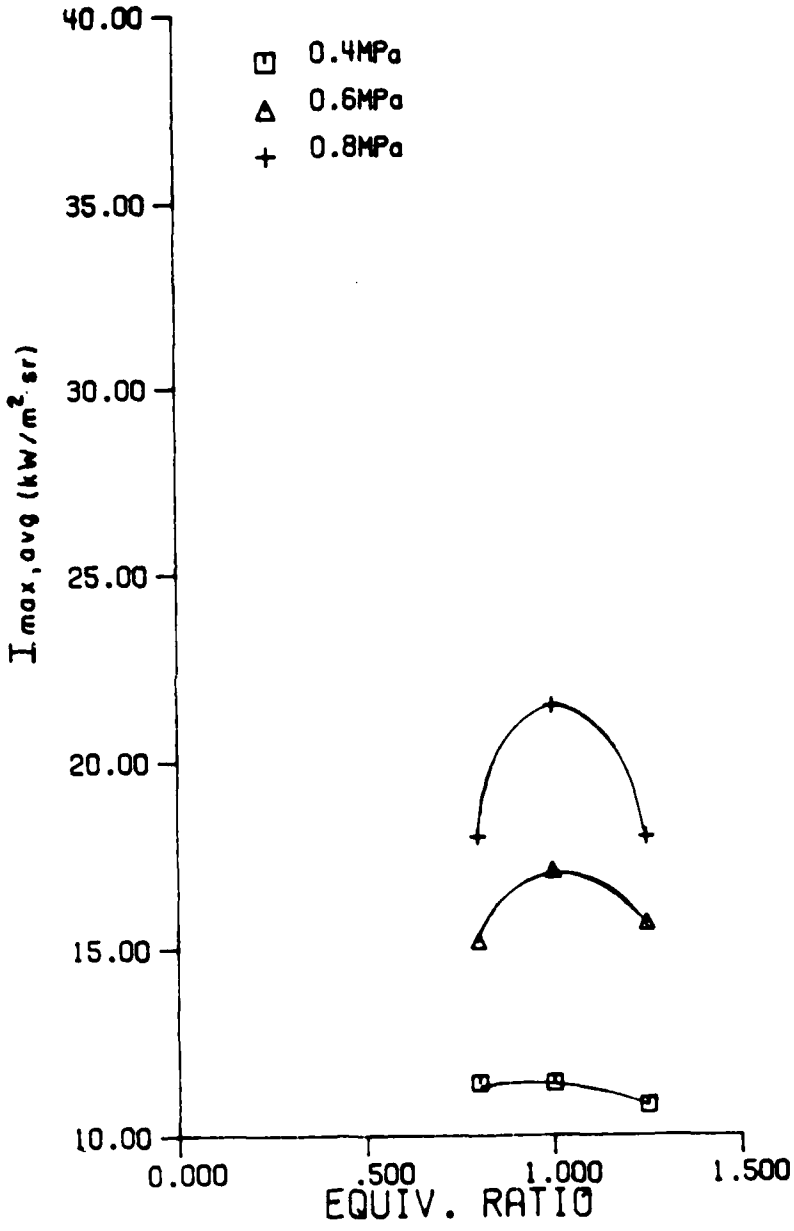

Figure 29. Peak Flame Radiation Intensity vs. ϕ; All Fuels.

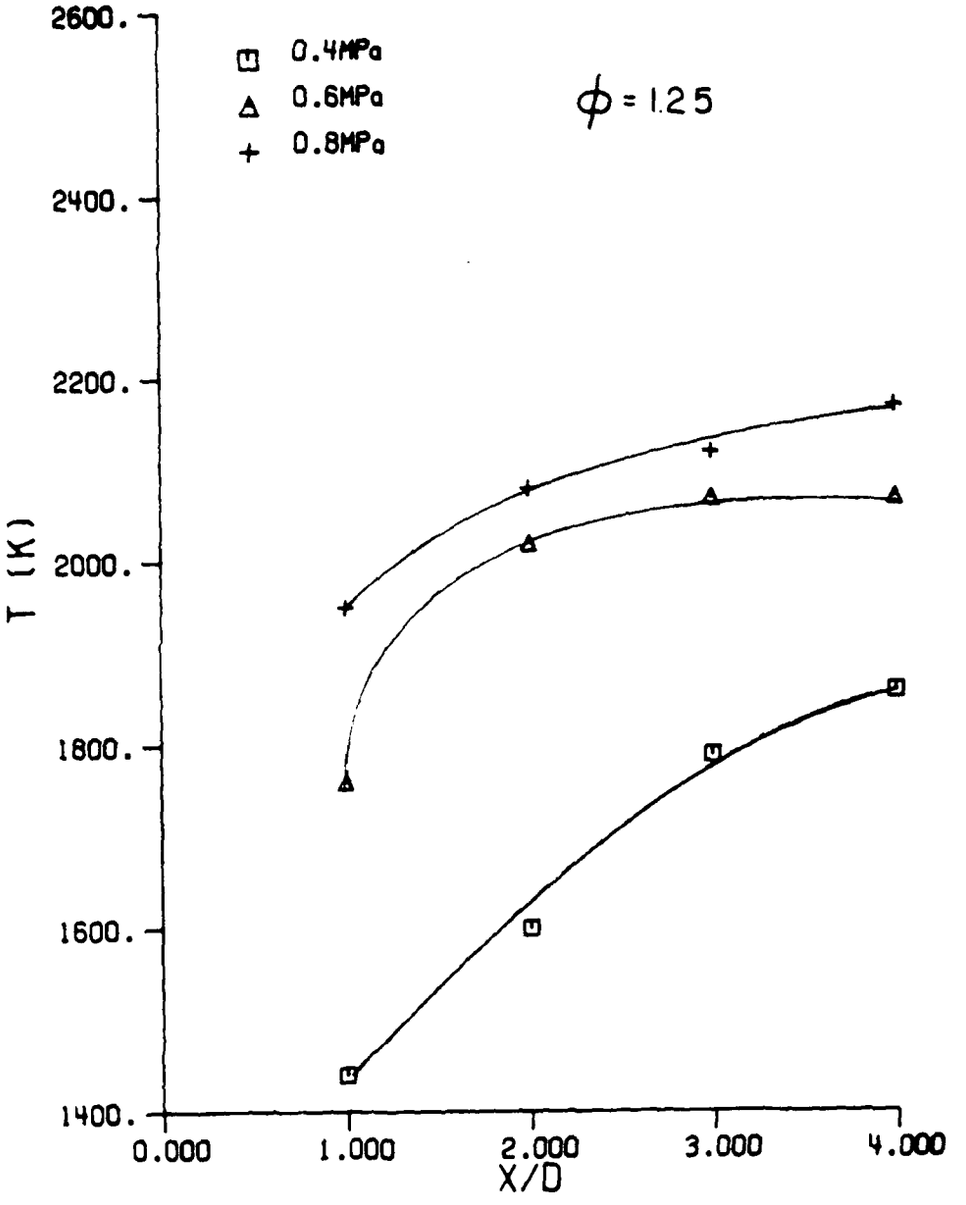

Figure 30. Combustor Temperature Profiles: $\phi = 1.25$.

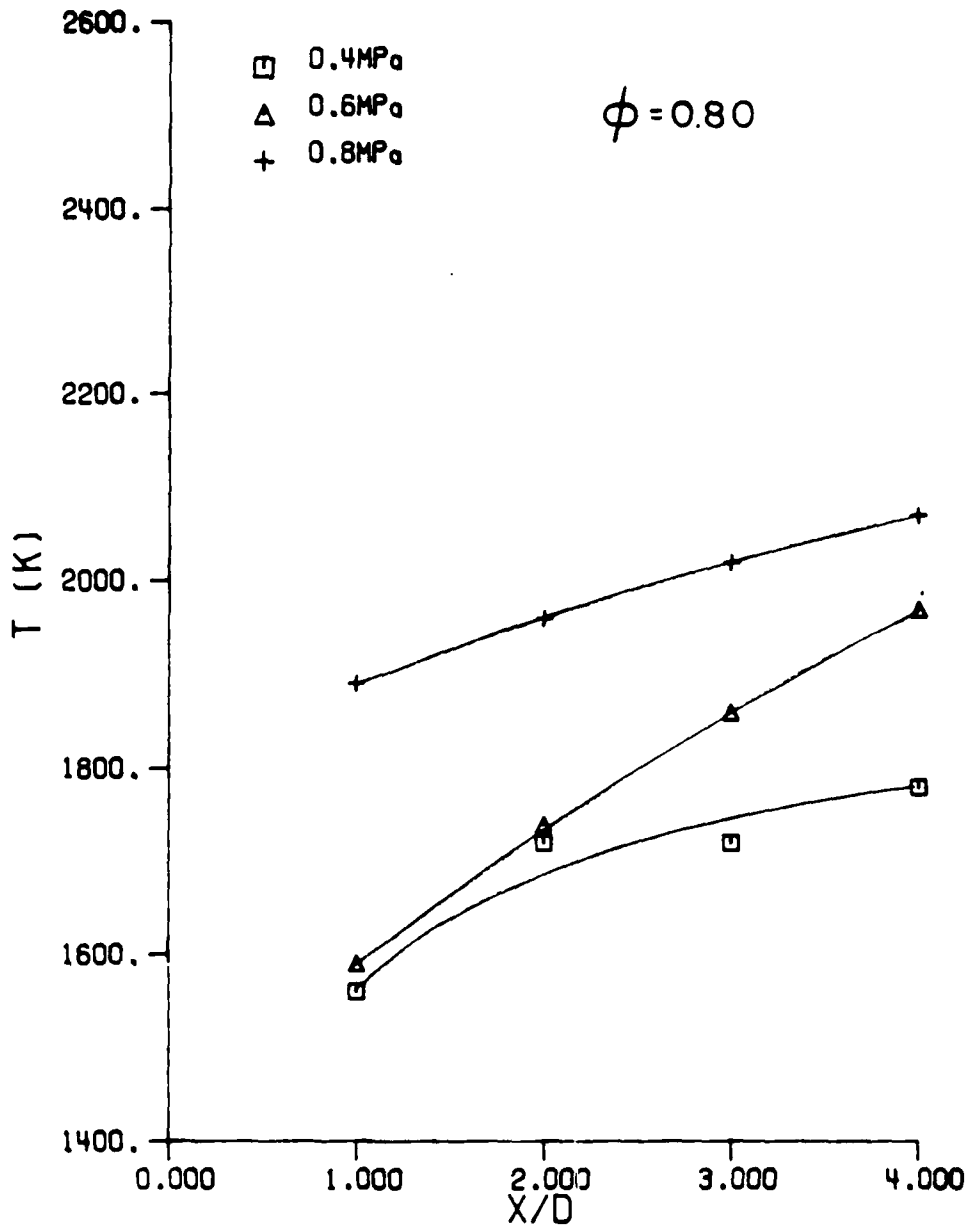

Figure 31. Combustor Temperature Profiles: $\phi = 0.80$.

flames exhibited, on average, a 20% higher intensity than flames burning at equivalence ratios of 0.8 and 1.25. This is also reasonable because the equilibrium H_2O concentrations of the stoichiometric flame were nearly equal to those for $\phi = 1.25$, and the equilibrium CO_2 concentrations were 10% higher than the values for $\phi = 0.80$. Moreover, stoichiometric flame temperatures were generally 5-10% higher than for $\phi = 1.25$. One observation, then, is that equivalence ratios of 0.80 and 1.25 yield nearly equal radiation intensities, which are about 20% lower than for stoichiometric mixtures.

Another observation is that flame length increases with equivalence ratio, so that the peak intensity moves downstream as the equivalence ratio is increased. This effect can be seen very clearly in a comparison of any curves depicting $\phi = 0.80$ and $\phi = 1.25$ (e.g. Figure 25). The former peak early, usually before x/D = 1.5; the $\phi = 1.25$ curves, on the other hand, continue to rise, peaking at x/D = 4. The explanation is that rich mixtures require a longer time (and therefore length) to achieve complete combustion because more fuel is burnt per unit volume of air.

Effect of Fuel Properties

The highest flame radiation levels were obtained with propylene, followed by propane, ethylene, and then ethane. These results indicate that flame radiation may depend on the hydrogen-to-carbon (H/C) ratio of the fuel, as suggested by gas turbine experiments [Naegeli et al., 1982; 1983], or on the number of bonds in the fuel molecule. Since the peak radiation levels appeared to be a function of the hydrogen-to-carbon ratio of the fuel, I_{max} was plotted against H/C. As Figure 33 shows, the radiant intensity generally

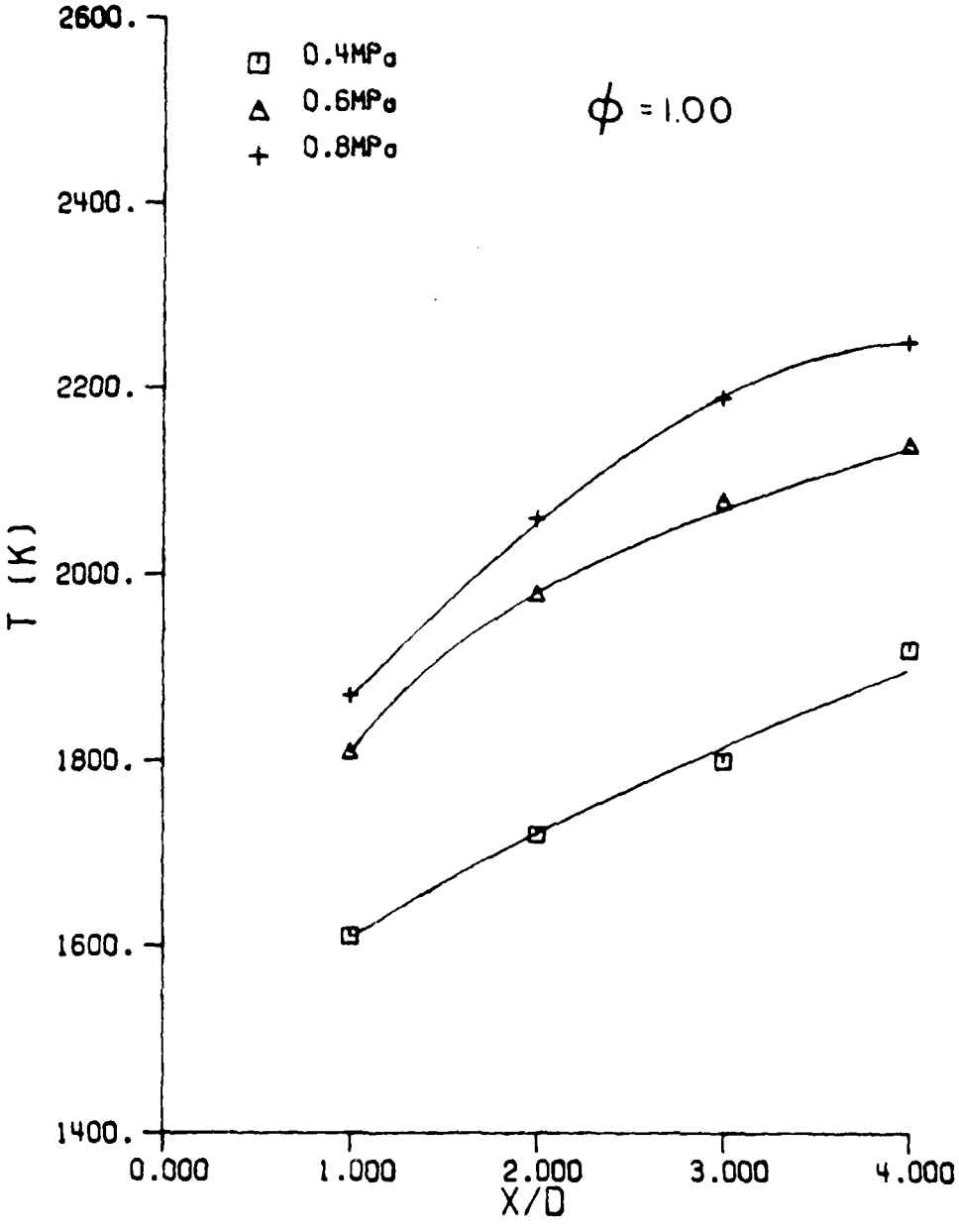

Figure 32. Combustor Temperature Profiles: $\phi = 1.00$.

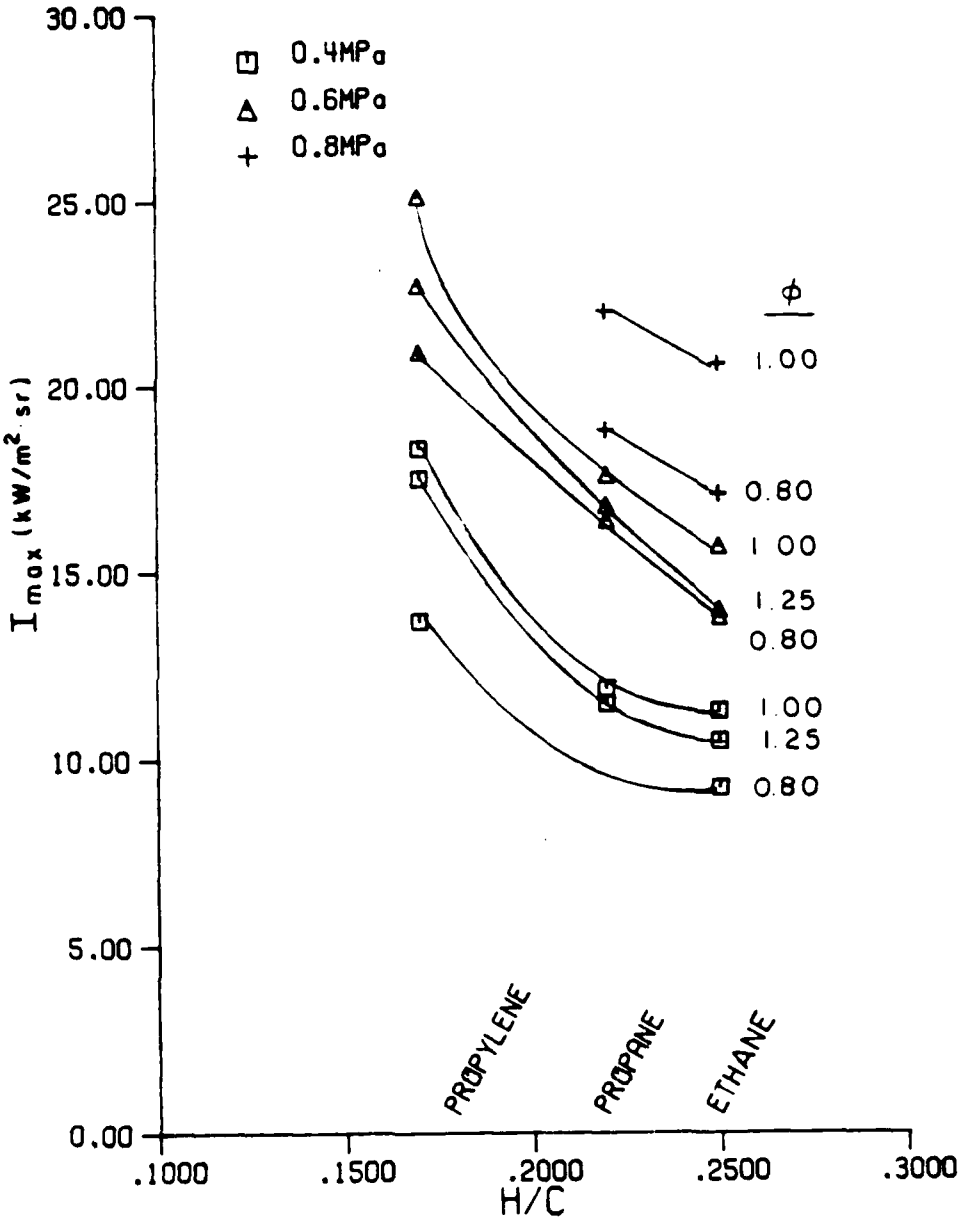

Figure 33. Intensity vs. H/C Ratio of Fuel.

falls with increasing H/C, which agrees with the results of Moses and Naegeli [1979]. This agreement indicates that although gas turbine flame radiation is certainly complicated by liquid fuel spray phenomena, it is also dependent upon the degree of fuel molecule saturation.

Because the curves in Figure 33 are qualitatively similar but vertically separated, other expressions were tested to determine if they more accurately described the data. Recalling that density played a role in flame gas concentrations for the soot threshold analysis, it might be expected to influence the CO_2 and H_2O concentrations in the same manner. A linear dependence of radiation intensity on gas density is not anticipated because of self absorption along the radiation path length, but a gas of higher density should emit more energy than one of low density. Figure 34 shows that the families of curves lie slightly closer together when corrected for differences in density, indicating that the gas density may be an important factor. The intensity, after being divided by the gas density, still shows a decrease with increasing H/C ratio.

A final expression was formulated by dividing the peak intensity by the number of carbon-to-carbon bonds in the fuel molecule. For three of the fuels, propane, ethylene, and propylene, this gave a linear relationship when plotted against pressure. Figure 35 shows that the value of $\frac{I_{max}}{\#\ C-C\ bonds}$ rises linearly with pressure, and the curves lie on top of each other. The slope of these lines, 12.5, is about 1/5 the slope from the work of Claus. The flames in Claus' study were, however, luminous, and the fuel was aviation kerosene.

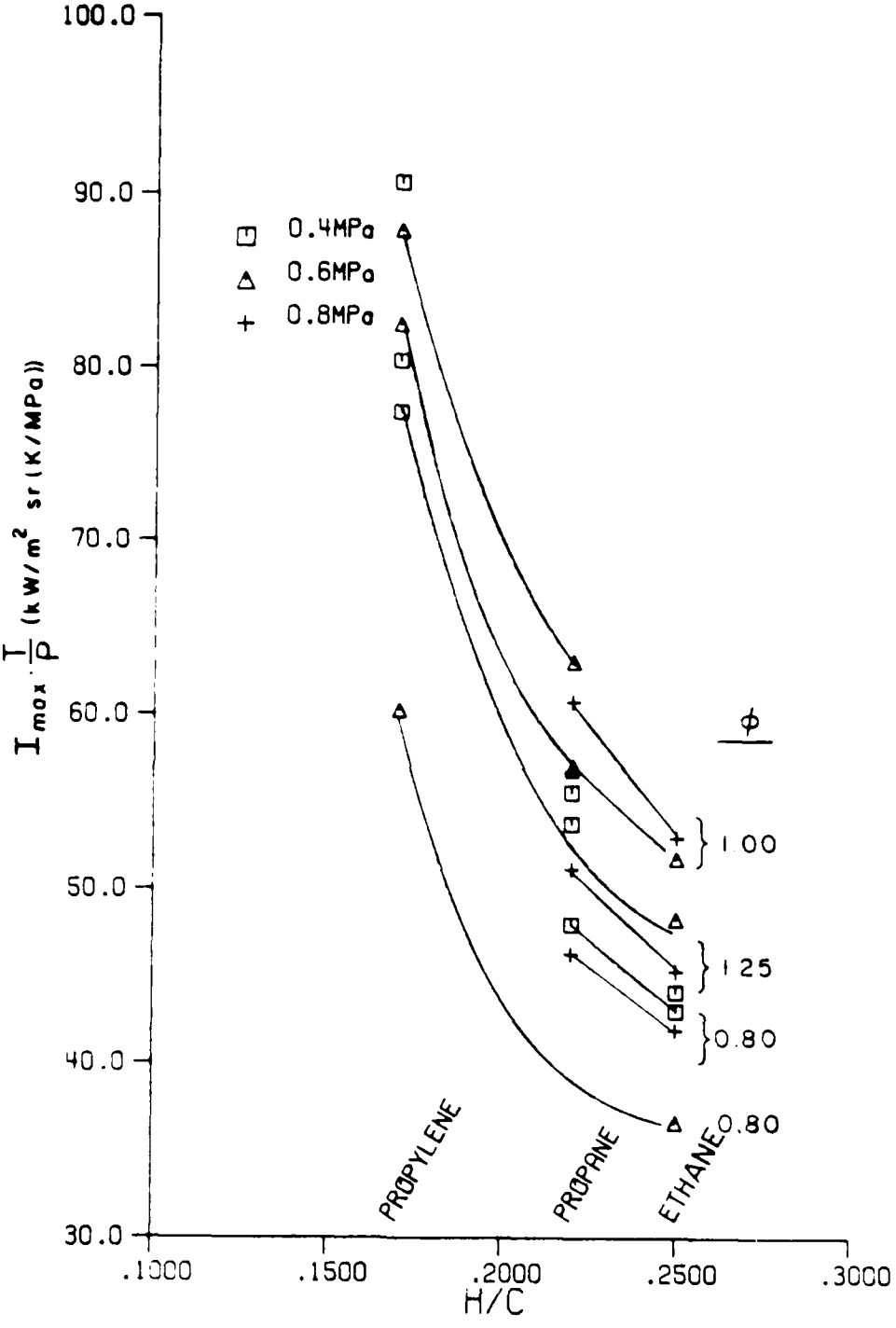

Figure 34. Intensity/ρ vs. H/C Ratio of Fuel.

AD-A191 991 SOOT AND RADIATION IN A GAS TURBINE COMBUSTOR(U) PURDUE 2/2
UNIV LAFAYETTE IN GAS TURBINE COMBUSTION LAB
A H LEFEBVRE ET AL 15 JUL 87 AFOSR-TR-88-0097
UNCLASSIFIED AFOSR-83-0374 F/G 21/2 NL

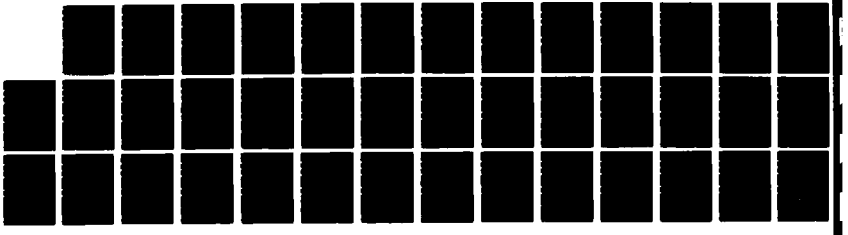

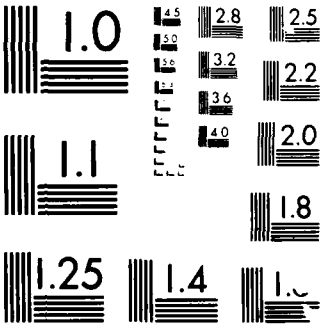

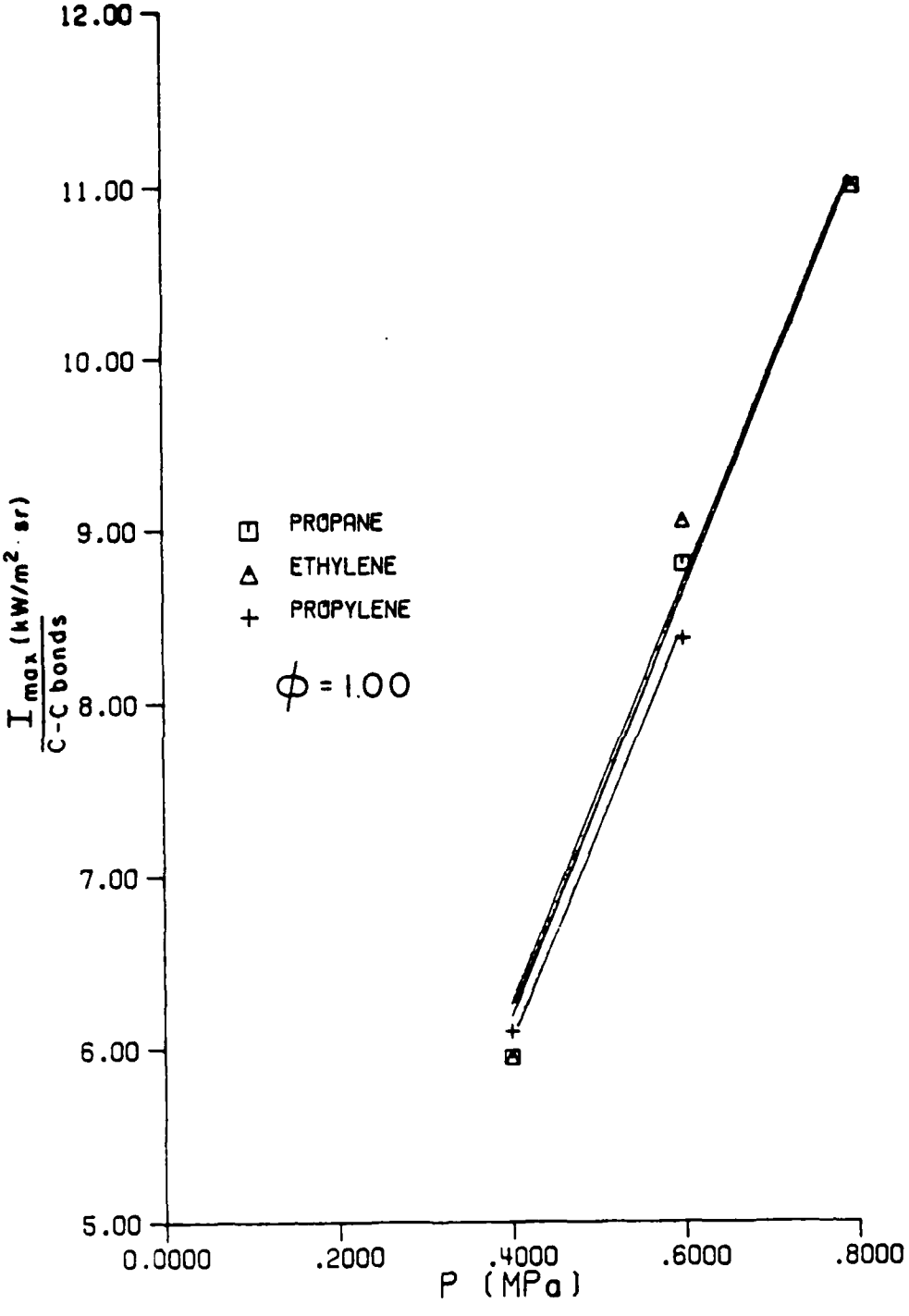

Figure 35. Intensity/C-C Bonds vs. Pressure.

Emissivities

A logical method of analyzing radiation data is to calculate emissivities for the different conditions studied. In this work, where the flame temperatures and emitted fluxes were measured, the emissivities were calculated as follows:

$$\epsilon = \frac{E_f}{\sigma T_f^4} \tag{46}$$

where

ϵ = emissivity

E = emitted flux (W/m^2)

σ = Stefan-Boltzmann constant ($5.67 \cdot 10^{-8}$ $W/m^2 \cdot K^4$)

T = temperature measured at the plane of the windows

and the subscript f denotes flame conditions.

The emissivities calculated from Eqn (46) showed considerable scatter. As Figure 36 shows for propane, no clear trends could be seen for the effects of equivalence ratio or pressure. Similar results were observed for ethane and propylene.

Lack of a simple relationship describing flame emissivity is not surprising, especially in light of the complex nature of gaseous radiation. For instance, the radiant energy emitted by CO_2 and H_2O is due to narrow bands in the infrared portion of the spectrum, and therefore does not provide a blackbody distribution (σT^4). Nevertheless, if the gas emissivity over each wavelength

band were unity, then the overall emissivity, ϵ, would scale as T^4. Since it does not, we can conclude that the individual band emissivities are different from unity and temperature dependent. Considering that the diameter of the combustion chamber is only 3.81 cm, this is not surprising, for only when the optical path length becomes large do the band emissivities approach unity.

Hottel's charts were applied to the results using the measured flame temperature and combustion pressure and calculated equilibrium concentrations of CO_2 and H_2O. Properties and concentrations were assumed to be uniform across the diameter of the combustor. The resulting (calculated) emissivities for the non-luminous gases show a clear increase with pressure. Figure 37 shows this behavior for ethane and also reveals a strong decrease in emissivity with increasing equivalence ratio. The increase in emissivity with pressure is logical because of collisional broadening of the emission-absorption bandwidths for CO_2 and H_2O. The decrease in emissivity with downstream location is probably a manifestation of increasing temperature as combustion approaches completion.

Figure 38 also shows emissivities calculated using Hottel's charts and indicates a decrease in emissivity with increasing distance from the flameholder. This behavior, coupled with the rise in temperature with downstream distance, explains why the profiles of radiation intensity show little variation with axial location. The variations in temperature and emissivity have competing effects, which serve to flatten the flame radiation profiles. As Figures 30 through 32 show, the flame temperature generally rises up to $x/D = 4$. The band emissivities are known to fall with rising gas temperature in this temperature range [Siegel and Howell].

Finally, the measured values for radiation intensity were compared to values using the calculated emissivities. This allows for estimation of radiation intensity via the equation

$$I = \frac{\epsilon \sigma T^4}{\pi} \tag{47}$$

Figure 39 shows the relationship between measured and estimated radiation intensities. The correlation coefficient of 0.535 indicates poor agreement. This is attributed to experimental error, both in the measurement of radiation intensity and in the determination of emissivity from Hottel's charts.

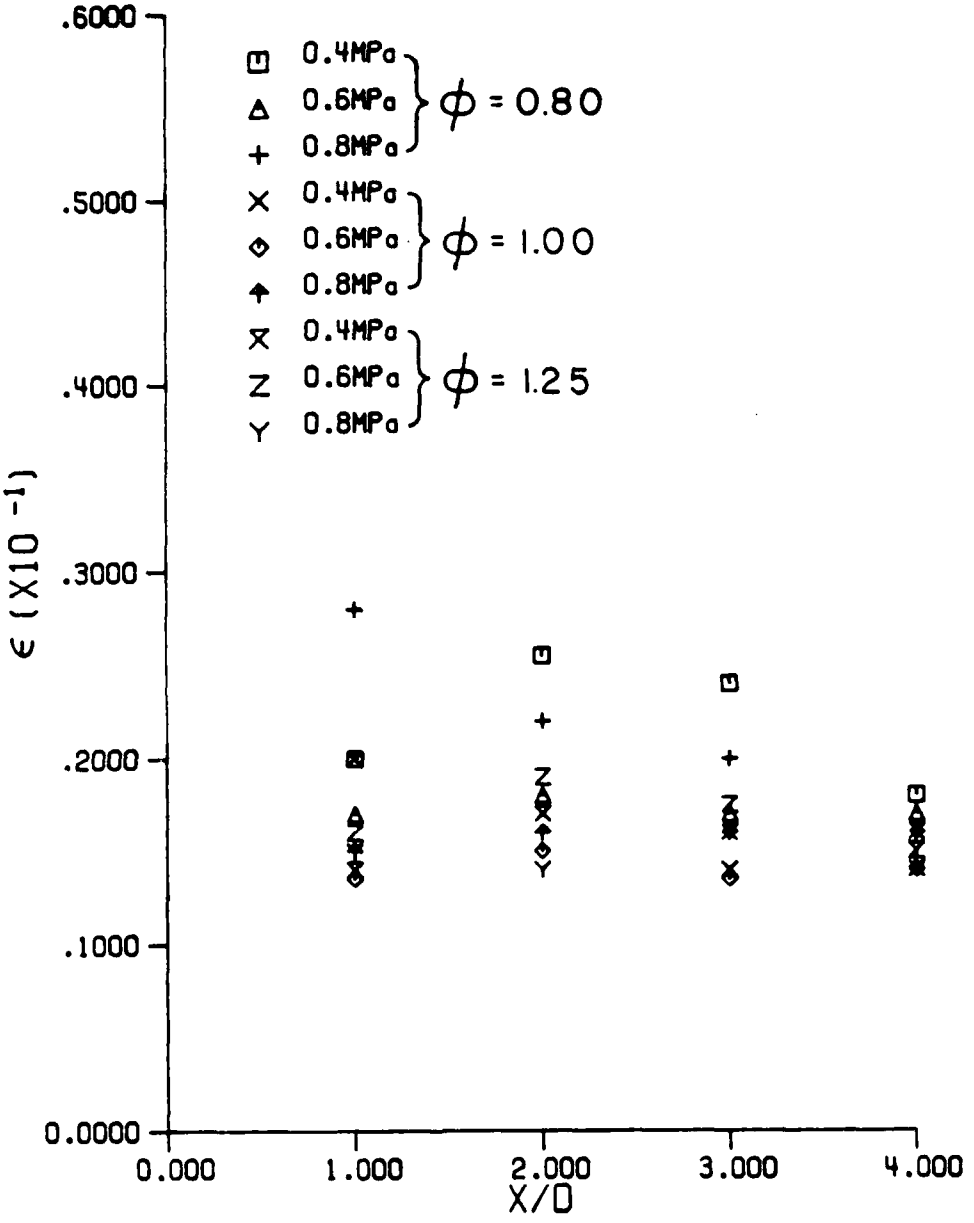

Figure 36. Calculated Emissivity Profiles.

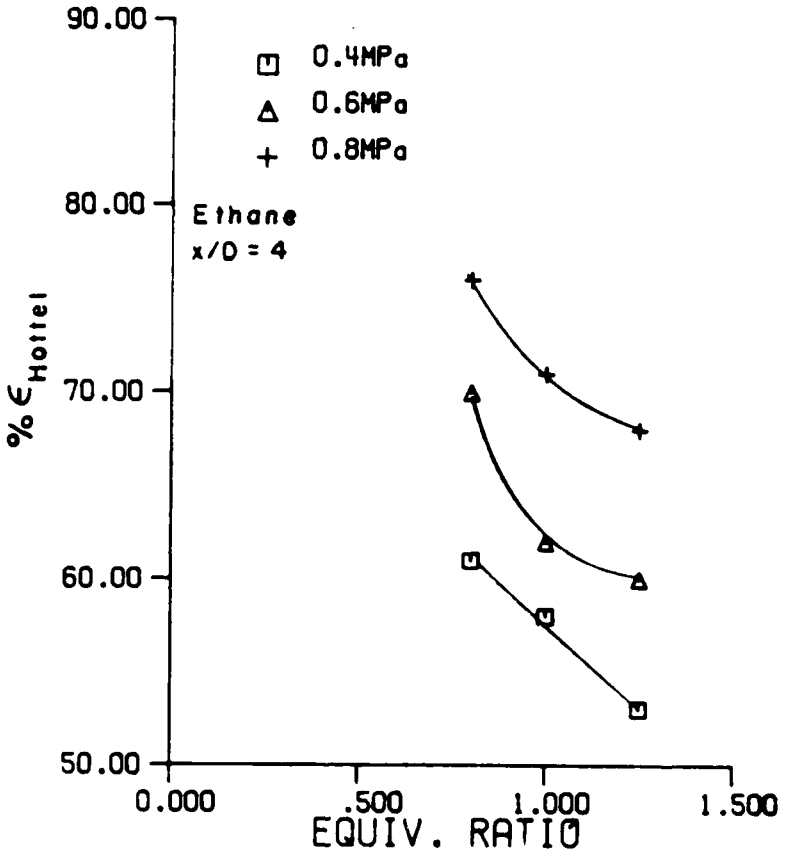

Figure 37. Ethane: Empirical Emissivity vs. ϕ.

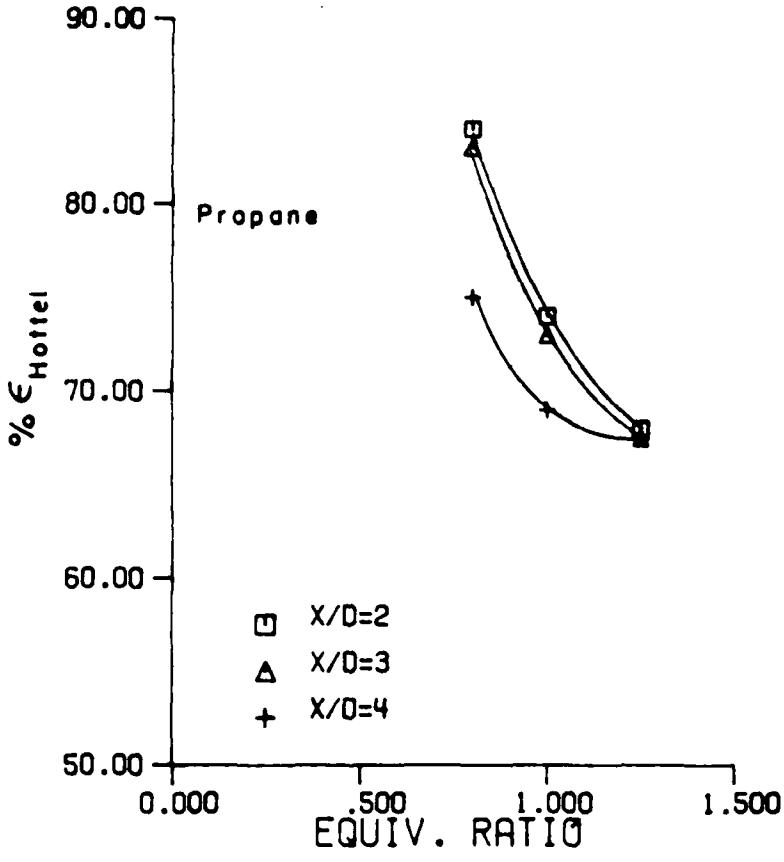

Figure 38. Propane: Empirical Emissivity vs. ϕ.

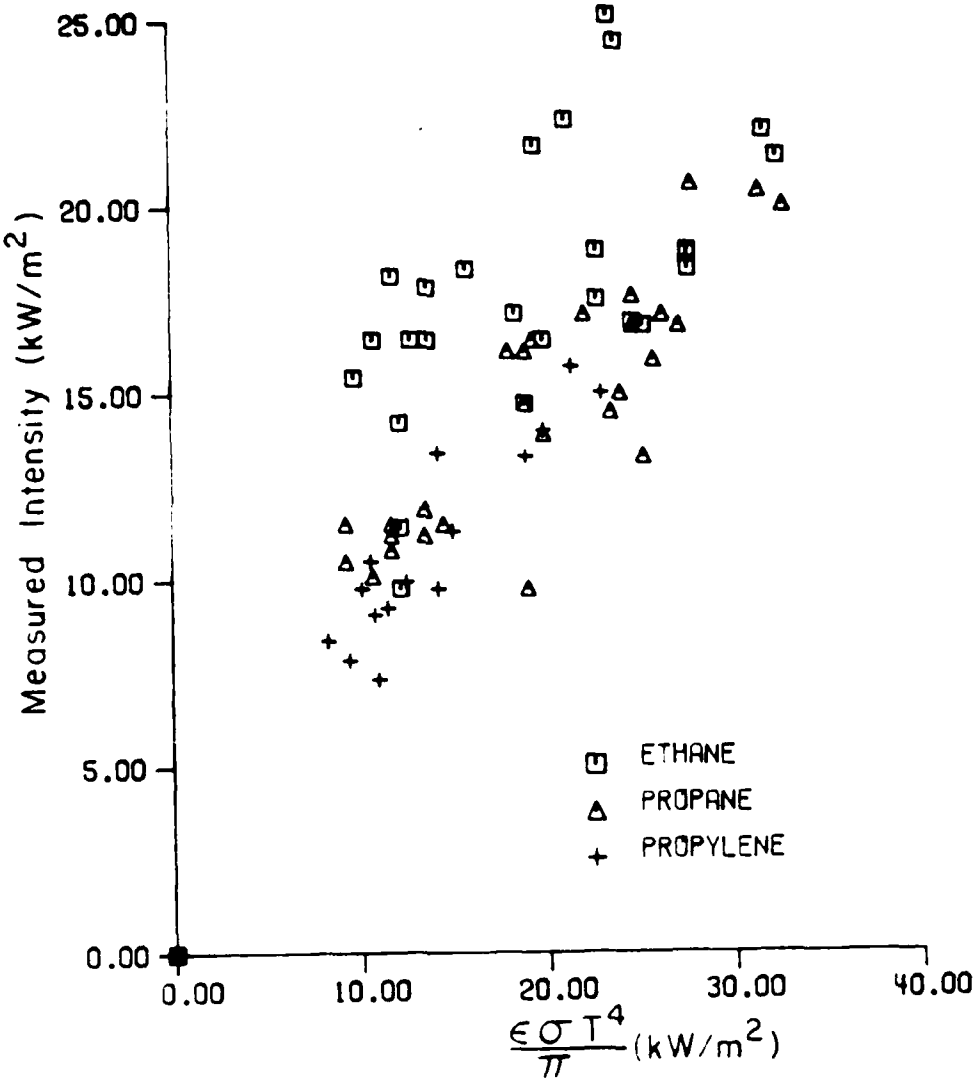

Figure 39. Measured vs. Estimated Radiation Intensities.

SUMMARY AND CONCLUSIONS

This concludes the study of the effects of pressure, temperature, and fuel type on soot threshold equivalence ratios and non-luminous flame radiation. To summarize, the pressure ranged from 0.1 MPa to 0.8 MPa, flame temperatures were as low as 1600K and as high as 2400K, and a variety of paraffins and olefins as well as cyclopropane were burned. All flames were completely premixed and either non-luminous or just sooting.

With regard to soot thresholds, this investigation has revealed several important findings.

— Higher pressures give lower soot threshold equivalence ratios (ϕ_c). The effect diminishes as pressure increases.

— The two-step model for soot precursor evolution is valid for wide ranges of pressures, flame temperatures, and fuels, i.e.

$$\ln\left[\frac{\phi_c}{\chi_{OH}}\cdot\frac{T}{P}\right] \text{ vs. } \frac{1}{T}$$

accurately describes incipient sooting behavior over the range of conditions listed above and for the fuels tested (CH_4, C_2H_6, C_3H_8, C_2H_4, C_3H_6, C_4H_{10} and cyclopropane).

— Measurement of flame temperature at the location of sooting is imperative; adiabatic flame temperatures fail to explain the results.

— The effect of fuel type on incipient soot formation appears negligible. This conclusion is based on an analysis using the measured temperature at that location where soot is first observed to form.

— That incipient soot behavior is independent of fuel type implies that a single chemical mechanism, and single precursor species, is responsible for the onset of sooting.

The second portion of this investigation revealed the effects of equivalence ratio, pressure and fuel type on total non-luminous flame radiation. Important features of this portion of the study were the use of premixed, pure hydrocarbon fuels. As a consequence, the effects of atomization, hydrocarbon blending and fuel-air mixing were absent. Flame radiation could therefore be examined as a separable function of individual physical and chemical properties without the complications associated with liquid-fuels. Several trends were apparent.

— Radiation intensity increased linearly with pressure up to 0.8 MPa. The greatest rate of increase was for $\phi = 1.00$, followed by $\phi = 1.25$ and $\phi = 0.80$.

— Radiation intensity was approximately equal for $\phi = 0.80$ and $\phi = 1.25$ and 20% higher for $\phi = 1.00$.

— Radiation intensity, normalized by the number of carbon-to-carbon bonds in the fuel, $\frac{I_{max}}{\#\ C{-}C\ bonds}$, scales with pressure.

— Radiation intensity decreases as the hydrogen-to-carbon (H/C) ratio of the fuel increases under all conditions, which agrees with previous liquid-fueled studies.

— Empirical, non-luminous emissivities increase with pressure and decrease with axial location and equivalence ratio.

— Emissivities calculated from total radiation and temperature measurements showed no trends, indicating gas band emissivities of less than one for the temperatures and geometry involved.

The results of this study suggest a follow up study be conducted to investigate the pressure and temperature dependence of the incipient soot behavior of mixtures of single component, vaporized fuels. An investigation into the ϕ_c behavior of mixtures would have obvious applications to the new class of "endothermic" fuels, not only because of the feasibility of modeling the decomposition products of these fuels as a mixture of hydrogen and another hydrocarbon, but also because current plans call for burning endothermic fuels as gases premixed with air. A study of this type would show whether the mechanism of incipient soot formation is independent of fuel type. In addition, it would have the added advantage of providing design engineers with values for ϕ_c versus pressure and temperature so that they could design soot-free combustors. Such combustors would have a smaller radiation signature, a characteristic of obvious importance to the Air Force.

BIBLIOGRAPHY

ASME [1971]. *Fluid Meters*, 6th ed., 234.

Calcote, H.F., and Manos, D.M. [1983]. "Effect of Molecular Structure on Incipient Soot Formation," Comb. and Flame, **49**, 289-304.

Calcote, H.F., and Miller, W.J. [1978]. "Ionic Mechanisms of Carbon Formation in Flames," AFOSR-TR-78-1082.

Calcote, H.F., and Olson, D.B. [1982]. "Importance of Temperature on Soot Formation in Premixed Flames," Comb. Sci. and Tech., **28**, 315-7.

Claus, R.W. [1981]. "Spectral Flame Radiance from a Tubular-Can Combustor," NASA TP 1722.

Daily, J.W. and Harleman, D.R.F. [1966]. *Fluid Dynamics*, 227-51, Addison-Wesley Publishing Co., Reading, MA.

Daws, L.F. and Thring, M.W. [1952]. J. Inst. of Fuel, International Committee on Flame Radiation at IJmuiden, Holland, **25**, S28.

Fenimore, C.P., Jones, G.W., and Moore, G.E. [1957]. "Carbon Formation in Quenched Flat Flames at 1600°K," 6th Symp. on Combustion, 242-7.

Flower, B. and Bowman, T. [1986]. "Soot Production Studied at High Pressures," Combustion Research Facility News, **8**, no. 2, 4.

Glassman, I. and Yaccarino, P. [1981]. "The Temperature Effect in Sooting Diffusion Flames," 18th Symp. on Combustion, 1175-83.

Goldstein, R.J. [1983]. *Fluid Mechanics Measurements*, 250-1, Hemisphere Publishing Corp., Washington.

Gordon, S. and McBride, B. [1971]. "Computer Program for Calculation of Complex Chemical Equilibrium Compositions, Rocket Performance, Incident Reflected Shocks, and Chapman-Jouguet Detonations," NASA SP-273.

Harris, M.M., King, G.B., and Laurendeau, N.M. [1986]. "Influence of Temperature and Hydroxyl Concentration on Incipient Soot Formation in Premixed Flames," Comb. and Flame, **64**, 99-112.

Humenik, F.M., Claus, R.W., and Neely, G.M. [1983]. "Parametric Study of Flame Radiation Characteristics of a Tubular-Can Combustor," NASA TM 83436.

Kunitomo, T. and Kodama, K. [1974]. "Radiation from Luminous Flame at High Pressures," Bulletin of the JSME, **17**, no. 113, 1486-93.

Lasers and Applications [1985]. "1986 Buying Guide Technical and Industry Directory," **4**, no. 13, 249.

Lefebvre, A.H. [1983]. *Gas Turbine Combustion*, McGraw-Hill Book Co., New York.

MacFarlane, J.J., Holderness, F.H., and Whitcher, F.S.E. [1964]. "Soot Formation Rates in Premixed C_5 and C_6 Hydrocarbon-Air Flames at Pressures up to 20 Atmospheres," Comb. and Flame, **8**, 215-29.

MacFarlane, J.J. [1975]. "Flame Radiation Studies Using a Model Gas Turbine Primary Zone," 12th Symp. on Combustion, 1255-64.

Marsland, J., Odgers, J. and Winter, J. [1975]. "The Effects of Flame Radiation on Flame-Tube Metal Temperatures," 12th Symp. on Combustion, 1265-1276.

Millikan, R.C. [1962]. "Non-Equilibrium Soot Formation in Premixed Flames," J. Phys. Chem., **66**, 794-9.

Moses, C.A. and Naegeli, D.W. [1979]. "Fuel Property Effects on Combustor Performance," ASME 79-GT-178.

Naegeli, D.W., Dodge, L.G., and Moses, C.A. [1983]. "Effects of Flame Temperature and Fuel Composition on Soot Formation in Gas Turbine Combustors," Comb. Sci. and Tech., **35**, 117-31.

Naegeli, D.W., Dodge, L.G., and Moses, C.A. [1982]. "Sooting Tendency of Fuels Containing Polycyclic Aromatics in a Research Combustor," J. Energy, **7**, no. 2, 168-75.

Olson, D.B. and Madronich, S. [1985]. "The Effect of Temperature on Soot Formation in Premixed Flames," Comb. and Flame, **60**, 203-13.

Olson, D.B. and Pickens, J.C. [1984]. "The Effects of Molecular Structure on Soot Formation, I. Soot Thresholds in Premixed Flames," Comb. and Flame, **57**, 199-208.

Schubauer, G.B., Spangenberg, W.G., and Klebanoff, P.S. [1948]. "Aerodynamic Characteristics of Damping Screens," NACA TN 2001.

Siegel, R. and Howell, J. [1981]. *Thermal Radiation Heat Transfer*, 2nd ed., McGraw-Hill Book Co., New York, chap. 13.

Takahashi, F. and Glassman, I. [1984]. "Sooting Correlations for Premixed Flames," Comb. Sci. and Tech., **37**, 1-19.

Wark, K. [1977]. *Thermodynamics*, 3rd ed., McGraw-Hill Publishing Co., New York.

Wright, F.J. [1969]. "The Formation of Carbon under Well-Stirred Conditions," 12th Symp. on Combustion, 867-74.

Appendix A. Data Tables

Table A1. Fuel Properties.

Fuel	Formula	M(g/gmol)	$\frac{m_{fuel}}{m_{air}}\|\phi=1$	$H_f°$(cal/mole)
Methane	CH_4	16	.058	-17890
Ethane	C_2H_6	30	.061	-20240
Propane	C_3H_8	44	.064	-24820
n-Butane	C_4H_{10}	58	.063	-29810
Ethylene	C_2H_4	28	.067	12500
Propylene	C_3H_6	42	.067	4880
1-Butylene	C_4H_8	56	.066	280
Cyclopropane	C_3H_6	42	.067	12800

Table A2. Critical Equivalence Ratios.

Fuel	T_{in}(K)	P(MPa)	ϕ_c	ψ_c
Methane	700	0.4	1.59	1.19
CH_4		0.5	1.41	1.06
		0.6	1.35	1.01
		0.7	1.28	0.96
		0.8	1.24	0.93
Ethane	500	0.4	1.24	0.89
C_2H_6		0.5	1.23	0.88
		0.6	1.09	0.78
	600	0.3	1.56	1.11
		0.5	1.35	0.96
		0.7	1.30	0.93
		0.8	1.29	0.92
	700	0.3	1.51	1.08
		0.4	1.40	1.00
		0.5	1.38	0.99
		0.6	1.31	0.94
		0.7	1.26	0.90
		0.8	1.24	0.89
Propane	400	0.5	1.50	1.05
C_3H_8		0.6	1.32	0.92
		0.7	1.27	0.89
		0.8	1.13	0.79
	500	0.3	1.60	1.12
		0.4	1.51	1.06
		0.5	1.42	0.99
		0.6	1.34	0.94
		0.7	1.23	0.86
		0.8	1.17	0.82
	600	0.2	1.71	1.20
		0.3	1.42	0.99
		0.4	1.32	0.92
		0.5	1.19	0.83
		0.6	1.16	0.81
		0.7	1.15	0.81
		0.8	1.12	0.78
	700	0.2	1.74	1.22
		0.3	1.50	1.05
		0.4	1.28	0.90
		0.5	1.28	0.90
		0.6	1.21	0.85
		0.7	1.18	0.83
		0.8	1.15	0.81

Fuel	T_{in}(K)	P(MPa)	ϕ_c	ψ_c
n-Butane C_4H_{10}	700	0.2	1.33	0.92
		0.3	1.12	0.78
Ethylene C_2H_4	500	0.3	1.19	0.79
		0.5	1.09	0.73
		0.6	1.07	0.71
	600	0.3	1.19	0.79
		0.4	1.15	0.77
		0.6	1.06	0.71
	700	0.1	1.67	1.11
		0.2	1.55	1.03
		0.3	1.37	0.91
		0.4	1.33	0.89
		0.5	1.28	0.85
		0.6	1.26	0.84
		0.7	1.25	0.83
		0.8	1.23	0.82
Propylene C_3H_6	700	0.1	1.70	1.13
		0.2	1.72	1.15
		0.3	1.48	0.99
		0.4	1.31	0.87
		0.5	1.29	0.86
		0.6	1.27	0.85
1-Butylene C_4H_8	700	0.1	1.22	0.81
		0.2	1.12	0.75
		0.3	1.05	0.70
Cyclopropane C_3H_6	700	0.1	1.34	0.89
		0.2	1.18	0.79
		0.3	1.11	0.74
		0.4	1.09	0.73

Table A3. Measured Flame Temperatures and Equilibrium OH Mole Fractions.

Fuel	T_{in}(K)	P(MPa)	T_f(K)	$\frac{10^6}{T_f}$	$\chi_{OH} \cdot 10^7$
Methane	700	0.4	1640	610	10
CH_4		0.5	1750	571	46
		0.6	2020	495	640
		0.7	2250	444	4140
		0.8	2230	448	3713
Ethane	500	0.4	1850	541	202
C_2H_6		0.5	2030	493	983
		0.6	2240	446	7820
	600	0.3	1690	592	19
		0.5	1990	503	495
		0.7	2230	448	3280
		0.8	2310	433	5110
	700	0.3	1450	688	0.5
		0.4	1800	556	74
		0.5	1850	541	117
		0.6	2010	498	582
		0.7	2090	478	1210
		0.8	2270	441	4690
Propane	400	0.5	1720	581	22
C_3H_8		0.6	1920	521	244
		0.7	1950	513	363
		0.8	2200	455	3893
	500	0.3	1530	654	2.2
		0.4	1720	581	24
		0.5	1860	538	119
		0.6	1965	509	357
		0.7	2220	450	3550
		0.8	2230	448	4348
	600	0.2	1320	758	-
		0.3	1570	637	5.2
		0.4	1840	543	132
		0.5	1925	519	395
		0.6	2070	483	1520
		0.7	2040	490	1080
		0.8	1980	505	684
	700	0.2	1350	741	-
		0.3	1550	645	3.5
		0.4	1780	562	76
		0.5	2030	493	800
		0.6	2170	461	2830
		0.7	2130	469	2140
		0.8	2360	424	11100

Fuel	T_{in}(K)	P(MPa)	T_f(K)	$\frac{10^6}{T_f}$	$\chi_{OH} \cdot 10^7$
n-Butane	700	0.2	1550	645	5
C_4H_{10}		0.3	2250	444	9810
Ethylene	500	0.3	1580	633	8
C_2H_4		0.5	2300	435	11304
		0.6	2140	467	4010
	600	0.3	1750	571	83
		0.4	1930	518	536
		0.6	2150	465	4670
	700	0.1	1370	730	-
		0.2	1580	633	4
		0.3	1610	621	8.8
		0.4	1730	578	40
		0.5	2000	500	566
		0.6	2080	481	1130
		0.7	2200	455	2638
		0.8	2430	412	12400
Propylene	700	0.1	1310	763	-
C_3H_6		0.2	1460	685	1
		0.3	1965	509	335
		0.4	2050	488	987
		0.5	2065	484	1040
		0.6	2140	467	1830
1-Butylene	700	0.1	1460	685	2
C_4H_8		0.2	1590	629	854
		0.3	1680	595	1628
Cyclopropane	700	0.1	1460	685	1
C_3H_6		0.2	1680	595	39
		0.3	1870	535	371
		0.4	2060	485	2110

Table A4. Adiabatic Flame Temperatures and Equilibrium OH Mole Fractions.

Fuel	T_{in}(K)	P(MPa)	T_{ad}(K)	$\frac{10^6}{T_{ad}}$	$\chi_{OH} \cdot 10^7$
Methane CH_4	700	0.4	2075	482	778
		0.5	2209	453	2659
		0.6	2257	443	3814
		0.7	2313	432	6023
		0.8	2345	426	7701
Ethane C_2H_6	500	0.4	2274	440	6545
		0.5	2283	438	6396
		0.6	2381	420	18475
	600	0.3	2095	477	1044
		0.5	2252	444	3877
		0.7	2292	436	4817
		0.8	2300	435	4880
	700	0.3	2194	456	2436
		0.4	2276	439	4628
		0.5	2292	436	4805
		0.6	2347	427	7274
		0.7	2385	419	9713
		0.8	2401	416	10574
Propane C_3H_8	400	0.5	2031	492	509
		0.6	2167	461	1987
		0.7	2207	453	2781
		0.8	2316	432	8731
	500	0.3	2020	495	508
		0.4	2085	480	885
		0.5	2153	464	1586
		0.6	2214	452	2697
		0.7	2300	435	5966
		0.8	2347	426	9137
	600	0.2	2004	499	458
		0.3	2214	452	3232
		0.4	2290	437	5889
		0.5	2388	419	13944
		0.6	2410	415	16110
		0.7	2419	413	16282
		0.8	2438	410	19226
	700	0.2	2046	489	630
		0.3	2218	451	2873
		0.4	2382	420	11706
		0.5	2384	419	10613
		0.6	2435	411	15970
		0.7	2457	407	18418
		0.8	2478	404	21393

Fuel	T_{in}(K)	P(MPa)	T_{ad}(K)	$\frac{10^6}{T_{ad}}$	$\chi_{OH} \cdot 10^7$
n-Butane	700	0.2	2343	427	11371
C_4H_{10}		0.3	2472	405	35711
Ethylene	500	0.3	2481	403	28900
C_2H_4		0.5	2518	397	38091
		0.6	2524	396	38867
	600	0.3	2529	395	37245
		0.4	2548	392	40173
		0.6	2565	390	47965
	700	0.1	2317	432	6841
		0.2	2392	418	9655
		0.3	2500	400	20937
		0.4	2526	396	22908
		0.5	2556	391	26969
		0.6	2569	389	27794
		0.7	2577	388	27575
		0.8	2589	386	28938
Propylene	700	0.1	2217	451	3260
C_3H_6		0.2	2208	453	2090
		0.3	2365	423	7533
		0.4	2476	404	18138
		0.5	2491	401	18577
		0.6	2506	399	19352
1-Butylene	700	0.1	2468	405	41349
C_4H_8		0.2	2515	398	49917
		0.3	2527	396	54334
Cyclopropane	700	0.1	2467	405	31441
C_3H_6		0.2	2544	393	49335
		0.3	2568	389	55153
		0.4	2579	388	54408

Table A5. ϕ_c and ψ_c vs Measured Flame Temperature.

Fuel	T_{in}(K)	P(MPa)	$\ln\left[\frac{\phi_c}{\chi_{OH}}\cdot\frac{T}{P}\right]$	$\ln\left[\frac{\phi_c}{\chi_{OH}}\cdot\frac{T}{P}\cdot\left[\frac{H}{C}\right]^{1/2}\right]$	$\ln\left[\frac{\psi_c}{\chi_{OH}}\cdot\frac{T}{P}\right]$
Methane CH_4	700	0.4	22.6	23.3	22.3
		0.5	20.8	21.1	20.5
		0.6	18.1	20.4	17.8
		0.7	16.1	18.7	15.9
		0.8	16.0	17.8	15.8
Ethane C_2H_6	500	0.4	19.5	20.0	19.1
		0.5	17.7	18.3	17.4
		0.6	15.5	16.0	15.1
	600	0.3	22.3	22.8	21.9
		0.5	18.5	19.1	18.2
		0.7	16.4	16.9	16.0
		0.8	15.8	16.4	15.5
	700	0.3	25.7	26.3	25.4
		0.4	20.6	21.1	20.2
		0.5	19.9	20.4	19.6
		0.6	18.1	18.7	17.8
		0.7	17.3	17.8	16.9
		0.8	15.8	16.4	15.5
Propane C_3H_8	400	0.5	21.6	22.1	21.2
		0.6	19.0	19.5	18.6
		0.7	18.4	18.9	18.0
		0.8	15.9	16.4	15.5
	500	0.3	24.3	24.8	24.0
		0.4	21.7	22.	21.4
		0.5	19.9	20.4	19.6
		0.6	18.6	19.1	18.3
		0.7	16.2	16.7	15.9
		0.8	15.8	16.3	15.5
	600	0.2	-	-	-
		0.3	23.4	23.9	23.0
		0.4	19.9	20.4	19.6
		0.5	18.6	19.1	18.2
		0.6	17.1	17.6	16.7
		0.7	-	-	-
		0.8	-	-	-
	700	0.2	-	-	-
		0.3	23.8	24.3	23.5
		0.4	20.4	20.9	20.1
		0.5	18.0	18.5	17.6
		0.6	16.6	17.0	16.2
		0.7	-	-	-
		0.8	14.9	15.4	14.6

Fuel	T_{in}(K)	P(MPa)	$\ln\left[\frac{\phi_c}{\chi_{OH}}\cdot\frac{T}{P}\right]$	$\ln\left[\frac{\phi_c}{\chi_{OH}}\cdot\frac{T}{P}\cdot\left[\frac{H}{C}\right]^{1/2}\right]$	$\ln\left[\frac{\psi_c}{\chi_{OH}}\cdot\frac{T}{P}\right]$
n-Butane C_4H_{10}	700	0.2	23.7	24.2	23.4
		0.3	16.0	16.4	15.6
Ethylene C_2H_4	500	0.3	22.8	23.1	22.4
		0.5	15.3	15.6	14.9
		0.6	16.1	16.4	15.7
	600	0.3	20.5	20.9	20.1
		0.4	18.5	18.8	18.1
		0.6	15.9	16.3	15.5
	700	0.1	-	-	-
		0.2	24.1	24.5	23.7
		0.3	22.8	23.2	22.4
		0.4	21.1	21.4	20.7
		0.5	18.3	18.7	17.9
		0.6	17.5	17.8	17.1
		0.7	16.5	16.9	16.1
		0.8	14.9	15.3	14.5
Propylene C_3H_6	700	0.1	-	-	-
		0.2	25.6	25.9	25.2
		0.3	19.5	19.8	19.1
		0.4	18.0	18.4	17.6
		0.5	17.8	18.1	17.3
		0.6	17.0	17.4	16.6
1-Butylene C_4H_8	700	0.1	25.2	25.6	24.8
		0.2	21.5	21.8	21.1
		0.3	18.9	19.2	18.5
Cyclo-propane C_3H_6	700	0.1	26.0	26.3	25.6
		0.2	21.7	22.0	21.3
		0.3	19.0	19.4	18.6
		0.4	17.1	17.4	16.7

Table A6. ϕ_c and ψ_c vs Adiabatic Flame Temperature.

Fuel	T_{in}(K)	P(MPa)	$\ln\left[\frac{\phi_c}{\chi_{OH}}\cdot\frac{T}{P}\right]$	$\ln\left[\frac{\psi_c}{\chi_{OH}}\cdot\frac{T}{P}\right]$
Methane	700	0.4	18.5	18.2
CH_4		0.5	17.0	16.7
		0.6	16.4	16.1
		0.7	15.8	15.5
		0.8	15.4	15.1
Ethane	500	0.4	16.2	15.9
C_2H_6		0.5	16.0	15.7
		0.6	14.7	14.3
	600	0.3	18.5	18.1
		0.5	16.6	16.2
		0.7	16.0	15.7
		0.8	15.8	15.5
	700	0.3	17.6	17.3
		0.4	16.7	16.3
		0.5	16.4	16.1
		0.6	15.8	15.4
		0.7	15.3	15.0
		0.8	15.1	14.7
Propane	400	0.5	18.6	18.2
C_3H_8		0.6	17.0	16.6
		0.7	16.5	16.1
		0.8	15.1	14.8
	500	0.3	19.2	18.8
		0.4	18.3	17.9
		0.5	17.5	17.1
		0.6	16.7	16.4
		0.7	15.7	15.4
		0.8	15.1	14.8
	600	0.2	19.7	19.4
		0.3	17.3	16.9
		0.4	16.3	16.0
		0.5	15.2	14.9
		0.6	14.9	14.5
		0.7	14.7	14.4
		0.8	14.4	14.0
	700	0.2	19.5	19.1
		0.3	17.5	17.1
		0.4	15.7	15.3
		0.5	15.6	15.2
		0.6	14.9	14.6
		0.7	14.6	14.3
		0.8	14.3	14.0

Fuel	T_{in}(K)	P(MPa)	$\ln\left[\frac{\phi_c}{\chi_{OH}}\cdot\frac{T}{P}\right]$	$\ln\left[\frac{\psi_c}{\chi_{OH}}\cdot\frac{T}{P}\right]$
n-Butane	700	0.2	16.4	15.7
C_4H_{10}		0.3	14.8	14.4
Ethylene	500	0.3	15.0	14.6
C_2H_4		0.5	14.2	13.8
		0.6	14.0	13.6
	600	0.3	14.8	14.4
		0.4	14.4	14.0
		0.6	13.8	13.4
	700	0.1	17.9	17.4
		0.2	16.8	16.4
		0.3	15.5	15.1
		0.4	15.1	14.7
		0.5	14.7	14.3
		0.6	14.5	14.1
		0.7	14.3	13.9
		0.8	14.1	13.7
Propylene	700	0.1	18.6	18.2
C_3H_6		0.2	18.3	17.9
		0.3	16.6	16.2
		0.4	15.3	14.9
		0.5	15.1	14.7
		0.6	14.8	14.4
1-Butylene	700	0.1	15.8	15.4
C_4H_8		0.2	14.9	14.5
		0.3	14.3	13.9
Cyclopropane	700	0.1	16.2	15.8
C_3H_6		0.2	14.9	14.5
		0.3	14.4	14.0
		0.4	14.1	13.7

Table A7. Maximum Radiant Intensities ($kW/m^2 \cdot sr$)

	Ethane	Propane	Ethylene	Propylene
		P = 0.4 MPa		
$\phi = 0.80$	11.3	11.5	11.5	17.5
$\phi = 1.00$	10.5	11.9	11.9	18.3
$\phi = 1.25$	9.25	11.5	11.5	13.7
P = 0.6 MPa				
$\phi = 0.80$	13.8	16.8	15.0	20.9
$\phi = 1.00$	15.7	17.6	18.1	25.1
$\phi = 1.25$	14.0	16.4	16.7	22.7
P = 0.8MPa				
$\phi = 0.80$	17.1	18.8	18.1	-
$\phi = 1.00$	20.6	22.0	22.0	-
$\phi = 1.25$	17.1	18.8	18.1	-

Temperature at Point of Maximum Intensity (K)

	Ethane	Propane	Ethylene	Propylene
P = 0.4 MPa				
$\phi = 0.80$	1560	1670	-	1770
$\phi = 1.00$	1680	1870	-	1980
$\phi = 1.25$	1860	1870	-	1960
P = 0.6 MPa				
$\phi = 0.80$	1590	2040	-	1730
$\phi = 1.00$	1980	2150	-	2100
$\phi = 1.25$	2070	2080	-	2180
P = 0.8MPa				
$\phi = 0.80$	1960	1970	-	-
$\phi = 1.00$	2060	2210	-	-
$\phi = 1.25$	2120	2180	-	-

Table A8. Ethane: Intensity, Temperature, and Emissivity Profiles.

Radiant Intensities ($kW/m^2 \cdot sr$)

	x/D = 1	x/D = 2	x/D = 3	x/D = 4
P = 0.4 MPa				
ϕ = 0.80	11.3	9.77	7.85	7.33
ϕ = 1.00	9.42	10.5	9.95	9.77
ϕ = 1.25	7.68	8.38	9.07	9.25
P = 0.6 MPa				
ϕ = 0.80	13.8	13.4	11.3	9.77
ϕ = 1.00	14.3	15.7	15.0	14.5
ϕ = 1.25	11.9	13.3	14.0	13.9
P = 0.8MPa				
ϕ = 0.80	16.1	17.1	15.0	13.3
ϕ = 1.00	19.5	20.6	20.4	20.0
ϕ = 1.25	14.7	15.9	17.1	16.8

Temperatures (K)

	x/D = 1	x/D = 2	x/D = 3	x/D = 4
P = 0.4 MPa				
ϕ = 0.80	1560	1720	1660	1780
ϕ = 1.00	1610	1680	1800	1920
ϕ = 1.25	1440	1600	1790	1860
P = 0.6 MPa				
ϕ = 0.80	1590	1740	1780	1970
ϕ = 1.00	1810	1980	2080	2140
ϕ = 1.25	1760	2020	2070	2070
P = 0.8MPa				
ϕ = 0.80	1890	1960	2020	2070
ϕ = 1.00	1870	2060	2190	2250
ϕ = 1.25	1950	2090	2120	2170

Emissivities

	x/D = 1	x/D = 2	x/D = 3	x/D = 4
P = 0.4 MPa				
ϕ = 0.80	.034	.020	.018	.013
ϕ = 1.00	.025	.023	.017	.013
ϕ = 1.25	.032	.023	.016	.014
P = 0.6 MPa				
ϕ = 0.80	.038	.026	.020	.011
ϕ = 1.00	.023	.018	.014	.012
ϕ = 1.25	.022	.014	.013	.013
P = 0.8MPa				
ϕ = 0.80	.022	.020	.016	.013
ϕ = 1.00	.028	.020	.016	.014
ϕ = 1.25	.018	.015	.015	.013

Table A9. Propane: Intensity, Temperature, and Emissivity Profiles.

Radiant Intensities ($kW/m^2 \cdot sr$)

	x/D = 1	x/D = 2	x/D = 3	x/D = 4
P = 0.4 MPa				
ϕ = 0.80	11.5	11.5	10.5	10.1
ϕ = 1.00	11.9	11.9	11.2	11.5
ϕ = 1.25	9.95	11.5	11.2	10.8
P = 0.6 MPa				
ϕ = 0.80	16.8	16.1	14.7	14.7
ϕ = 1.00	16.1	17.6	16.8	16.9
ϕ = 1.25	14.0	16.1	16.4	16.4
P = 0.8MPa				
ϕ = 0.80	18.1	18.8	17.5	16.8
ϕ = 1.00	18.1	22.0	22.0	21.3
ϕ = 1.25	16.8	18.8	18.3	18.7

Temperatures (K)

	x/D = 1	x/D = 2	x/D = 3	x/D = 4
P = 0.4 MPa				
ϕ = 0.80	1780	1670	1670	1780
ϕ = 1.00	1790	1870	1870	1930
ϕ = 1.25	1870	1870	1870	1870
P = 0.6 MPa				
ϕ = 0.80	2040	1980	1980	1980
ϕ = 1.00	2120	2150	2150	2150
ϕ = 1.25	1970	1970	2030	2080
P = 0.8MPa				
ϕ = 0.80	1830	1970	1970	2080
ϕ = 1.00	2160	2210	2210	2260
ϕ = 1.25	2100	2180	2180	2180

Emissivities

	x/D = 1	x/D = 2	x/D = 3	x/D = 4
P = 0.4 MPa				
ϕ = 0.80	.020	.026	.024	.018
ϕ = 1.00	.020	.017	.016	.015
ϕ = 1.25	.014	.017	.016	.016
P = 0.6 MPa				
ϕ = 0.80	.017	.018	.017	.017
ϕ = 1.00	.014	.015	.014	.014
ϕ = 1.25	.016	.019	.017	.015
P = 0.8MPa				
ϕ = 0.80	.028	.022	.020	.016
ϕ = 1.00	.015	.016	.016	.014
ϕ = 1.25	.015	.015	.014	.015

Table A10. Ethylene: Intensity Profiles.

Radiant Intensities ($kW/m^2 \cdot sr$)

	x/D = 1	x/D = 2	x/D = 3	x/D = 4
P = 0.4 MPa				
$\phi = 0.80$	13.3	11.9	11.9	10.6
$\phi = 1.00$	11.5	12.6	12.9	12.2
$\phi = 1.25$	8.73	10.5	11.5	11.9
P = 0.6 MPa				
$\phi = 0.80$	15.0	14.7	12.6	9.42
$\phi = 1.00$	14.3	17.5	18.1	17.6
$\phi = 1.25$	12.2	15.4	16.4	16.4
P = 0.8MPa				
$\phi = 0.80$	18.1	16.4	14.7	14.0
$\phi = 1.00$	18.1	21.6	22.0	21.1
$\phi = 1.25$	15.5	17.3	18.1	18.1

Table A11. Propylene: Intensity, Temperature, and Emissivity Profiles.

Radiant Intensities ($kW/m^2 \cdot sr$)

	x/D = 1	x/D = 2	x/D = 3	x/D = 4
P = 0.4 MPa				
ϕ = 0.80	17.5	14.2	11.4	9.77
ϕ = 1.00	14.0	16.4	17.8	18.3
ϕ = 1.25	11.9	15.4	16.4	16.4
P = 0.6 MPa				
ϕ = 0.80	20.9	18.1	17.1	14.5
ϕ = 1.00	23.7	25.1	24.4	23.7
ϕ = 1.25	20.2	21.6	22.3	22.7

Temperatures (K)

	x/D = 1	x/D = 2	x/D = 3	x/D = 4
P = 0.4 MPa				
ϕ = 0.80	1770	1840	1840	1840
ϕ = 1.00	1740	1920	1920	1980
ϕ = 1.25	1670	1740	1800	1960
P = 0.6 MPa				
ϕ = 0.80	1730	1810	1960	2050
ϕ = 1.00	1950	2100	2150	2210
ϕ = 1.25	1900	2070	2180	2180

Emissivities

	x/D = 1	x/D = 2	x/D = 3	x/D = 4
P = 0.4 MPa				
ϕ = 0.80	.031	.022	.018	.015
ϕ = 1.00	.027	.021	.023	.021
ϕ = 1.25	.027	.030	.028	.020
P = 0.6 MPa				
ϕ = 0.80	.041	.030	.020	.014
ϕ = 1.00	.029	.023	.020	.018
ϕ = 1.25	.027	.021	.017	.018

Table A12. Empirical Emissivities Using Measured Flame Properties.

Fuel	x/D = 2	x/D = 3	x/D = 4
Ethane			
P = 0.4 MPa			
$\phi = 0.80$	.064	.069	.061
$\phi = 1.00$	.074	.066	.058
$\phi = 1.25$	.070	.058	.053
P = 0.6 MPa			
$\phi = 0.80$	.086	.083	.070
$\phi = 1.00$	.077	.068	.062
$\phi = 1.25$	.063	.060	.060
P = 0.8MPa			
$\phi = 0.80$	.083	.080	.076
$\phi = 1.00$	.086	.076	.071
$\phi = 1.25$	.075	.072	.068
Propane			
P = 0.4 MPa			
$\phi = 0.80$	.066	.066	.059
$\phi = 1.00$	.061	.061	.058
$\phi = 1.25$	.053	.053	.053
P = 0.6 MPa			
$\phi = 0.80$	.068	.068	.068
$\phi = 1.00$	.064	.064	.064
$\phi = 1.25$	.066	.063	.059
P = 0.8MPa			
$\phi = 0.80$	.084	.084	.075
$\phi = 1.00$	.074	.074	.069
$\phi = 1.25$	.068	.068	.068

Propylene

P = 0.4 MPa

$\phi = 0.80$	.059	.059	.059
$\phi = 1.00$	.056	.056	.057
$\phi = 1.25$	.059	.057	.048

P = 0.6 MPa

$\phi = 0.80$	.061	.069	.062
$\phi = 1.00$	.067	.062	.058
$\phi = 1.25$	.059	.052	.052

Appendix B. Journal Publications

The following journal publications have resulted from this work, have been submitted, or are in preparation.

1. "The Influence of Pressure and Temperature on Incipient Soot Formation in Premixed Flames," W.G. Cummings, III, P.E. Sojka, and A.H. Lefebvre, submitted to *Combustion and Flame* (July, 1987).

2. "Measurements of Thermal Radiation in Pressurized Turbulent Flames," W.G. Cummings, III, A.H. Lefebvre, and P.E. Sojka, submitted to *ASME Journal of Engineering for Gas Turbines and Power* (July, 1987).

Appendix C. Professional Personnel

Three people have been associated with this contract: A.H. Lefebvre, Reilly Professor of Combustion, P.E. Sojka, Assistant Professor of Mechanical Engineering, and W.G. Cummings, III. Mr. Cummings' M.S.M.E. (Master of Science in Mechanical Engineering) thesis was a direct result of the work performed under this contract. The title was "Soot Thresholds and Flame Radiation in High Pressure, Gaseous Fuel Flames." Mr. Cummings degree was conferred December 12, 1986.

Appendix D. Interactions

Several technical interactions have occurred during this contract. They are divided into two parts. Critical soot equivalence ratio and flame radiation.

Critical Soot Equivalence Ratio

W.G. Cummings, III, P.E. Sojka, and A.H. Lefebvre, "The Influence of Pressure and Temperature on Incipient Soot Formation in Premixed Flames," Central States Section/Combustion Institute Spring Technical Meeting, Argonne National Lab, Chicago (May 1987).

W.G. Cummings, III, P.E. Sojka and A.H. Lefebvre, "The Effects of Temperature, Pressure and Fuel Type on Flame Radiation and Soot Formation in Gaseous Hydrocarbon + Air Flames," Central States Section/Combustion Institute Spring Technical Meeting, NASA LeRC, Cleveland (May 1986).

Radiation

W.G. Cummings, III, P.E. Sojka, and A.H. Lefebvre, "Measurements of Thermal Radiation in Pressurized Turbulent Flames," ASME 1987 National Heat Transfer Conference, Pittsburgh (Aug. 1987).

W.G. Cummings, III, P.E. Sojka, and A.H. Lefebvre, "Flame Radiation in a Gas Turbine Combustor," SAE Paper No. 85208, SAE International Fuels and Lubricant Meeting, Tulsa (Oct. 1985).

W.G. Cummings, III, P.E. Sojka, and A.H. Lefebvre, "Flame Radiation in a

Gas Turbine Combustor," Central States Section Combustion Institute Spring Technical Meeting, Univ. of MN, St. Paul (March 1984).

END

DATE

FILMED

6-88

DTIC